Quality control in cone-beam computed tomography (CBCT)

EFOMP-ESTRO-IAEA protocol

EFOMP
European Federation of Organisations for Medical Physics

ESTRO

IAEA
International Atomic Energy Agency

EFOMP

2nd edition, May 2019

QUALITY CONTROL IN CONE-BEAM COMPUTED TOMOGRAPHY (CBCT)

EFOMP-ESTRO-IAEA PROTOCOL

Hugo de las Heras Gala, Alberto Torresin, Alexandru Dasu, Osvaldo Rampado, Harry Delis, Irene Hernández Girón, Chrysoula Theodorakou, Jonas Andersson, John Holroyd, Mats Nilsson, Sue Edyvean, Vesna Gershan, Lama Hadid-Beurrier, Christopher Hoog, Gregory Delpon, Ismael Sancho Kolster, Primož Peterlin, Julia Garayoa Roca, Paola Caprile, Costas Zervides, Annalisa Trianni

This report is dedicated to our deceased colleague and friend Wil van der Putten, who co-founded this working group.

http://dx.medra.org/10.19285/CBCTEFOMP.V1.0.2017.06

Working Group (alphabetically)	Affiliation
Jonas Andersson	University Hospital of Umeå, Umeå, Sweden
Paola Caprile	Pontificia Universidad Católica de Chile, Santiago, Chile
Alexandru Dasu	The Skandion Clinic, Uppsala, Sweden Linköping University, Linköping, Sweden
Harry Delis (IAEA liaison)	International Atomic Energy Agency, Vienna, Austria
Gregory Delpon (ESTRO)	Centre René Gauducheau, Nantes, France
Sue Edyvean	Public Health England (PHE), Chilton, Didcot, Oxfordshire, UK
Julia Garayoa Roca	Fundación Jiménez Díaz, Madrid, Spain
Vesna Gershan	Faculty of Natural Sciences and Mathematics, Skopje, Macedonia
Lama Hadid-Beurrier	Hôpital Jean-Verdier, Paris, France
Hugo de las Heras Gala (group leader)	QUART GmbH & Helmholtz Zentrum München, Munich, Germany
Irene Hernández Girón	Leiden University Medical Center, Leiden, The Netherlands
John Holroyd	Dental x-ray Protection Services, PHE, UK
Christopher Hoog	Centre Antoine Lacassagne, Nice, France
Mats Nilsson	Skane University Hospital, Malmö, Sweden
Primož Peterlin	Institute of Oncology Ljubljana, Slovenia
Osvaldo Rampado	A.O.U. Città della Salute e della Scienza, Torino, Italy
Ismael Sancho Kolster (ESTRO)	Institut Catalàd'Oncologia, L'Hospitalet de Llobregat, Spain

Chrysoula Theodorakou	The Christie NHS Foundation Trust, Manchester, UK
Annalisa Trianni	Azienda Sanitaria Universitaria Integrata, Udine, Italy
Alberto Torresin (EFOMP supervisor)	EFOMP Education and Training Committee Past Chair ASST Grande Ospedale Metropolitano Niguarda, Milano, Italy
Costas Zervides	Zervides Radiation Protection Services, Limassol, Cyprus University of Nicosia, Medical School, Nicosia, Cyprus

EFOMP Scientific Committee chairpersons:

Manuel Bardiès	Cancer Research Center of Toulouse, France
Mika Kortesniemi	HUS Medical Imaging Center, University of Helsinki, Finland

Consultants

For their comments and support we are very thankful to the liaisons with AAPM (Eric Gingold), EURADOS (Annalisa Trianni), IAEA (Ahmed Meghzifene) and ESTRO (Nuria Jornet Sala and Eduard Gershkevitsh), as well as the additional ESTRO reviewer Tufve Nyholm.

For their comments at the virtual meetings, photos and help during data acquisition we are also thankful to Anne Thilander-Klang, Wouter Veldkamp, Federica Zanca, Ana Roda, José Afonso, Dina Tamras, Stefan Thunberg, Henrik Bertilsson, Paul Charnock, Gerald R. Torgersen, Valerie Jarrige, Julien Darreon, Marçal Salvadó, Hua Li, Sandra Sandstrom, Renato Padovani, Katharina Mair, Bernhard Renger, Patricia Mora, Klara Jarczyk and Paolo Russo.

For the numerous and careful corrections of style we are very thankful to EFOMP Past president Peter Sharp. His input has radically improved the readability of the document. We are also thankful to the EFOMP team, especially Efi Koutsouveli and Magdalena Stoeva, for their efforts to bring our work into a beautiful format.

For the appendix 7 we are especially thankful to EURADOS WG 12 Dosimetry in medical imaging, and in particular to Olivera Ciraj Bjelac, Jad Farah, Aoife Gallagher, Željka Knežević and Marija Majer.

For his interest in our work we want to thank EFOMP President Marco Brambilla.

Finally for his encouragement, support to our activities and his writing of the introduction we want to thank EFOMP Past President John Damilakis.

Foreword

Quality control of cone-beam computed tomography (CBCT) systems is an essential part of quality assurance to periodically check that quality requirements are met, reduce uncertainties and errors and reduce the likelihood of accidents and incidents. Radiation exposure levels must be measured to ensure that patient doses associated with CBCT examinations are kept as low as reasonably achievable consistent with the required diagnostic information. The main purpose of this document is to present procedures for quality control of CBCT systems used for dental, radiotherapy, interventional radiology and guided surgery applications.

The 'Quality control in cone-beam computed tomography' is the second of the series on quality control protocols. The European Federation of Organizations for Medical Physics (EFOMP) published the first document on 'Quality Controls in digital mammography' in 2015. These books are freely available online at efomp.org and can be used as both, in-depth working guides to everyday practice and an up-to-date reference sources for medical physicists engaged in quality control of medical imaging systems.

This book is the result of the experience and knowledge of an international group of leading medical physics experts and an excellent illustration of the synergy that can be achieved when every team member works at their best and collaboratively follows the whole process through its completion. Representing the European Medical Physics professional-scientific community (EFOMP), I would like to thank each co-author for sharing their invaluable expertise and insights and especially the Group Leader Dr. Hugo de las Heras Gala and the Past Chair of the EFOMP Education and Training Committee Dr. Alberto Torresin.

Prof. John Damilakis
EFOMP President (2015-2017)

Table of Contents

List of Abbreviations

AAPM	American Association of Physicists in Medicine
QA	Quality assurance
QC	Quality control
CBCT	Cone beam computed tomography
CBDI	Cone beam dose index
CHO	Channelized Hotelling observer
CNR	Contrast-to-noise ratio
CT	Computed tomography
CTDI	Computed tomography dose index
DICOM	Digital imaging and communications in medicine
DIN	Deutsches Institut für Normung (German insititute for standards)
DFOV	Dose over the diameter of the field of view
EFOMP	European Federation of Organisations for Medical Physics
ESTRO	European Society for Therapeutic Radiation Oncology
EURADOS	European radiation dosimetry group
FOV	Field of view
Gy	Gray

EFOMP-ESTRO-IAEA CBCT Protocol

List of Abbreviations

HU	Hounsfield units
IAEA	International atomic energy agency
IGRT	Image-guided radiotherapy
$K_{a,i}$	Incident air kerma
$K_{a,i}$(FDD)	Incident air kerma at the focus-detector distance
KAP	Kerma area product
Lp/mm	Line-pairs per millimetre
MTF	Modulation transfer function
NPS	Noise power spectrum
NPWE	Non-prewhitening matched filter with an eye filter
PMMA	Polymethylmethacrylate
PVC	Polyvinyl chloride (PVC)
ROI	Region of interest
SRS/SBRT	Stereotactic radiosurgery / Stereotactic body radiotherapy

CHAPTER 1

Introduction

CHAPTER 1

Introduction

The goal of quality assurance (QA) is to provide health care practitioners with consistent and reliable diagnostic image quality with regard to patient radiation dose, in conformance with manufacturer specifications and present regulatory demands. QA is initiated with the analysis of the need and the purchase specifications of a device, continues at the installation of a cone-beam computed tomography (CBCT) unit, where baseline measurements are performed, and extends until end of life for a given unit to ensure functionality. Furthermore, QA shall provide actionable information to initiate corrective maintenance when required.

As part of QA, quality control (QC), as defined by EURATOM[1], "means the set of operations (programming, coordinating, implementing) intended to maintain or to improve quality. It includes monitoring, evaluation and maintenance at required levels of all characteristics of performance of equipment that can be defined, measured, and controlled". Different practitioners perform QC tests and measurements depending on present regulatory demands. Manufacturer representatives, as well as medical physicists, additionally evaluate results from QC testing.

Motivation

Current guidelines for quality control of cone-beam CT (CBCT) and general documents on radiology physics regard the different CBCT applications (dental, radiotherapy, interventional radiology and guided surgery) as different entities[2,3]. However, the data acquisition, reconstruction and the test parameters for image quality and dose evaluation are the same. This guideline was born to unify the image quality controls for all CBCT systems. A further unification with multi slice CT systems, which are closely related to CBCT, is planned for a future edition.

In the past few years, the concern about doses received by patients undergoing CT scans has grown in parallel with the number of examinations performed per year worldwide. Different initiatives, like the EUROsafe[4], Image Gently[5], Image Wisely[6] or recent efforts by the AAPM and EFOMP recommending standard protocols for different common indications, have been developed. This document is part of them.

In the particular case of external radiotherapy, patients undergo high energy x-ray treatments with total absorbed doses in the range of several tens of Gy. In addition, for image-guided radiotherapy (IGRT) several CBCT scans are performed on the patient during treatment[7]. In this regard, the present document focuses on the quality control of the CBCT system and not the whole IGRT system. Adaptive radiotherapy (ART) has been considered as an extension of IGRT.

Our unifying approach

Test parameters and methods have been sought so they can be used to assess the image quality and the exposure related to any CBCT device. Detailed procedures using free software have been included for the image quality evaluation. Action levels and frequency of the tests are indicated together with references wherever possible. However, due to a lack of long worldwide experience with applications of CBCT in radiotherapy, interventional radiology and guided surgery, the recommended action levels for these modalities are still not as well established as in the dental field[8,9,10].

For quantitative (or technical) image quality evaluation, the recently developed technology for CBCT is well served by objective measures for quality control, such as contrast-to-noise[11] ratio and the modulation transfer function[9,10] (MTF). These objective measures are reproducible, they are not dependent on the observer and they can be conveniently assessed by computer software. The new measures have been proposed as methods to quantitatively and objectively assess image quality, so replacing the evaluation and measures based on contrast detail objects and bar patterns, which have been in use for quality control for more than 20 years[12,13,14,15,16].

This guideline includes the minimum tests that should be performed to ensure proper functioning of the CBCT devices. The tests have been limited to image quality and dosimetric checks, which can be easily (and thus often) performed by technicians and physicists with a minimum of experience anywhere in the world. They provide a means to evaluate the whole imaging chain with a minimum effort. If the dose or the image quality deviate from expected values, or exceed the action levels, the support from a service engineer or a more time-consuming analysis of the device is required.

Purpose

The purpose of this document is to present an objective, practical and unifying procedure for quality control of CBCT. This includes CBCT for dental, radiotherapy, interventional radiology and guided surgery applications. Simplicity in terminology and methodology has been favoured in every occasion where different but equivalent terms or methods were available. The proposed tools and procedures aim to simplify the work of professionals involved in the quality control of CBCT, but they may also satisfy the research interest of many physicists in objective comparisons among different technologies[17-21]. Finally, consensus among the group and with existing national and international guidelines has been pursued to define action levels for the different technologies.

Structure

Previous work related to CBCT devices is outlined in chapter 2, together with short descriptions and references to perform conventional tests that are necessary, but not specific, for CBCT.

Chapter 3 describes the image quality test parameters. Each section provides a definition and an explanation for the need to perform the test. Afterwards, the recommended methods to measure this parameter are described in detail, and action levels are suggested. Several phantoms that enable the recommended tests to be performed are presented in chapter 4.

Two alternative solutions for radiation dosimetry for quality control are described in chapter 5.

The appendix contains important remarks that are not necessarily part of the quality controls described in this document.

British spelling has been substituted by US spelling in the cases where the word is literally contained in software from the US (such as “analyze” within ImageJ).

CHAPTER 2

Review of Previous Work

CHAPTER 2

Review of previous work

The ICRP publication 129 Radiological protection in cone beam computed tomography (CBCT)[22] constitutes the most recent international effort to provide recommendations for quality control of CBCT devices. However, the recommendations are focused on the measurement of dose and they only briefly mention measurements of image quality.

Action levels for CBCT image quality parameters can be found in the recent European Criteria for acceptability of medical radiological equipment used in diagnostic radiology, nuclear medicine and radiotherapy[3]. However, this document only refers to dental applications of CBCT and does not go into detail.

The most recent and practical guidelines, directed to the end users of dental CBCT, are the work of German and British institutions, as well as the evidence based guidelines of the European Union[8,9,10].

The German standard DIN 6868-16110 Acceptance testing of dental radiographic equipment for digital cone beam computed tomography and its complementary DIN 6868-1523 provide a complete and detailed method for acceptance and constancy tests in dental CBCT applications. The method focuses on objective image quality and point dose measurements.

The British guidelines Guidance on the safe use of dental CBCT equipment[9] include some detail about image quality and dose measurements, but it focuses on a comprehensive approach to all aspects related to handling CBCT devices.

The European document: Cone beam CT for dental and maxillofacial radiology. Evidence based guidelines8 also provides comprehensive recommendations that are useful for handling CBCT devices. In terms of image quality, this document focuses on the use of one single phantom for image quality measurements.

Regarding applications of CBCT to radiotherapy, the French guideline Radiothérapie guidée par l'image - contrôle de qualité des équipements à rayons X - Rapport SFPM N° 29[24] summarizes the different controls in tables. The controls are presented and adapted according to the different manufacturers and the frequencies are adapted to the clinical routine. Other useful information is given in the AAPM guideline Quality assurance for image-guided radiation therapy utilizing CT-based technologies[25].

Regarding applications of CBCT to interventional radiology, angiography and guided surgery then to the authors1 best knowledge there is no information apart from the research work indicated in the corresponding sections of this work.

The recent publication by IAEA, Diagnostic radiology physics: a handbook for teachers and students[2] is recommended for giving general information about the concepts that are handled in these guidelines.

2.1 | Conventional tests

This section includes short descriptions and advice for finding references describing additional, conventional tests that are not specific to CBCT technology. These recommendations do not supersede existing national regulations.

X-ray tube potential

Using a digital kV meter, the x-ray tube potential over a range of values that contain all the clinically used kV settings is measured and must be within ±5 kilovolts or ±10 percent, whichever is greater, of the indicated value[8,26,27,28].

X-ray tube leakage

Using a suitable leakage detector, the air kerma from leakage at 1m from the focal spot can be measured. This must be done at every rating specified by the manufacturer, averaged over an area not bigger than 100 cm^2 and must not exceed 1 mGy/h[26,27,29]. A comprehensive description of the test can be found in references 8 and 30.

Total Filtration

Using a suitable meter of half-value layer (HVL) or aluminium filters, the equivalent aluminium HVL is measured for a range of x-ray tube potentials and is used to determine the total beam filtration[26, 27]. Alternatively, you can also use a suitable meter that directly measures total beam filtration. The total filtration should be equivalent to at least 2.5 mm Al. More information can be found in references 8 and 30.

Repeatability of radiation output

Using a radiation dosimeter, the consistency of the radiation output for at least three exposures using constant exposure parameters is found[26,27]. The calculated coefficient of variation must be less than or equal to 5 %[30]. Using a multifunction meter, the consistency of the x-ray tube potential and the exposure time can be verified[8].

Reproducibility of radiation output

This test monitors the effect that x-ray tube potential, current and exposure time have on radiation output[7]. Using a radiation dosimeter, measurements of radiation output are made at a range of x-ray tube potentials and at a range of clinically used current-exposure time product (mAs) settings[8]. The calculated coefficient of variation must be less than or equal to 10 %[31].

Beam collimation

Citing reference 2, "limiting the radiation field to the area of interest will both reduce the radiation risk and improve image quality (as, for a smaller irradiated volume, less scattered radiation will reach the image detector)". In CBCT it is particularly important to check that the radiation field is not larger than the dimensions of the detector. Fluorescent screens, film or the recently developed electronic x-ray ruler can be used for this purpose, the same way they have been used in the past to check proper collimation in mammography, tomosynthesis or fluoroscopy[32].

Using these tools, the decay of the x-ray intensity along the field edge (beam penumbra) is measured. The position at which the intensity decays to one half of its maximum is assumed to be the actual position of the edge. This position should ideally not deviate from the expected beam edge by more than 2 % of the focus-to-detector distance (FDD). However, a larger deviation is acceptable if the total deviation (of all four edges) is not larger than 4 % of the FDD. Image slice thickness / Resolution in the z-direction

A test phantom with inclined plates is needed in order to measure the profile of the z-sensitivity over a representative sample of clinically used slice thicknesses. The measured value must be within ±1 mm or ±20 percent, whichever is the greater, of the indicated value[26,27].
Equivalently a measurement of the spatial resolution in the z axis may be performed (See end of section 3.6).

Image display

Quality control for image displays is explained in detail in guidelines for mammography, such as the recent EFOMP guidelines33. As a practical rule, the room illumination hitting the monitor should be between 20 and 60 lux.

In addition, the luminance from a purely white screen in the monitor should be above 200 cd/m^2. If this value is between 350 and 500 cd/m^{2}one should make sure that this strong luminance is not uncomfortable for the radiologists.

Image artefacts

The absence of strong artefacts should be regularly checked in all kinds of x-ray devices. Some tests described in this guideline, such as the uniformity test of section 3.1., will help to detect cupping artefacts. However, ring and crescent artefacts may not be detected by the described tests. For this reason, an additional visual inspection of the images is recommended even if all the tests described in this guideline are passed.

A complete description of artefacts in CBCT, specifically focused on dental CBCT can be found in the appendix of reference 10. A short description of artefacts in computed tomography can be found in section 11.6.4 of reference 2. A detailed description of artefacts in tomography, including CBCT, can be found in reference 34.

Operator protection

Operator doses should be as low as reasonably achievable (ALARA). The radiation protection requirements should be assessed by a radiation protection expert (such as a radiation protection adviser in the UK, Sachverständige in Germany or unidad técnica de protección radiológica (UTPR) in Spain). Measurements made during installation to confirm adequate protection must be provided[30,35].

CHAPTER 3

Image Quality Parameters

CHAPTER 3

Image Quality Parameters

Introduction

The following parameters have been selected for image quality control of CBCT devices: uniformity, voxel density values, geometry evaluation, noise, low-contrast resolution and spatial (high-contrast) resolution. Each one of them is explained in this chapter. Practical hints to measure and evaluate them, as well as recommended test frequencies, are given. Although monthly tests would be desirable for all modalities, in general test frequencies and action levels are stricter for radiotherapy applications. This is because the CBCT images are often used in the context of image guided radiotherapy (IGRT) to aid the accuracy of the delivery (patient/tumour positioning before the delivery and/or within treatment fractions) and can be used sometimes to (re-)plan a treatment in adaptive radiotherapy (ART).

If additional or more frequent tests are recommended by the manufacturer these should also be undertaken.

3.1 | Uniformity

Introduction

Ideally the images should show the same quality across the whole of the image and therefore, testing the uniformity is an essential quality control test. A lack of uniformity is usually unavoidable though, especially because of the heel effect (see 5.3.3 in reference 18) but also due to the detector (see 4.5.2. in reference 18) and, specifically for tomographic modalities, due to beam hardening and other artefacts (see 11.2.1. and 11.6.4. in reference 2). This section presents methods to objectively quantify uniformity.

Definition

Uniformity is a measure of the CBCT scanner´s ability to produce an image of a homogeneous object with mean pixel values that do not depend on the position of the pixel.

Purpose

Checking the axial uniformity regularly is one of the simplest methods to make sure that there are no functional errors (appearing as artefacts) affecting the reconstruction. In particular, for all applications (e.g. radiotherapy) that rely on quantitative measurements in the image (e.g., mean Hounsfield value in a region of interest, ROI, drawn inside a pathological structure) the uniformity is a crucial parameter.

Equipment

For this test one phantom is strictly needed: a head phantom (diameter approximately 16 cm). Although an additional Teflon ring can be used to simulate the cranial bone, especially for brain studies, its use is not necessary for the purpose of QC. In the case of a device being used also for body scans, a body phantom (diameter approximately 32 cm) is recommended to check the body imaging protocols (for example in radiotherapy CBCT).

Both phantoms should be cylindrical, homogeneous and ideally made of water (in this case distilled water is recommended), but any plastic material that will produce images with mean Hounsfield values (for medical CT scanners) between -50 and +50 HU may also be used.

The length of the phantom (in the z-direction), for constancy tests, should be at least 2 cm. For absolute measurements and inter-device comparisons, this length should be at least two times the maximum extension of the x-ray beam in the z-direction at the isocentre.

Test frequency

In radiotherapy, the uniformity test should be performed at acceptance and once a month afterwards. The frequency could be reduced to every 4 months after stability has been demonstrated. In addition, the test should be performed after a breakdown of the system.
For dental and interventional radiology applications, annual tests are enough, but monthly tests are desirable.

Procedures

The phantom is centred at the isocentre. Images are acquired using the largest pixel size and tube current available. The most common value(s) of the tube voltage (kVp) should be used. A stack of images with a slice thickness of around 2 mm should be produced.

Then, one of the following two methods may be used to check the uniformity.

Procedure 1: xyz uniformity curves

Uniformity is evaluated in all images by placing five circular ROIs as indicated in figure 3.1.1. The diameter of each ROI should be approximately 20% of the diameter of the phantom. The peripheral ROIs should not be placed too close to the phantom edge, as this will affect the mean pixel value.

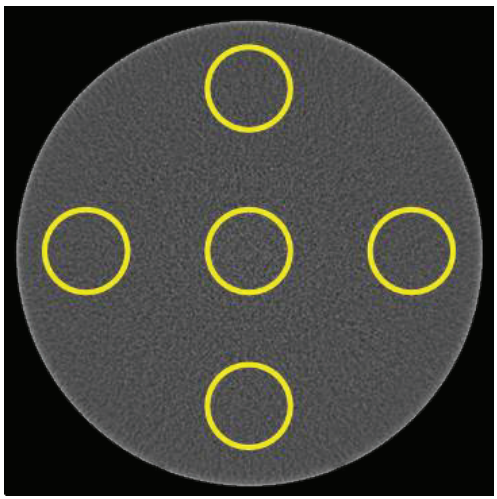

FIGURE 3.1.1. Position of the ROIs for the calculation of the uniformity.

The ROI values are plotted in a diagram as five curves with mean ROI values on the y-axis and z-coordinate on the x-axis. At acceptance, the values measured are used as baseline values for following QA procedures. Following any service change in the device that may affect the uniformity new baseline values should be produced.

Procedure 2: DIN method

The DIN standard describes an evaluation of the axial uniformity using the five ROIs shown in figure 3.1.1, but for a single axial image. The procedure can be summarized as follows[10]:

1. Obtain the mean pixel value of each ROI (centre, top, bottom, left and right).
2. Obtain the average, H_M, of the five values obtained in step 1.
3. Calculate the difference between H_M and each of the five values obtained in step 1.
4. Select the maximum of the five differences, D_{max}.
5. Obtain the uniformity, U, as

$$U = \frac{|P1\text{-}P2|}{D_{max}} \qquad [3.1.1.]$$

where |P1-P2| is the contrast between two materials (defined as part of the CNR in section 3.5). In the DIN standard those materials are PMMA and PVC.

The advantage of this procedure is that it is independent of the chosen scale range of the pixels in the evaluated systems (because D_{max} is normalized by the CNR). Although the DIN procedure does not evaluate the uniformity along the z axis, the proposed method can be repeated in different reconstruction slices to check the uniformity in other axial planes if desired.

The measurements can be performed in any workstation linked to the equipment without the need to extract the images. To perform the evaluation in external software (e.g., ImageJ) the DICOM image files need to be retrieved first.

Freeware tip: To measure average pixel values, as required to check the uniformity, the freeware ImageJ[40] can be used. For this purpose, open the desired DICOM image using the menu File -> Open, select the rectangular or the circular tool and draw an ROI in the desired position. To obtain the mean pixel value in that region, use the menu Analize -> Measure. A pop-up window containing a table of results will show the mean of the pixel values and the standard deviation in the columns "mean" and "StdDev".

If you wish to obtain the result of more parameters, use the menu within the pop-up window "Results -> Set measurements" and tick the box next to the values you would like to obtain. Click OK and repeat the measurement.

Action levels

For the results of procedure 1, the deviation from baseline values should not exceed ± 10 HU[18] in radiotherapy applications. For dental and interventional radiology applications, the action levels should follow manufacturer specifications. In any case, the uniformity should be below 10 % of the difference between the air and water-like regions.

Following procedure 2 (DIN method), the value of the uniformity should be above five[10] for all applications. This action level has proved reasonable for dental applications. In radiotherapy, this value might be too lax for images used for dose calculations (currently under research), so it should be revised once evidence has been collected from practice.

3.2 | Geometrical accuracy

Introduction

The value of CBCT relies on its ability to produce a three-dimensional description of the anatomy of the patients. In this respect, it is essential that the relative spatial relationship of the internal structures in the image is representative of the imaged structures, and that the image is rigidly related to the coordinate system of the machine. The latter aspect is especially important for radiotherapy applications, where mismatches between the imaging isocentre and the treatment isocentre must be avoided in order to ensure that the strict positioning requirements are met. Both mechanical sag and flex of the CBCT arms, and limitations of the reconstruction algorithms, are responsible for limitations of the geometrical accuracy of CBCT images. Therefore, it is essential to regularly check the geometrical calibration of the CBCT.

In general, two features must be checked to evaluate the geometrical stability of the CBCT equipment: the geometrical accuracy, i.e., that the positioning of the movable components is spatially reproducible, and that the linearity, i.e., the relative spatial relationship of the imaged structures, is reflected in the CBCT image. For the specific case of radiotherapy CBCT equipment, a further control that the image space obtained with the CBCT system is accurately related to the radiation beam geometry must also be included in the QC procedure.

Image reconstruction for CBCT is usually performed with 3D back-projection (Feldkamp[37]) methods that take into account the particulars of the imaging method, as opposed to conventional CT, where 2D back-projection is generally used.

The reconstruction algorithms generally perform well near the isocentre, but their accuracy usually decreases further away from the isocentre, and consequently distortions and resolution degradations can be expected in the longitudinal direction.

From this perspective, geometrical controls of linearity should be performed in several regions of the reconstructed image, in the transversal plane as well as in the direction parallel to the rotation axis. By extending these considerations, HU constancy (see section 3.3.) should be checked in several regions in the reconstructed image and the performance of the algorithm should also be checked for small and large phantoms.

Definitions

Geometrical accuracy: the movable components are spatially reproducible.

Linearity: the relative spatial relationship of the imaged structures is linearly reflected in the CBCT image.
Spatial stability (for radiotherapy equipment): the image space obtained with the CBCT system is rigidly related to the radiation beam geometry.

Purpose

The purpose of the test is to monitor the geometrical accuracy and the linearity of the CBCT image. For radiotherapy, a further test is recommended aimed at monitoring the position of the imaging isocentre in relation to the treatment isocentre.

Equipment

Geometric accuracy is checked using dedicated phantoms with embedded ball bearings or other bead structures. To check linearity, phantoms with known internal structures or grids are required. Dedicated phantoms are necessary to check for spatial stability.

Test frequency

In radiotherapy, at least monthly checks are recommended after acceptance, but the frequency could be reduced after stability has been demonstrated. The recommended frequencies of the controls from the manufacturers for the verification and recalibration of the imaging systems should also be followed, unless studies have been performed showing that these frequencies can safely be reduced (see references 25, 38 and 39).

The coincidence of the treatment and imaging isocentres should be checked daily either with planar imaging or with CBCT. The frequency of the CBCT controls could be adapted according to the complexity of the treatment techniques used and the weight of CBCT for image guidance.

For dental and interventional radiology applications, annual tests are enough if no upgrade of the system has occurred, but monthly tests are desirable.

Procedures

Imaging a phantom with several structures with known dimensions can be used to check the linearity performance of the CBCT equipment (see an example in Figure 3.2.1). Grid phantoms would probably offer the best means to perform linearity checks both in the transversal plane, as well as in the axial plane, as part of the QA program.

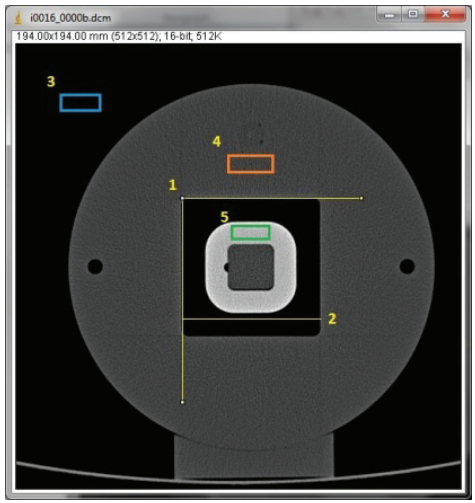

FIGURE 3.2.1.Illustration of geometrical measurements on a phantom. The 90-degree angle (1) and the 60 mm-side of the air gap (2) can be used to check the linearity in the xy-plane.

Freeware tip: To measure angles and distances in the DICOM image, the freeware ImageJ[40] can be used. For this purpose, select the straight line or the angle tool, click on the image object that you want to measure (see Figure 3.2.1) and select "measure" on the Analyze menu. A pop-up window containing a table of results will show the values of the angle and/or the length on the right columns.

The geometrical stability of the CBCT systems is usually checked with a variation of the Winston-Lutz procedure from stereotactic radiosurgery[41]. The procedure involves the placing of a bead near the mechanical isocentre of the CBCT system and comparing the positions of the sphere on the imaging device relative to the position of the image centroid for several projection angles. The apparent movement of the image of the ball on the projection images used for reconstruction provides a measure of the mechanical movement (sag and flex) of the CBCT components as a function of the projection angle[42,43]. The plot of the distance between the projected isocentre and the nominal isocentre is known as a flexmap and could be used to correct for mechanical imperfections of the CBCT system. Flexmap corrections remove the blur in the images due to mechanical imperfections. Special phantoms and methods based on this test have been reported in references [44, 45 and 46].

Several options for phantoms and methods are available for checking the agreement between imaging and treatment isocentre for radiotherapy CBCT. These range from in-house developments to manufacturer specific recommendations like the Penta-Guide[47] used by Elekta and IsoCal used by Varian (Figure 3.2.2). The performance recommendations, however, would vary depending on the intended use of the CBCT imaging. Thus, a stricter tolerance should be required for treatment platforms delivering stereotactic treatments[38,48].

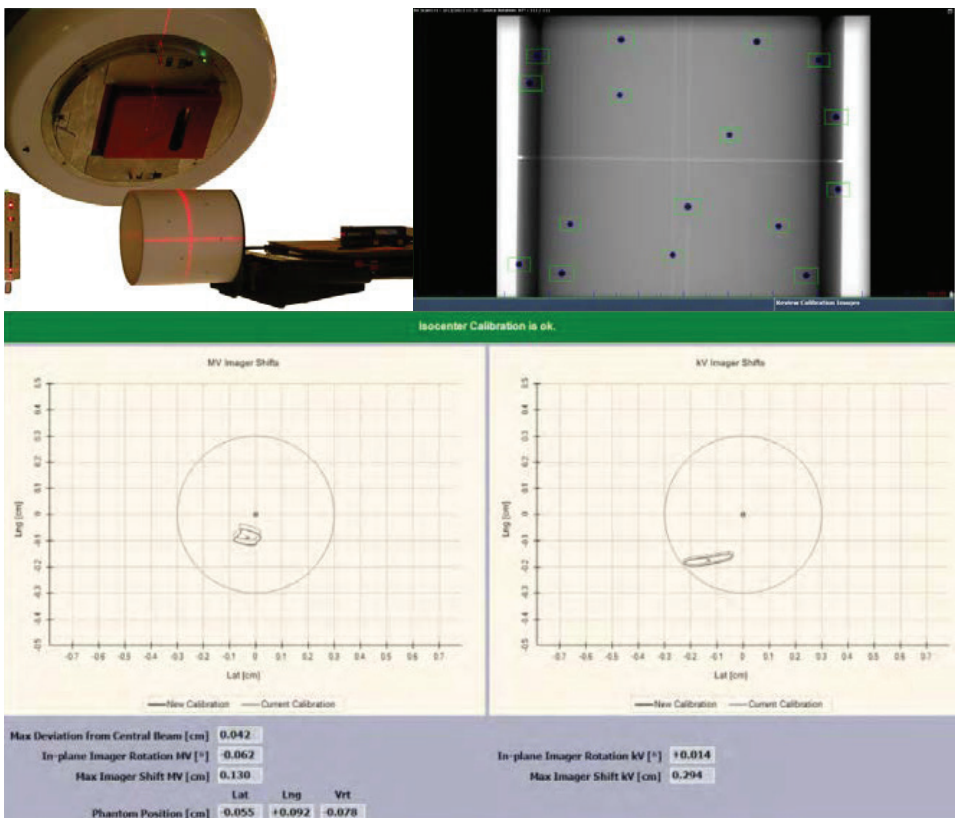

FIGURE 3.2.2.Set-up (upper left), phantom image (upper right) and software interface (bottom) used on Varian accelerators to check the agreement between treatment and imaging isocentres (reproduced with permission from Varian Medical Systems).

Action levels

For radiotherapy applications, TG142[38] recommends tolerances better than 2 mm for conventional treatments and better than 1 mm for stereotactic radiosurgery or stereotactic body radiotherapy (SRS/SBRT), both for geometrical scaling and for imaging and treatment coordinate coincidence.

UK[9] and SEDENTEXCT[8] guidelines have a tolerance of 0.5 mm for linearity in dental CBCT devices. A value of 1 mm is suggested in this document because it is difficult to ensure an uncertainty below 0.5 mm in this kind of measurement. For interventional radiology applications, a tolerance of 2 mm should be applied if there are no stricter indications from the manufacturer.

The DIN standard for dental CBCT[10] does not explicitly mention the test of geometrical precision. It is nevertheless included in the test for "spatial resolution of the reconstruction". In this test, the Nyquist frequency FN of the reconstruction is calculated from the known thickness of a highly attenuating object. Comparing the result with the actual pixel size provides an objective method to check linearity. Spatial stability (required for radiotherapy) and geometrical accuracy are part of the "visual and functionality tests", also included in the DIN standard. The geometrical definition of the DIN phantom allows for further software analysis of geometrical distortion. These are not mandatory for acceptance and constancy test of dental equipment to keep the efforts in a reasonable range.

3.3 | Voxel density values

Introduction

Voxel density values describe the different x-ray attenuation properties of matter in a tomographic image. The more radiodense the material is in the image, the higher is the voxel density value.

It is important to be able to distinguish between the different densities of materials in a radiographic image, in order to perform accurate clinical diagnoses. Accurately relating physical density to voxel density values is particularly important when these values are used to perform a clinical diagnosis, such as assessing bone density. It is also essential to accurately relate the voxel density (in Hounsfield units) to the electron density of the material if the CBCT images are used to perform dose computations in adaptive radiotherapy, which is currently an active area of research. To this respect, a robust method could be to segment and assign bulk densities (see for example reference 49).

The relationship between physical (or electron) density and voxel density values can be influenced by many different factors:

- Scattered radiation in the image, caused by x-rays being scattered from the patient and the detector, which can artificially increase or decrease the voxel density.
- Beam hardening, resulting in the central part of dense objects being effectively subject to harder x-rays than the periphery, hence the object appears as if it were less radiodense at the centre (cupping artefact).
- The presence of very high density materials (e.g. a tooth implant), causing the x-ray beam to be almost fully attenuated, which leads to dark streaks being visible on the image.

- The whole patient not being contained within the field of view, which can yield changes in voxel values. The image reconstruction process assumes that all the x-ray attenuation occurs within the imaging volume, therefore when part of the patient is outside the image volume (the part outside the image volume is referred to as the exomass) voxel densities values will be altered. This is particularly applicable to dental CBCT where only a small part of the patient's jaw is contained within the field of view (FOV) and the majority of the patient is outside.
- The version of the imaging software that is being used.

Definition

Radiodensity values are typically defined using Hounsfield units (HU). This scale was originally defined for conventional computed tomography but the same principles apply for CBCT.

The HU scale is related to the linear attenuation coefficient of a material, where water is defined with a HU of 0 and air with a HU of -1000. Materials are then assigned a HU value based on the following formula:

$$HU = 1000 \times \frac{\mu_{\chi} - \mu_{water}}{\mu_{water} - \mu_{air}} \qquad [3.3.1.]$$

where μ_x is the linear attenuation coefficient of the material in question and μ_{water} and μ_{air} are the linear attenuation coefficients of water and air, respectively. It is important to note that some CBCT units, especially many dental CBCT units, do not use the HU scale and instead just report a greyscale value. Greyscale values are assigned during the image reconstruction process such that, usually, a value of 0 is the lowest image density (e.g. air) up to a maximum greyscale value (usually between 2^{10} [1024] and 2^{16} [65536] depending on the particular machine) of a very radiodense material.

Purpose

The purpose of this test is to check whether the system is able to reproduce the voxel density values that are expected for the given materials. If the system does not claim conformity with the HU scale the purpose of this test is just to check that the density values assigned to a certain material do not deviate from the baseline values.

Equipment

A test phantom containing a number of materials of varying densities is required. Ideally, these materials should cover the whole range of densities likely to be seen in clinical practice and should include the two standard materials of the HU scale, air and water (or a water-equivalent solid material). An example of such a phantom for dental applications is shown in Figure 3.3.1.

FIGURE 3.3.1. Example of a voxel density value phantom used for dental CBCT containing air, low-density polyethylene (LDPE), Teflon and acrylic inserts.

Test Frequency

Voxel density values should be measured at commissioning of the x-ray set, after any major maintenance (including software upgrades) and as part of the routine QA programme at the following frequencies: in dental and interventional radiology, the tests should be performed at least annually. In radiation therapy, a monthly frequency is recommended. If any software upgrades have been carried out, this may affect the calibration between physical density and voxel values, in which case new baseline values would need to be established.

Procedure

An axial slice should be selected in the image, and voxel density values from each material in the test phantom should be measured. The reported values for this test should always include the mean and standard deviation

Freeware tip: You can use free software like ImageJ[40] to measure the voxel density values. For this purpose open the axial slice containing the materials, select the rectangular or the oval tool and draw a region of interest containing at least 30 pixels corresponding to one single material and avoiding the edges (See figure 3.3.2 below). To measure the density value, click on "Measure" under the "Analyze" menu (or use the key shortcut CTRL+m). The average voxel density value (in the scale of Hounsfield units or in the scale chosen by the manufacturer) appears in the column "Mean". The standard deviation appears in the column "StdDev".
If the value of the standard deviation does not appear in the results pop-up window, go to "Results -> Set measurements" and tick the box next to "standard deviation". Click OK and repeat the measurement.

The average voxel density in the material should be compared to reference values. An example image of a test phantom is shown in figure 3.3.2.

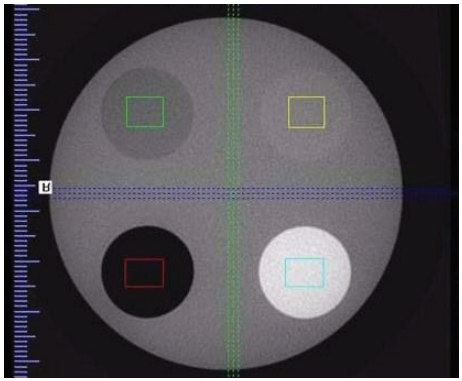

FIGURE 3.3.2.An axial slice view of the voxel density value phantom shown in figure 3.3.1.

It is essential to position the test phantom exactly in the same way during the constancy tests, because the relative contribution of factors affecting density values could change significantly for different positions of the phantom. For the same reason all the exposure parameters must be kept constant for periodic tests, and the ROI measurements must be performed using the same slice. The test phantom should ideally have a smaller diameter than the imaging FOV to remove issues associated with the exomass.

Action levels

The requirement for voxel density values should be a certain tolerance on the expected voxel value. As a minimum this should include values for air and water. If images are not calibrated to the HU scale then the requirement should be a certain tolerance from reference grey scale values, which should be reported by the equipment manufacturer as part of the equipment performance specification.

Acceptable requirements will depend on the particular application. When measurements of physical density are used in clinical practice, very accurate results are required. Suggested action levels are presented hereafter.

For dental applications, if the manufacturer does not specify any level, the action level is any density value that deviates from the baseline measurement by more than 25% of the difference between the values for water and air. For example, if the density value of air was -1000 and the value for water was 0, the applicable action level would be greater than ± 250.

In interventional radiology applications, as well as in radiotherapy if images are used for dose calculations, an action level of ± 50 HU from the baseline value[24] is recommended as a minimum requirement. However, it must be noted that dose calculation is still being a research topic and it is not implemented in the clinical routine.

The authors of this section would like to acknowledge the information obtained from the following sources, although they are not specifically cited in this section:

1. Bryant JA, Drage NA, Richmond S. Study of the scan uniformity from an i-CAT cone beam computed tomography dental imaging system. DentomaxillofacRadiol. 2008 Oct;37(7):365-374.
2. Katsumata A, Hirukawa A, Okumura S, Naitoh M, Fujishita M, Ariji E, Langlais RP. Relationship between density variability and imaging volume size in cone-beam computerized tomographic scanning of the maxillofacial region: an in vitro study. Oral Surg Oral Med Oral Pathol Oral RadiolEndod. 2009 Mar;107(3):420-5.
3. Mah P, Reeves TE, McDavid WD. Deriving Hounsfield units using grey levels in cone beam computed tomography. DentomaxillofacRadiol. 2010 Sep;39(6):323-35.
4. Molteni R. Prospects and challenges of rendering tissue density in Hounsfield units for cone beam computed tomography. Oral Surg Oral Med Oral Pathol Oral Radiol. 2013 Jul;116(1):105-19.
5. Nackaerts O, Maes F, Yan H, Couto Souza P, Pauwels R, Jacobs R. Analysis of intensity variability in multislice and cone beam computed tomography. Clin Oral Implants Res. 2011 Aug;22(8):873-9.
6. Rong Y, Smilowitz J, Tewatia D, Tomé WA and Paliwal B. Dose calculation on kV CBCT images: an investigation of the Hu-density conversion stability and dose accuracy using the site-specific calibration. Med Dosim. 2010; 35(3):195-207.

3.4 | Noise

Introduction

Image noise refers to the fluctuations in pixel values in the image that can mask lesions or structures of interest, interfering with detection or diagnostic tasks.

Noise has three main contributions:

1. **Electronic noise** is the signal captured by a system in the absence of x-ray exposure. It can be related to dark currents inside the circuits or to the mechanism of image acquisition electronics. It represents a constant contribution to the variance of the pixel values. It can be reduced improving circuit and detectors design or with appropriate cooling systems in the detectors.

2. **Quantum noise** represents the pixel variations associated to the stochastic nature of radiation and can be modelled using a Poisson distribution. This is the most important contribution to noise in terms of quality control.

3. **Structural noise** represents the objects or structures in the image that can be confounded with the target that is being looked for in the image, such as a lesion or tumour. If these structures are related to anatomical parts, one of the possible solutions is image subtraction or selecting the appropriate acquisition and reconstruction parameters to enhance the pixel value differences between lesions and their surroundings. Some artefacts can be regarded as structural noise.

Many acquisition and reconstruction parameters can be tuned to reduce image noise. For example, in CBCT applied to radiotherapy or conventional CT, different kV or mAs values can be selected depending on the patient characteristics or medical indication. Figure 3.4.1 depicts the effect of changing the mAs in image noise for the low contrast module of a phantom and how the visibility of the objects improves as the noise decreases. Image noise decreases with the square root of mAs.

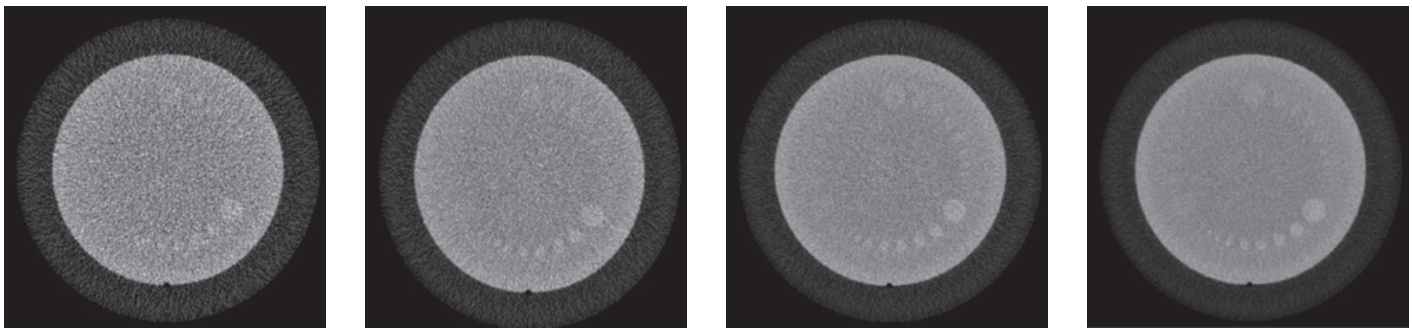

$CTDI_{vol}$= 5.7 mGy
Pixel noise = 8.6 HU

$CTDI_{vol}$= 11.3mGy
Pixel noise = 5.9 HU

$CTDI_{vol}$= 22.6 mGy
Pixel noise = 3.9 HU

$CTDI_{vol}$= 49.4 mGy
Pixel noise = 2.8 HU

FIGURE 3.4.1. Images of a phantom acquired varying the tube current (50, 100, 200, 400 mAs from left to right), corresponding to the indicated values of CT dose index (CTDIvol, see appendix 3).

A high noise level in the images is related to inconsistent attenuation values in the projection images, affecting the uniformity of regions that correspond to the same tissue in the patient. This can produce artefacts in the reconstructed volume[50].

The acceptable noise level for CBCT dedicated to dentistry devices is normally higher than in conventional CT or other CBCT applications, because the high contrast between the studied tissues (teeth, bones and soft tissue) cancels out the effect of the high noise. See figure 3.4.2. for an example.

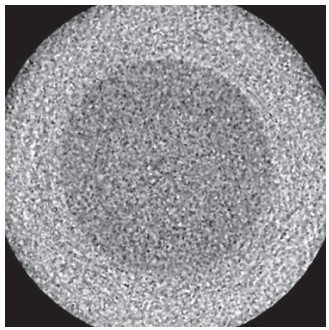

FIGURE 3.4.2.Example of an acceptable level of noise in dental CBCT (see "action levels" below). The image corresponds to a small field of view obtained from a homogeneous PMMA phantom.

Definition

The image noise corresponds to fluctuations in the values of the individual pixels inside a region of interest (ROI) in the image of a homogeneous phantom.

Purpose

The purpose of this measurement is to ensure that the level of noise in the images is not too high, and thus the visibility of structures or lesions is not compromised. A measurement of noise is also a simple method to detect failures in the performance of the x-ray device, by comparing the values with a performance baseline.

Equipment

The same phantom used for the uniformity is required for this test.

Test Frequency

This test should be performed at acceptance, monthly, and after changes in the device. Depending on the work load and the use of the CBCT device, this frequency may be reduced to yearly tests. It may be performed as part of the measurement of contrast-to-noise ratio.

Procedure

Image noise is traditionally measured as the standard deviation of the pixel values within a ROI taken in the central region of a homogeneous section of a phantom, preferably equivalent in attenuation to water. The size of this ROI depends on the size of the phantom. If we take a too small ROI,the result may be affected by local inhomogeneity (in this case it is necessary to average the noise value between several slices, at least 5, see references 8 and 19). On the other hand, if the ROI is too big, the result may be affected by artefacts in the image. For this reason, the ROI should optimally be as large as possible taking care that no artefact is included.

Even if the ROI is large, it is recommended to measure noise in several consecutive axial slices, at least once during the acceptance test, to investigate the possible differences between different slices. These differences might arise during the acquisition and reconstruction process. At acceptance, a baseline has to be established to serve as a guide for future tests of the system.Note that if the difference between consecutive slices is lower than 20 %, it is enough to check the noise during constancy tests in one single slice.

Freeware tip: You can use the free software ImageJ[40] to perform the measurements of noise. For this purpose, select the rectangular or the oval tool, draw an ROI in the homogeneous portion of the phantom (see figure 3.4.4) and click "Measure" from the "Analyze" drop-down menu. If the value of the standard deviation does not appear in the results pop-up window, go to "Results -> Set measurements" and tick the box next to "standard deviation". Click OK and repeat the measurement. If a stack of images is available, noise can be measured with the plugin "Stacks->Measure Stack".

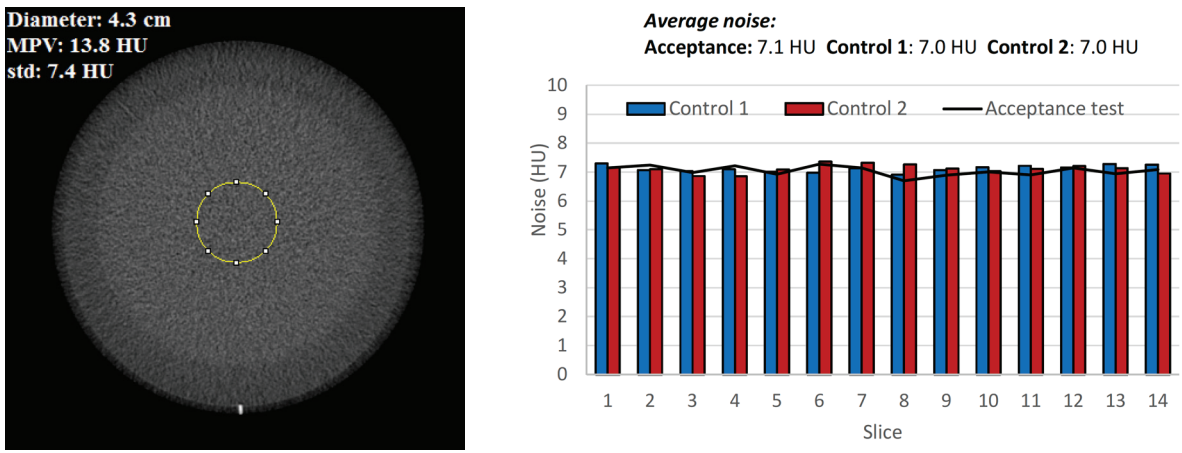

FIGURE 3.4.3. Left: Illustration of noise measurements in an image of a uniform phantom (acquired in a CT) used in radiotherapy selecting 120kV, 250 mAs, filter B and 2 mm as slice thickness). Image noise is 7.3 HU or 0.7% (mean pixel value for air = -1002 HU, mean pixel value of the background module = 14 HU). On the right, noise measurements in different controls for the same abdomen protocol for this unit are shown.

Action levels

The measured image noise has to be within 20% of the reference value (baseline) for the reference protocols. Image noise is sometimes expressed as a percentage, dividing the statistical deviation by the difference in HU between the phantom material and air. It should be noted that, as many reconstruction and acquisition parameters affect image noise, this value should always be given together with the information related to the selected protocol in the acquisition as a reference (figure 3.4.3.).

Due to the fact that the actual factor affecting detectability is the relation between the contrast of a signal and the surrounding noise (or the contrast-to-noise ratio), the German standard DIN 6868-161[10] foresees the measurement of noise only as an intermediate step to calculate the contrast-to-noise ratio. The corresponding action levels are thus defined for the contrast-to-noise ratio indicator (See section 3.5).

Optional Procedure: Calculation of noise power spectrum (NPS)

The noise power spectrum (NPS) is a Fourier tool that shows the amount of each noise frequency present in a certain ROI. The integral of this spectrum gives the standard deviation. The NPS can be considered as a second level check when other results are inconsistent and there is no obvious explanation.

The NPS can be very useful for studying reconstruction algorithms or other parameters that influence the performance of small object detection of any x-ray device. Therefore, the NPS is included, for example, in the calculation of DQE (detective quantum efficiency). However, it is very difficult to come up with an easy method that enables a quantitative evaluation of NPS and the definition of consequent acceptance thresholds. For this reason, the NPS is not recommended for routine quality control. In spite of that, the NPS is recommended for optionally comparing the structure of the noise in different systems. For this purpose, a specific macro in the free software ImageJ[40,52] has been created and is explained here.

Freeware tip: You can qualitatively analyse the NPS using ImageJ. For this purpose, open one slice corresponding to the reconstruction of a uniform portion of a phantom. Select an ROI inside this uniform portion of the phantom (avoid the edges of the container). In the main menu of ImageJ, click Process > FFT > FFT.

For quantitative, more detailed analysis of the NPS, a specific macro for the free software ImageJ[40,52] has been created and is found in appendix 5.The macro runs over a stack of tomographic images of a uniform phantom, and it computes the average 2-dimensional NPS of the images in the stack. In order to run the macro, the user needs to download the macro, open ImageJ, open the image stack and run the macro using the command "Plugins/Macro/Run" and selecting the location of the macro.

The macro returns the NPS obtained averaging the NPSs of all the images in the stack. The resulting NPS contains all noise sources: random noise and structural noise. The NPS is a 2-dimensional function as presented in Figure 3.4.4. If the 2-dimensional NPS has rotational symmetry a 1-dimensional NPS, as a function of the spatial frequency r = (u2 + v2)1/2, can be obtained performing an average radial profile[53], as presented in Figure 3.4.5.

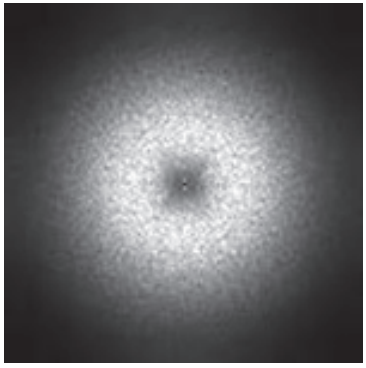

FIGURE 3.4.4.Two-dimensional NPS

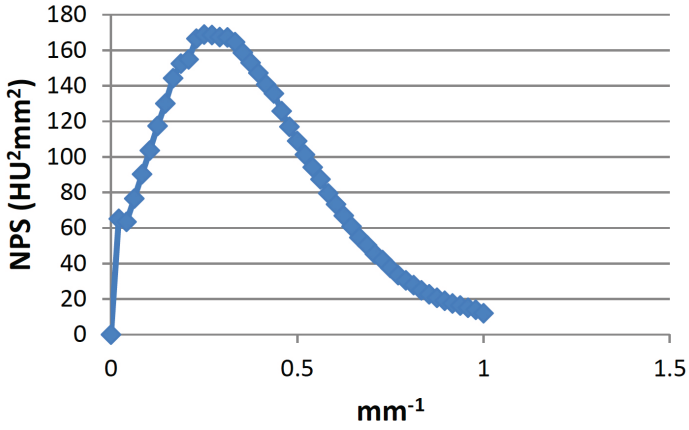

FIGURE 3.4.5 One-dimensional NPS obtained from the average radial profiles of the 2-dimensional NPS.

One can also subtract pairs of images acquired in the same conditions so that the noise structural component is removed in the subtracted image. In this case, the macro will return an NPS containing only the random noise contribution. The resulting NPS should be divided by 2 because we do not want to count the random noise twice (there are two random contributions in the subtracted image).

Finally, the random contribution of noise can be removed by averaging many images acquired in the same conditions. The NPS of the average image contains the structural noise contribution almost exclusively.

Another option is to compute the 3-dimensional NPS of the volumetric images provided by a CBCT. In this case one can use the FFTJ plugin[54] that runs over volumetric images (stacks are interpreted as a volume). One can inspect the resulting 3-dimensional NPS using an ImageJ 3D viewer[55].

3.5 | Low-contrast resolution

Introduction

The traditional method to evaluate low-contrast resolution is based on detecting subtle signals within a noisy background. The drawback of this method is that it is highly subjective. Different observers, and even the same observer on different occasions, can give different results when they are presented the same signals[56]. Although costly human observer studies are valid under certain circumstances of performance, the results can be biased and/or be difficult to reproduce. Thus, substituting subjective methods for objective techniques is a high priority when determining procedures for radiology image quality assurance. This principal standpoint is shared by the authors of the recently published paper on image quality assessment (IQA) of CBCT devices[57].

For the evaluation of digital images, subjective methods have different sources of error (and probably an even greater potential for error) than they had for analogue x-ray film images. Aside from observer variability, the digital environment introduces a number of confounding factors that make subjective IQA very uncertain. Examples of such factors include variability due to:

- Condition, calibration, and settings of the viewing display
- Quality of the graphics card to which the display is connected
- Interaction of the viewing software with the graphics card
- Viewing conditions such as reflections on the display screen, the ratio of diffuse/specular light impinging on the display surface, and the ambient light level (illuminance) in the room.

Image quality assessment in digital radiology depends on the devices used to display images. One key issue for image quality control in the analogue era was daily sensitometry/densitometry measurements for monitoring the film development process in order to have a constant film response for a step-wedge image. Today, the quality of the viewing display is just as important as the quality of film development in the analogue era.

In this chapter and in appendix 6 we consider objective methods to measure low-contrast resolution, including contrast-to-noise ratio, contrast-detail tests and model observers.

It must be noted that objective methods do not take into account the whole imaging chain. This means that the computer will always produce the same result, even if the monitor is not working well, or if the illumination of the room is incorrect, or if the contrast window is wrongly set. Therefore, it is especially important to test these observing conditions separately.

Definition

The low-contrast resolution represents the ability to distinguish a signal against its background, when the value of the signal is similar to the value of the background. This ability can be quantified measuring the contrast-to-noise ratio (CNR), defined in the following.

The absolute contrast of a signal against a given background is the difference of the mean pixel values in each of these regions. The relative contrast is this signal difference normalized to either the background signal or to the sum of the signal and the background (see section 4.3.1 in reference 2). Instead of this normalization, in medical imaging it is common to divide the absolute contrast by the background noise to obtain the CNR (see equation 3.5.1).

Purpose

Tumours and other pathologies are most often composed of organic tissue that has some malignant behaviour. Therefore, the malignant tissue has almost the same characteristics as the background, in particular almost the same attenuation coefficient for x-rays. Also the different regions of the brain and the different organs in the abdomen have very similar attenuation properties. Being able to clearly define the boundaries of a tumour, or the boundaries between those different regions or organs, is critical in radiotherapy planning, for example, to avoid unnecessary irradiation of healthy tissue. For this reason, it is very important that x-ray systems can distinguish very similar tissues next to each other or, in other words, that they have a good low-contrast resolution.

In the particular case of CBCT, large beam collimations are associated with high levels of scatter radiation, with a consequent degradation of soft tissue distinction and loss in CNR[58]. Apart from that, low contrast resolution is linked to the patient dose and to the kilovoltage of the x-ray tube (see section 6.2.7.1. in reference 2 "Effect of tube voltage on contrast, noise and dose"). Therefore, observing the change of this parameter we can indirectly check if the x-ray tube is working properly, as well as detect changes in its performance.

Equipment

A phantom containing at least two structures: one signal and one background. The structures should be large enough to enable reproducible measurements of the mean pixel values, but small enough to fit both in the field of view of any CBCT system.

Test Frequency

Traditionally, this test is performed at least at acceptance and yearly. However, with the help of appropriate software, it can be easily performed every month. Frequently, objective tests enable the early detection of relevant changes in the performance of the x-ray tube. If a regular decrease (or increase) in the performance is detected, maintenance service should also be alerted.

Procedure

An objective option to assess low-contrast resolution is to fix a certain signal and background and measure the actual ratio between its contrast and the background noise (the CNR). The main advantage of this method is that it is easy and reproducible, because it is a simple mathematical calculation, and thus it is recommended for frequent constancy checks.

In the standard DIN 6868-161 for dental CBCT, for example, two contiguous regions of polymethylmetacrylate (PMMA), representing a background of soft tissue, and polyvinyl chloride (PVC), representing a bone signal, are used to calculate a contrast-to-noise indicatora. In general, the contrast between a signal and its background is divided by the noise in the background (or by the average of the noise in the two regions) to obtain the contrast-to-noise ratio (CNR),

$$CNR = \frac{|P_{PVC} - P_{PMMA}|}{\sigma_{PMMA}} \qquad [3.5.1.]$$

where P_{PVC} and P_{PMMA} are the average pixel values of an ROI chosen in the PVC and the PMMA regions of the phantom; and σ_{PMMA} is the corresponding standard deviation of the pixel value in the PMMA region, representing the background (see figure 3.5.1).

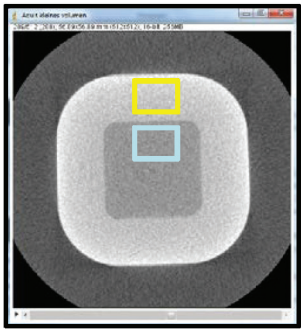

FIGURE. 3.5.1. Example of two ROIs chosen for the CNR calculation. In this example, the yellow and blue ROIs provide the mean and standard deviation corresponding to the signal and the background, respectively.

[a]In fact, the DIN standard 6868-161 describes a special algorithm to obtain P_{PMMA} and P_{PVC}, which is useful to take into account the edge enhancement performed in some reconstructions. However, this algorithm is not necessary for the calculation of a simple CNR as described here.

Freeware tip: To easily obtain the CNR using open source software like ImageJ follow the procedure below:

1. Open the image (File-open)
2. Click on the rectangle tool
3. Draw a region of interest (ROI) inside the signal (in the example above the signal would be the PVC)
4. Click on the menu Analyze->Measure (or press CTRL+M) to measure the mean (P_{PVC}) within that ROI.
5. Shift the region of interest (ROI) to the background (in the example above this would be the PMMA portion of the image)
6. Click CTRL + M again to measure the mean (P_{PMMA}) and standard deviation (σ_{PMMA}) within that ROI.
7. Copy and paste the results obtained in a spreadsheet or use a calculator to apply equation [3.5.1].

In appendix 6 we explain how to deal correctly with subjective methods and indicate two objective methods that are, unfortunately, more complex. They may become easier to apply as software develops and experience with them becomes more widespread. In this respect, an overview regarding iterative reconstruction is included in appendix 1.

Action levels

For constancy tests, the score of the low-contrast resolution should remain within 40 % of the value measured at the acceptance of the device. This large percentage takes into account the normal variability within the x-ray devices.
The action levels for acceptance tests are strongly dependent on the phantom that is used to test low-contrast resolution. The only official definition of a limiting value is given in reference 10, which states a minimum value of 100 for the so-called acceptance indicator (AI) for the case of contrast being measured between PVC and PMMA.

Action levels

This parameter combines the contrast-to-noise ratio CNR (see section 3.5), the dose quantity DFOV (free in air), as described in chapter 5, and the frequency at which the MTF falls to 50 % of its maximum F50 (See section 3.6),

$$AI = \frac{CNR}{D_{FOV}\left(\frac{1}{F_{50}}\right)^2} \qquad [3.5.2.]$$

The F_{50} (in line-pairs per millimeter) informs about the smallest size of low contrast objects that can still be adequately imaged by the x-ray device (see description of the modulation transfer function in the next section). This is thus an *objective* measure for low-contrast resolution. It upgrades the conventional methods based on subjective tests with low-contrast objects.

The threshold value of the acceptance indicator should be modified using long-term studies for CBCT applications in radiotherapy, interventional radiology and guided surgery and/or other materials, but the formula and its application are the same as in the example described here.

3.6 | Spatial resolution

Introduction

The relative high spatial resolution is one of the main advantages of CBCT methodology, and it is particularly important in dental clinical applications and peripheral vascular applications (see section 4.3). It is important to test it because its value depends on the technical characteristics of the equipment, such as focal spot dimension and detector performance, which could change over the time. In CBCT the voxel is usually isotropic, and as a consequence spatial resolution should be assessed along the three Cartesian axes, and similar values should be expected.

Spatial resolution is essentially affected by three scan parameters in CBCT:

- Field of view. Every CBCT has a limited number of available field of views, and each one is associated with a voxel dimension and a spatial resolution (eg. figure 3.6.1);
- Number of projection views. Different spatial resolutions could also be selected for different numbers of projection views, obtained for example by partial or full rotation scan or by different rotation times;
- Reconstruction algorithm. The choice of the convolution kernel for back projection methods or the kind of iterative approach affect the final spatial resolution and noise of the obtained image.

It is also important to underline that spatial resolution is not stationary inside a CBCT volume, as a consequence of the acquisition process and 3D back projection. MTF values at periphery of the volume could differ from that in the centre by about 20-30%[16,59].

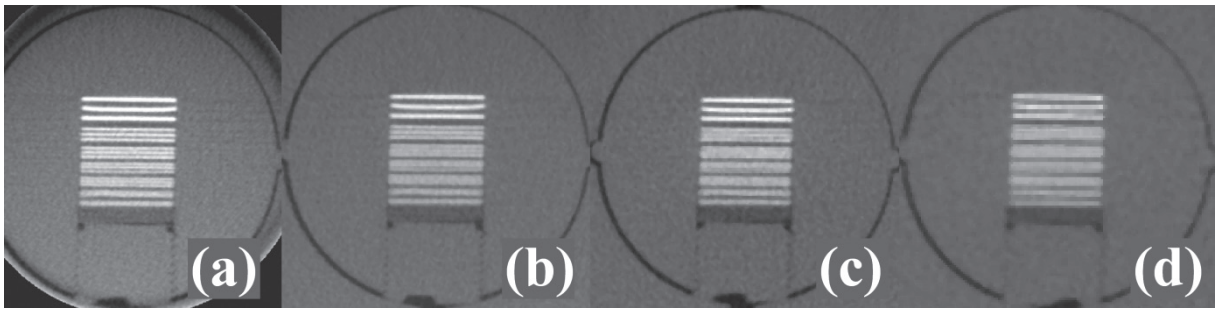

FIGURE. 3.6.1. Example of images acquired with the same dental CBCT equipment and different FOV and voxel size: (a) FOV 4x4 (diameter x height), voxel 80 µm (b) FOV 6x6, voxel 125 µm (c) FOV 8x8, voxel 160 µm (d) FOV 10x10, voxel 250 µm.

Definition

Spatial resolution refers to the size of the smallest object that can be resolved in a volumetric dataset resulting from a computed tomography acquisition. It is limited by voxel dimensions, but it does not coincide with it. It is usually expressed in terms of line pairs per centimetre (lp/cm), although recently, for high resolution CBCT, lp/mm are also often used.

It can be assessed by following two approaches:

- A subjective method, with the observation of a spatial resolution phantom with periodic pairs of high and low density materials representing different frequencies; the highest spatial frequency clearly resolved by the observer is assumed as the limiting resolution;

- A quantitative objective method, by evaluation of the modulation transfer function (MTF). More specifically, a spatial frequency value from the modulation transfer function should be used, and the limiting spatial resolution is usually associated with the 10% MTF value (F_{10}). Sometimes also the line-pair value corresponding to 50% of the MTF maximum (F_{50}) is indicated. Indeed the F_{10} informs of the smallest size of high contrast objects that can still be adequately imaged by the x-ray device. That is why it is often called "high-contrast resolution". Similarly, the F_{50} informs of the smallest size of low contrast objects that can still be adequately imaged by the x-ray device. That is why it is a measure for low-contrast resolution. Both values offer the advantages of quantified stable measures replacing all visual tests of high and low contrast resolution.

Purpose

The purpose of this test is to provide a quantitative spatial resolution evaluation and to verify that obtained values are consistent with baseline values measured during acceptance test or declared by manufacturers.

Equipment

For the MTF evaluation, a point or a wire or an edge could be used depending on phantom used. Test objects should allow a line or point spread function to be extracted along the three Cartesian axes, with an adequate oversampling to avoid aliasing effects. In particular problems are reported in literature with microbead phantoms[60,61], and these problems can be emphasized with fixed voxel and FOV dimensions of CBCT equipment. Methods with inclined wires[62] or foils[63] or edges[10] are preferable to achieve a correct line spread function. Evaluation based on a sphere phantom[16] has also been used recently, with the additional possibility to evaluate an edge profile along all directions.

It is important to stress that using an edge can introduce distortion of the edge spread function due to beam hardening, which will affect the MTF. Such problems are of no consequence when the high attenuating part is not too dense (and not a metal to avoid large artefacts), or when a point spread function is derived from a scan of a very thin wire (e.g. 0.1 mm diameter) of material with extremely high attenuation, such as tungsten. The wire should be suspended in air, so that a correction for beam hardening becomes unnecessary and a practically noise-free scan results.

Test Frequency

As in the case of the CNR test, this test is performed at least at acceptance and yearly. However, with the help of appropriate software, it can be easily performed every month.

Procedure

It is essential to position the test phantom exactly in the same way during the constancy tests, as a consequence of the spatial resolution location dependence inside the FOV previously described. High kV and mA values are preferable to limit the noise at minimum without affecting the resolution measurement.

To assess spatial resolution along longitudinal axis directions, images of a plane perpendicular to the axial plane should be used. It is advisable to check spatial resolution at least with two different exposure conditions, a standard approach and a high resolution modality (small FOV, maximum number of projection views, sharp kernel).

If a phantom with a wire is used, the wire should be orientated at a slight angle to all principal planes. Using data from several adjacent slices will result in an oversampling of point spread function data, which is needed for an adequate Gaussian fit in order to analytically generate the MTF (figure 3.6.2).

Freeware tip: there is no direct method to measure the MTF using ImageJ, although there are specific Plugins that can be used together with that software for this purpose. Instead of that, you can use the free software IQworks to measure the MTF (see appendix 4).

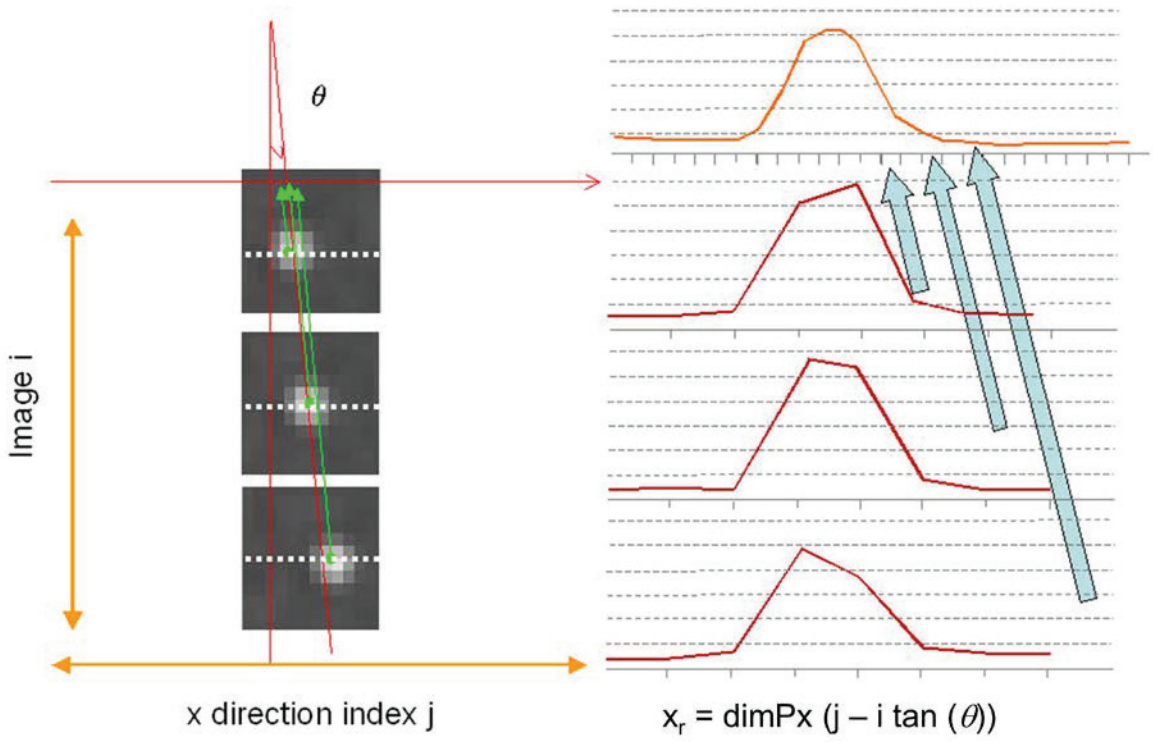

FIGURE 3.6.2 Example of resampling process of a point spread function derived from different slices of a wire. For each slice a profile is extracted, then the relative position xr of each profile value is recalculated considering the angle of the wire and in this way a resampled profile is obtained.

Action levels

Spatial resolution values measured during constancy tests should be within 20 % of the baseline values[64] (declared by the manufacturer or measured in the acceptance test).
For different clinical applications an absolute value of spatial resolution could be specified:

- for radiotherapy CBCT equipment, in the AAPM TG 179 report[25] a spatial resolution equal or greater than 5 lp/cm is required, considering that values reported in literature are in the range of 6-9 lp/cm;
- for dental CBCT a suspension level of 1 lp/mm (10 lp/cm) is reported for high resolution mode in the RP 162 document3. The same threshold (1 lp/mm) for the frequency corresponding to 10 % of the MTF maximum ($MTF_{10\%}$) in the transversal plane is reported in the standard DIN 6868-161[10] for acceptance tests. In addition, this reference states an action level of 100 for the value of the acceptance indicator, which includes the result from the MTF measurement.
- for interventional radiology and guided surgery applications currently there are no specific guidelines, but probably tolerance values similar to radiotherapy applications can be adopted.

As stated in the introduction, the measurement of spatial resolution in the z axis can be a substitute for the measurement of the image slice thickness. The measured value must also be within ±1 lp/mm or ±20 percent, whichever is the greater, of the value indicated by the manufacturer. Note that this equivalence is a suggestion of this report. No tolerances for the spatial resolution in the z axis have been published by the publication date of this report (Summer 2017).

3.7 | Summary table

<table>
<tr><th rowspan="2">Parameter</th><th rowspan="2">Procedures</th><th colspan="3">Frequency*</th><th colspan="3">Action level</th></tr>
<tr><th>Dental</th><th>Interven-tional radiology</th><th>Radio-therapy</th><th>Dental</th><th>Interven-tional radiology</th><th>Radio-therapy</th></tr>
<tr><td rowspan="2">3.1 Uniformity</td><td>XYZ uniformity curves</td><td colspan="2" rowspan="2">Annual</td><td rowspan="2">Monthly</td><td colspan="2">Manufacturer specifications, or > 10% difference air water</td><td>Deviation from baseline > 10 HU</td></tr>
<tr><td>DIN method</td><td colspan="3">Uniformity parameter U < 5</td></tr>
<tr><td rowspan="3">3.2 Geometrical precision</td><td>Geometrical accuracy</td><td colspan="2">Annual</td><td>Monthly</td><td rowspan="2">>1 mm</td><td rowspan="2">> 2 mm</td><td rowspan="3">> 2 mm for conventional treatments,> 1 mm for SRS/SBRT</td></tr>
<tr><td>Linearity</td><td colspan="2">Annual</td><td>Monthly</td></tr>
<tr><td>Spatial Stability</td><td colspan="2">n.r.</td><td>Monthly (coincidence of isocentres daily)</td><td>n.r.</td><td>n.r.</td></tr>
</table>

TABLE 3.7.1. Summary of image quality tests including suggested frequencies and action levels for the described procedures.

Parameter	Procedures	Frequency*			Action level		
		Dental	Interven-tional radiology	Radio-therapy	Dental	Interven-tional radiology	Radio-therapy
3.3 Voxel density values	Voxel values for different materials	Annual		Monthly	Manufacturer specifications, or > 25% difference air water	Deviations > 50 HU from the baseline value (still under research)	
3.4 Noise	ROI standard deviation	Annual		Monthly	Differences from baseline > 20%		
3.5 Low contrast resolution	Contrast-to-noise ratio	Annual			Differences from baseline > 40% Acceptance indicator < 100[§]		
3.6 Spatial resolution	Frequency at 10 % of the modulation transfer function	Annual			< 10 lp/cm (high resolution mode)	< 5 lp/cm	

TABLE 3.7.1. (cont.) Summary of image quality tests including suggested frequencies and action levels for the described procedures.

* Depending on the complexity of the treatment techniques used and the weight of CBCT for image guidance, the monthly tests in radiotherapy facilities may be carried out quarterly or every half a year. In addition to the indicated frequency, the tests should be performed at acceptance of the device as well as after maintenance work or upgrades that could affect the integrity of the system.

For dental and interventional radiology applications annual tests are suggested as a minimum requirement (in addition to the acceptance tests and the tests after changes in the device). However, we support the decision of some countries to enforce the tests on a monthly basis[10]. Indeed, with the help of dedicated software it is possible and desirable to perform the indicated tests on a monthly basis.

§ A value of 100 is given for the described example of contrast being calculated between PVC and PMMA.

n.r. = not relevant.

CHAPTER 4

Image Quality Phantoms

CHAPTER 4

Image Quality Phantoms

Introduction

Assessment of the equipment performance is achieved by evaluating phantom images against levels set by the manufacturer or by national or international standards and criteria. The focus of this section is to review the different aspects of the image quality phantoms for dental, interventional radiology and radiotherapy CBCT. A review of dosimetry methods for CBCT is covered in chapter 5.

An image quality phantom should allow the user to evaluate the different aspects of the imaging chain in a standardised, reproducible and consistent way. The level of expertise of the target user group in quality control testing should be taken into consideration at the design stage. Phantoms intended for medical physicists are used for assessing a wide range of image quality aspects of the equipment, e.g. uniformity, spatial and contrast resolution, noise, artefacts, image density values, geometric accuracy and reconstruction for a range of clinical protocols, usually on an annual basis. However, monthly, quarterly or biannual tests are aimed to highlight issues that require immediate attention. These tests are usually simple, time efficient and can be readily performed by the local clinical team. The phantoms used for these test are designed to assess a limited number of image quality parameters, most commonly uniformity, noise and spatial resolution.

Phantoms dedicated to CBCT should allow the assessment of the 3D performance of the system and therefore, should be designed to allow the evaluation of the image quality parameters across the axial, sagittal, coronal planes and at the volume rendering mode of the system. The size and shape of the phantoms should be optimised for the particular clinical applications e.g. head/neck, body, peripheral or paediatric imaging. Ideally, the phantoms optimised for body imaging should allow the evaluation of the imaging parameters across a range of body thicknesses.

CHAPTER 4 / Image Quality Phantoms

Dental and interventional radiology CBCT scanners are optimised for high contrast clinical applications with higher spatial resolution compared to clinical CT scanners and therefore, the phantoms should be designed accordingly. However, modern interventional radiology CBCT scanners offer the option of low contrast imaging in addition to high contrast imaging which ideally should be taken into consideration when designing a phantom for this type of scanners. The low/high contrast and spatial resolution details of the phantom should be designed to allow clear definitions of action levels for the performance of the equipment.

All the available CBCT phantoms are designed to simulate adult heads and torsos. However, for applications dedicated to paediatric imaging, dose optimisation and image quality assessment with adult phantoms is far from ideal especially for young children. The phantoms companies and the CBCT scanners manufacturers need to address this issue in the near future.

Software that allows automated handling and interpretation of the data would facilitate assessment of the performance especially for the local clinical staff[104]. Therefore, it is essential for CBCT manufacturers and phantom companies to provide simple but reliable software together with their phantoms. For dental CBCT, automated image analysis software is available for all phantoms. However, this comes with additional costs.

The following sections review the current status and challenges for phantoms in dental, interventional radiology and radiotherapy CBCT. A table summarizing the available phantom properties is presented at the end of the chapter.

CHAPTER 4 / Image Quality Phantoms

4.1 | Dental CBCT

The challenge in quality control of dental CBCT scanners is to design a universal phantom which would allow the assessment of the imaging properties of the available scanners. A universal phantom should fulfil the following requirements:

- Size of a typical adult and/or paediatric head
- Diameter and height for small, medium and large FOVs
- Contrast resolution materials that simulate soft tissue, air, bone and teeth
- Size and type of the detail applicable to all scanners and all FOVs, allowing clear definitions of action levels
- Assessment of spatial resolution using subjective and objective methods, line pairs and modulation transfer function
- Spatial and contrast resolution details that would allow the assessment of the 3D performance of the system
- A uniform section for allowing the assessment of homogeneity and noise for small, medium and large fields of view
- Materials to assess artefacts from metal restorations
- Capability of different detail placing positions at the periphery or centre of the phantom allowing limited interference on other details of the image quality parameter of interest
- Accurate and reproducible positioning across the axial, coronal and sagittal planes
- Capability for acquiring all the image quality parameters with one scan
- Automated software to facilitate the analysis and interpretation of the results.

Currently there are 20 manufacturers offering more than 40 different models of dental and maxillofacial CBCT scanners produced in 7 countries. The majority of the scanners support seated or standing patient positioning and only very few scanners offer horizontal positioning of the patient.

Field of view varies depending on the clinical application. For imaging single or very few teeth, scanners offer small fields of view, for dentoalveolar imaging, scanners are equipped with medium fields of view and for maxillofacial imaging, scanners offer large fields of view. The smallest FOV available in the market is 4 cm in diameter and 3.75 cm in height and the largest is 14 cm in diameter and 24 cm in height. Several scanners are equipped with a range of FOV from very small (4 cm x 4 cm) to very large (14 cm x 24 cm). The majority of the scanners are based on flat panel detector technology but there are a few available in the market which are equipped with image intensifiers. Depending on the CBCT device, the tube voltage and tube current are either fixed or can be manually adjusted. Some CBCT devices operate under automatic exposure control. Most of the scanners operate at 360o rotation angle but there are systems available which operate on partial rotation mode e.g. 180˚. In addition, there are several models that offer a range of rotation angles. The number of projections acquired during a scan varies from 180 to 1024 and there is a wide range of isotropic voxel sizes ranging between 75 μm^3 to 600 μm^3.

To the best of the author's knowledge, there are six commercial phantoms for image quality assessment for dental CBCT scanners as shown in the following table. Steiding et *al*, 2014[16] and Torgersen et al[97], 2014 research studies presented two CBCT image quality phantoms which are not commercially available at the time of this report.

TABLE 4.1.1. Phantoms for quality control in dental CBCT.

Phantom	**Manufacturer**	**Compliance with**
Quart DVT_AP	Quart GmbH	DIN 6868-161 standard (acceptance test)
Quart DVT_KP	Quart GmbH	DIN 6868-15 standard (constancy test)
Quart DVT_150	Quart GmbH	DIN 6868-150 standard
SedentexCT IQ	Leeds Test Objects	EC report 172
CBCT 161	Leeds Test Objects	DIN 6868-15 standard (constancy test)
QRM ConeBeam Phantom	QRM GmbH	

CHAPTER 4 / Image Quality Phantoms

In dental CBCT, positioning of the phantoms is achieved with the use of tripods but all of them offer positioning aids (see figure 4.1.1.). However, users should keep in mind that positioning can be challenging because of the design of the gantry, chair and chin rest and it is recommended that the experimental set-up is planned ahead of the survey.

CBCT manufacturers are increasingly offering quality control phantoms which are tailored to their CBCT scanners. These phantoms are simple, are accompanied by automated software and can be readily used by the local clinical staff. However, the local clinical staff should discuss and review the quality control programme recommended by the manufacturer with the medical physics team.

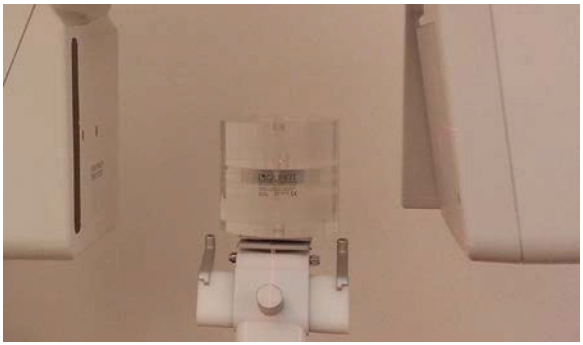

FIGURE 4.1.1. An example of the DIN phantom for acceptance tests (QUART DVTap) on the positioning aid (holder) of a dental CBCT system. Image courtesy of Chang Eui Lee and Ralph Schulze (Mannheim).

4.2 | CBCT for interventional radiology and guided surgery

Currently some C-arm equipment for fluoroscopically guided surgical procedures and for interventional radiology and cardiology enable volumetric images by cone beam acquisitions. The term "rotational angiography" is sometimes used in the interventional field, but the indication "C-arm CBCT" is more general and can include all volumetric modalities performed both with mobile C-arm and complex angiographic equipment. Some acquisition systems produce only three dimensional volume rendering of high contrast structures (e.g. vessels with contrast medium or bone segments in orthopaedic surgery), whereas other systems allow to view volumetric data as slices over axial or other planes, as for surgical navigation systems. For orthopaedic applications, a dedicated mobile CBCT with a circular gantry was recently developed. Furthermore, there are CBCT applications specifically developed for extremity imaging, which allow the patient to stand up and therefore image the joints while carrying its person's weight.

A good review of the value of CBCT imaging for interventional radiology is presented in reference65. For general vascular applications, tomographic images offer the possibility to evaluate dimension and shapes of lesions before and after the treatment, so a good geometrical accuracy is fundamental. A good contrast for soft tissue is also useful, for example for hepatic embolization procedures, to achieve a visualization of which hepatic segments are to be preserved before treatment and after the treatment and to enable the operator to better understand the quantity of parenchyma that has been embolized. For peripheral vascular applications stent placement, a high-resolution acquisition (0.25 mm pixel size) is generally required for stent placement to get a good definition of the vessel lumen, stent struts, and vessel wall, whereas a larger field of view and lower spatial resolution (0.5 mm pixel size) are usually preferred for stent-graft procedures.

A few studies investigated C-arm CBCT image quality with geometrical phantoms or semi anthropomorphic phantoms. A Catphan 600 phantom was used to assess image quality of an angiographic C-arm system for three-dimensional neuro-imaging[66], with the use of low contrast and spatial resolution modules.

Shafer et al[67] evaluated image quality in terms of CNR for bone and soft tissue in spinal surgery for different doses and slice thickness, using a semi anthropomorphic oblate thoracic phantom including low-density regions. Home-made phantoms were developed to study positioning accuracy in CBCT guided stereotactic liver punctures[68] or in laparoscopic liver surgery[69]. A phantom consisting of two plane-parallel circles of ball bearings encased in a cylindrical acrylic tube was used for geometric calibration of a mobile C-arm[70], finding sub millimetres short and long term reproducibility.

Some manufacturers provide quality phantoms for calibration and also for acceptance and constancy tests with the radiological equipment. As an example, with the XperCT CBCT systems of Philips angiographic equipment a contrast resolution phantom is provided, which has inserts constituted by cylinders of diameter in the range 0.5 – 2.25 mm inside two disks of PMMA and of PE200. A minimum resolution of 1 mm for the PMMA disk and of 1.25 mm for the PE200 disk is recommended by the manufacturer. Figure 4.2.1 shows the phantom section resolution targets and two example images.

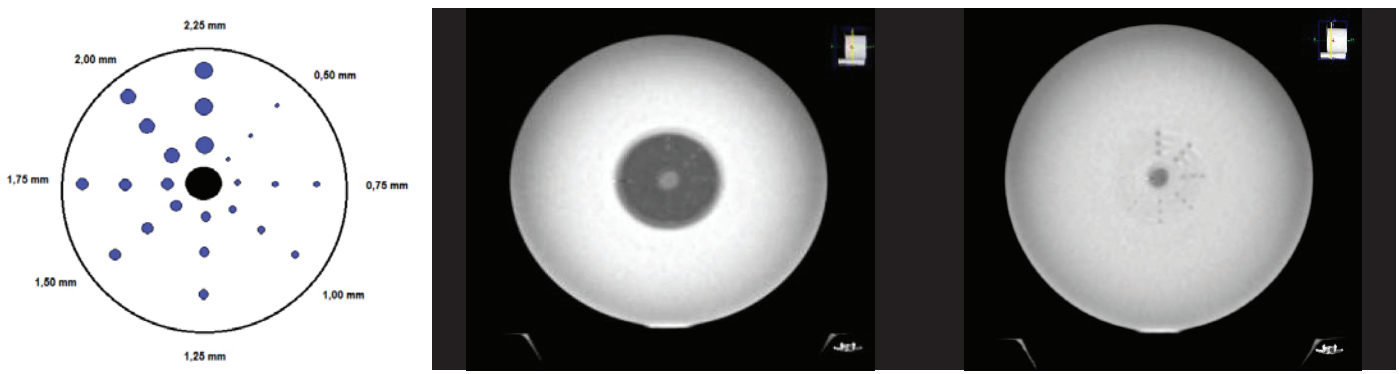

FIGURE 4.2.1.Phantom provided by a manufacturer for interventional radiology CBCT.

Another example of manufacturer's phantoms and quality assurance procedures is available from Siemens, for3D applications with Axiom Artis Systems and Artis zee/zeego. The following quality tests are defined:

- Geometric definition: qualitatively evaluated by thin metallic wires (1-2 mm diameter) positioned along the longitudinal direction over the examination table and acquired with the 3D application. The wires should be well visible in volume rendering. Their profile shall be well defined, with sharp edges.
- Spatial resolution: a phantom constituted by a resolution test pattern for radiography positioned on the top of a 2.1 mm Cu plate at the isocentre. From the 3D dataset a coronal plane should be reconstructed and 1.2 lp/mm should be visible both in horizontal and in vertical planes.
- Registration accuracy: this test aims to investigate the accuracy of virtual reconstructed 2D projections from the 3D dataset acquired. Three metallic wires of 2 mm are positioned on the patient table, two parallel and one vertical to the patient axis. A 3D acquisition is performed and then a 2D reconstructed projection is overlaid on actual 2D acquisition. The overall accuracy of superposition must be better than 2 mm in the isocentre, so with a wire diameter of 2 mm the wire images must "touch each other".
- Uniformity and low contrast: a cylindrical phantom with a uniform section and a low contrast pattern is used. In the homogeneity section, a mean value between –85 and 115 is expected, together with a standard deviation less than 15. In the low contrast section the detail of diameter 20 mm and contrast 6 HU must be visible for a 10 mm thick section.

At the time of this report, there are no commercial phantoms specifically dedicated to C-arm CBCT. However, several phantom manufacturers indicated the suitability of their CT and CBCT phantoms for angiography or surgery CBCT. The QRM CBCT phantom is presented as a tool for 3-D dental imaging, C-arm or angio x-ray machines with options for 3-D imaging or CT scanners with flat-panel detectors covering a large scan volume. It contains three different low contrast sections providing contrasts between 3 Hounsfield Units and 200 HU, spatial resolution bar patterns ranging from 4 to 30 lp/cm, an edge insert to assess the system MTF in different orientations and an image contrast and HU-scale section.

The QUART DVT_AP phantom, already cited in the previous paragraph of dental phantoms, is designed for QA/QC at CBCT including applications in interventional radiology and guided surgery. The CBCT Electron Density & Image Quality Phantom System is promulgated primarily for radiotherapy CBCT, but the manufacturer states that in the spatial resolution layer, line pairs from 1 lp/cm to 16 lp/cm are present with attenuation of about 420 HU, a difference that is often used in cardiac angiography imaging.

4.3 | CBCT for radiotherapy

Image-guided radiotherapy is frequently performed using the images obtained with on-board or in-room CBCT system to aid in patient positioning and to accurately locate the target with regard to the planned treatment radiation beam. Therefore, geometrical precision (see section 3.2) is critical for radiation treatment to ensure correct irradiation of the target volumes while minimizing the dose irradiation to surrounding organs. In addition, the action levels in radiotherapy are stricter than with other CBCT devices.

Image contrast has to be adequate to resolve the high and low contrast anatomical structures (see sections 3.5 and 3.6). Besides, in current research works, the CBCT images are used for dose calculation and thus appropriate voxel density values (HU) are crucial (See section 3.3). Image noise (section 3.4) is normally higher than in conventional CT. Also in many CBCT devices for radiotherapy, the number of projections can be selected (normally full or half fan) and also some reconstruction parameters, depending on the anatomical region.

The most commonly analysed parameters for radiotherapy CBCT are geometrical stability, uniformity, voxel density values for different materials, MTF and CNR. The basics about how to calculate them have been explained in the previous sections. An example of phantom images obtained in a radiotherapy CBCT system is shown in figure 4.3.1. An example of the set-up of another phantom is shown in figure 4.3.2.

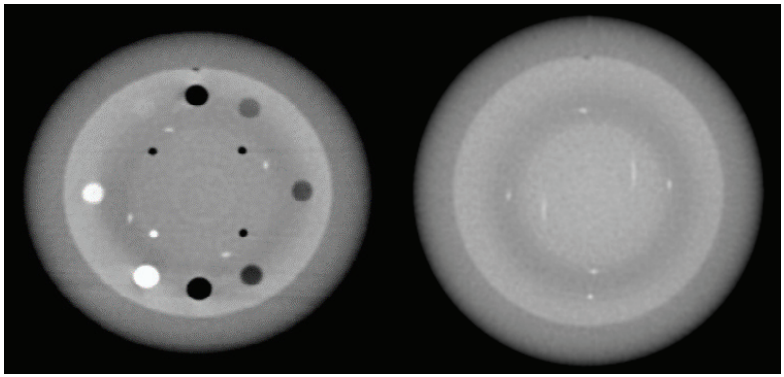

FIGURE 4.3.1. Images of the Catphan phantom obtained in a radiotherapy CBCT system (Elekta XVI) for the voxel density values measurements (left) and geometrical precision (right).

FIGURE 4.3.2.Left: An example of the DIN phantom for constancy tests (QUART DVTkp) placed in a TrueBeam Varian linear accelerator (left) and the acquired image of the uniformity module of the phantom (right).

CHAPTER 4 / Image Quality Phantoms

In the literature, for routine image quality QC, the recommendations for these CBCT radiotherapy devices are based in evaluating the constancy of these image quality parameters, with respect to a baseline for the typical protocols used (for example head and abdomen), and there are not established quantitative action levels[38,39,43,71,72].

As tolerances, some authors propose to use the baseline (obtained at acceptance for the different protocols) plus or minus three times the standard deviation (99% confidence interval)[73]. The baseline value for the different image quality parameters should be obtained as an average over different slices, and even better, over several scans selecting the same conditions in each test at acceptance or after major changes in the device.

4.4 | Summary table

Phantom	Diameter (mm)	Height (mm)	Materials	Noise/ Uniform.	CNR	Spatial res.	Low contrast	Density values	Artefacts	Geom. accuracy	Applica-tions
Quart DVT_AP	160	150	PMMA PVC Air Enhancement set[2]	Y	Y	Y	Y	Y	Y	Y	Universal CBCT[1]
Quart DVT_KP CBCT 161	160	40	PMMA PVC Air	Y	Y	Y	Y	Y	Y	Y	Universal CBCT[3]
Quart DVT_150	120 x 120 x 60 mm[3]			N	N	Y	N	N	N	N	Dental 3D
SedentexCT IQ	160	162	PMMA Aluminium PTFE Delrin LDPE Air	Y	Y	Y	Y	Y	Y	Y	Dental CBCT
QRM ConeBeam CT	160	143	Water eq Bone eq Air -200HU to -3HU	Y	Y	Y	Y	Y	N	N	Universal CBCT[4]

TABLE 4.4.1. Summary of commercial phantoms available

Phantom	Diameter (mm)	Height (mm)	Materials	Noise/ Uniform.	CNR	Spatial res.	Low Contrast	Density values	Artefacts	Geom. accuracy	Applica-tions
Steidinget al	100	100	-1000HU -30HU 0 30HU HA100- bone eq	Y	Y	Y	N	Y	Y	N	Universal CBCT[5]
Torgersen et al	160	70	Polyethene Nylon Acetal Teflon	Y	Y	Y	Y	Y	N	Y	Dental CBCT
Catphan	150	250	Teflon, Delrin Acrylic, Polystyren e, H20, LDPE, PMP, Air	Y	Y	Y	Y	Y	Y	Y	Universal CBCT[5]
CIRS radiotherapy	250	330	Electron Density anatomic insert , uniform slab, bone,	Y	Y	Y	Y	Y	Y	Y	Universal CBCT[5]

TABLE 4.4.1. Summary of commercial phantoms available

[1]As stated by the manufacturer: dental volume tomography, C-arm angiography, CT
[2]Enhancement set includes: Water, Soft Tissue, Bone and Bone and Tooth equivalent materials
[3]As stated by the manufacturer: dental volume tomography, CBCT, 3D imaging
[4]As stated by the manufacturer: dental volume tomography, C-arm, angiography, CT scanners with large flat panel detectors
[5]As stated by the manufacturer: CBCT systems

CHAPTER 5

Tests of Radiation Output

CHAPTER 5

Tests of Radiation Output

Introduction

Presently there are many different medical and dental applications employing CBCT, e.g. imaging in the fields of surgery, interventional radiology, dental radiology and radiotherapy. Due to the heterogeneity of applications, the manufacturers of these devices have accommodated the healthcare industry with technical innovations designed for each specific task. For CBCT there is a multitude of different solutions for the x-ray beam geometry commonly including a variety of large x-ray fields compared to those found in MDCT, central or off-axis exposure geometries, full or partial rotation of the x-ray tube during imaging, as well as combined functionality of CT and Fluoroscopy. While this is desirable for the end users, the situation has made it difficult to achieve a standardization of radiation dosimetry to characterise machine output, or to determine patient exposure following a CBCT examination.

Action levels and frequency

For QC to yield actionable results, measurements must be traceable to actual action levels that are relevant for a given type of CBCT unit, as specified by the manufacturer and/or regulatory bodies. Individual practitioners may undertake testing of parameters that are not traceable, which may be of use in the process of optimization but not for the purpose of QC. For dosimetry QC with CBCT, measurements are recommended to be performed at least annually, as well as when a unit has undergone maintenance that may affect x-ray radiation output[25,8,9,64]. Action levels and frequencies are suggested in the summary table at the end of this chapter.

Present dose metrics

Due to the lack of standardization of radiation dosimetry for general CBCT applications, there are different formalisms commonly used to quantify radiation output in CBCT, i.e. as a basis for radiation dosimetry QC. These are the kerma Area Product (KAP), the air kerma at the focus-to-detector distance, K_a(FDD) and in phantom dose indicators (traditional CTDI, cone-beam dose index 'CBDI', AAPM cumulative dose and SedentexCT indexes as described in appendix 3). For QC purposes, all these formalisms have some advantages for the different CBCT applications. However, they will also be insufficient for applied patient radiation dosimetry.

Challenges with present dose metrics

In-phantom dosimetry raises two kinds of problems: 1) the formalisms use phantoms that are too small to properly represent radiation scatter from the large x-ray fields commonly used in CBCT applications, and 2) the positioning of the phantom can be problematic in particular for dental CBCT (see appendix 3)[74]. However, QC measurements without phantoms may be used with a complete description of the x-ray beam geometry of a CBCT unit, e.g. from the manufacturer, to characterise the radiation output and even derive estimates of patient radiation dose for a given unit. The air kerma shall be used for periodic (and fast) constancy measurements of the x-ray tube output. This means that a medical physicist may decrease the uncertainty in patient dose estimates substantially, i.e. from manufacturer stated tolerances that may be as large as ±40% to uncertainty levels associated with best practice radiation dosimetry for diagnostic radiology[75,76]. Appendix 3 contains an overview of in phantom dose indicators and how they may be applied to CBCT applications. For a comprehensive discussion on the CTDI interested readers are encouraged to consult references 22 and 77 (under review).

A troublesome shortcoming of the KAP and the K_a(FDD) formalism is that they require measurements performed free in air, with a large plane parallel ionization chamber close to the x-ray tube (KAP) or a flat probe attached to the image detector (in the case of K_a(FDD)). This means that for measurements of KAP or K_a(FDD), no information is provided in regard to a patient or phantom exposure, which is required for further estimates of patient radiation dose. Nevertheless, for QC purposes the quantification provided by these radiation dosimetry metrics free in air is sufficient for CBCT applications. Thus the KAP and the air kerma methods are proposed to be used as dosimetric indexes. The measurement methodology, a discussion of advantages and drawbacks, test frequencies and action levels are suggested in the rest of this chapter.

Further refinement is always required when QC metrics are to be used to estimate patient radiation dose. Given the diversity and continuing growth of CBCT applications in health care, as well as the lack of a general standardization of radiation dosimetry in the field, a general overview of applied patient dosimetry with CBCT applications was prepared by the European Radiation Dosimetry Group (EURADOS) and shown in appendix 7.

5.1 | The kerma area product (KAP)

Quantification of the KAP metric is performed using a large plane parallel ionization chamber mounted on the x-ray tube assembly, if possible. This ionization chamber type is commonly called a "KAP meter" (or even "DAP meter" representing a Dose Area Product if the ionization chamber has been calibrated for absorbed dose instead of air kerma[78]). The usage of a KAP meter to quantify x-ray radiation output in practice is straightforward: after mounting the meter on the x-ray tube housing an exposure is made with the parameters settings chosen. The resulting KAP measurement is given as air kerma (or absorbed dose) multiplied by area, e.g. μGy m^2 or mGy cm^2 or dGy m^2.

FIGURE 5.1. A KAP meter mounted on the x-ray tube housing of a dental CBCT. Image courtesy of H. de las Heras.

As shown in Figure 5.1, the KAP meter measurement volume covers all possible collimation settings that may be relevant for QC measurements, and the KAP metric is thus not sensitive to differences in nominal collimation (field of view sizes), which is a limiting factor for the CTDI. Furthermore, for consideration of patient dose estimates the KAP metric is also robust when it comes to off-axis exposure geometries, as well as partial rotations of the x-ray tube during imaging, both of which are common in CBCT applications. Like all air-filled ionization chambers, the KAP meter readings should be corrected for air temperature and pressure[75]. There are commercial programs that use KAP as input dosimetry quantity for organ and effective dose evaluation in CBCT[79].

Discussion

The measurement formalism of the KAP metric does not require the use of a phantom, which may be considered both as a strength and a weakness. As previously discussed (see also Appendix 3), free in air measurements (i.e. no phantom) are adequate for QC purposes, and even preferable for practical reasons. However, if results from QC are to be used for further radiation dosimetry considerations involving patients, the lack of a phantom is definitely a weakness, although the KAP is can be used as input data for software involving patient modelling. For a practical discussion on the calibration of KAP meters see section 5.1 of reference[76].

5.2 | The incident air kerma at the detector, $K_{a,i}$ (FDD)

As a practical alternative, point measurements of the incident air kerma ($K_{a,i}$ as abbreviated by ICRU[80]) at the focal spot-to-detector distance (FDD) can be easily performed with a flat probe. Appropriate solid-state probes are used for measurements of $K_{a,i}$ in projection radiography and mammography, so they are already available in most clinics. They should be back-shielded in order to not measure backscatter. The advantage of solid-state dosimeters is that their calibration and their results are not dependent on the atmospheric pressure or the temperature in the room (as opposed to KAP meters and CTDI chambers). However, in contrast to ionisation chambers the energy dependence of solid-state dosimeters is not negligible, which limits their accuracy for patient dose estimations in the presence of scattered radiation from a phantom or a patient.

Procedure

The method mentioned here is described in detail in the DIN standard 6868-161[10]. The $K_{a,i}$(FDD) is measured free in air without a phantom, simulating an actual examination by placing the probe as close as possible to the plane of the imaging detector (figure 5.2). Caution must be taken to place the probe so that it collects radiation during a whole rotation of the x-ray system, which may include physically removing the head support in CBCT units for oral radiology.The probe must be placed at the centre of the imaging detector and, most important, its position must be marked (preferably on the detector) to ensure reproducibility. This is especially important when the longitudinal size of the scanned volume is user-defined. For the data acquisition, the exposure parameters for a standard patient are used following indications of the manufacturer. If the x-ray device makes use of an automatic exposure control, it is necessary to manually enter the appropriate exposure parameters. As some users reported ghosting after repeated tests, the use of a copper or aluminium plate to protect the flat panel during tests is recommended.

FIGURE 5.2. Position of a flat solid-state probe to measure the Ka,i(FDD) in a dental CBCT (left), a C-arm for angiography CBCT (center) and a CBCT in radiotherapy (right). Images courtesy of F. Schöfer, B. Renger and K. Mair.

The advantage of this simple measurement is that it enables the calculation of a dose quantity, D_{FOV}, which takes into account the kind of geometry, size of the field of view and rotation angle. This quantity is an estimation of the average dose calculated over the diameter of the FOV, and it can be determined from the $K_{a,i}$(FDD) using a simple geometrical relation:

$$D_{FOV}=K_{a,i}\,(\mathrm{FDD})\cdot\frac{b}{a}\cdot\frac{d}{c}, \qquad [5.1]$$

where *a* is the distance from the focal spot to the isocentre, *b* the distance from the focal spot to the place of measurement, *c* the horizontal diameter of the scanned volume, and *d* the horizontal diameter of the radiation field at the place of measurement (see figure 5.3.).

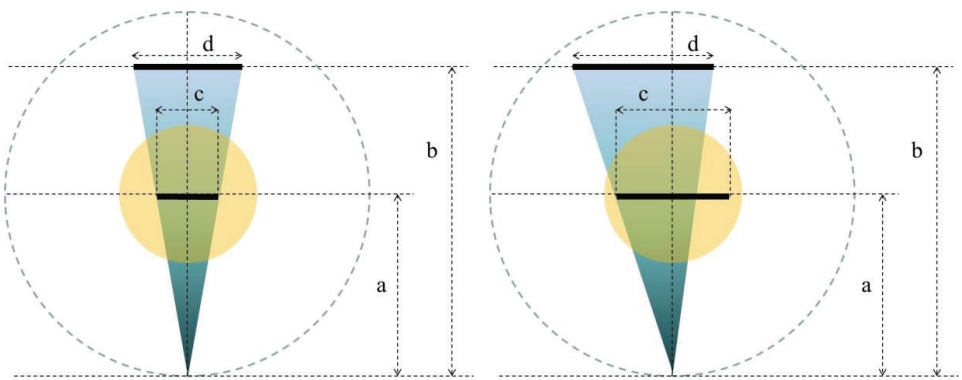

FIGURE 5.3. Description of the quantities a, b, c and d required to apply equation 5.1 in the case of symmetric scan geometry (left) and asymmetric scan geometry (right).

Tests of Radiation Output

Action levels

The DIN standard 6868-16110 enforces an action level of $D_{FOV} \geq 50$ mGy. A practical example of a test report is shown in Appendix 2. The bottom part of the report shows the $K_{a,i}$(FDD) measurements and the relevant results.

Discussion

The geometrical relation 5.1. reduces to the well-known inverse-square law for symmetric data acquisition geometries (see 3.2.1 in reference[80]). In fact, for the simplest scan geometries and homogeneous fields, the $K_{a,i}$(FDD) can be used to estimate the $CTDI_{free\text{-}in\text{-}air}$. In the case of asymmetric geometries (such as those using only one "half beam"), the ratio d/c is much smaller than b/a. For this reason, for a fixed value of measured $K_{a,i}$(FDD), D_{FOV} is smaller than in the case of symmetric geometries. This reflects the fact that, for a fixed value of $K_{a,i}$(FDD), patients receive a lower dose in the case of asymmetric geometries.

It should also be noted that the distances b and d are measured at the "place of measurement", i.e. the surface or front plate of the detector. These distance scan be estimated if it is not exactly indicated in the specifications of the device. However, this estimation can be a substantial source of uncertainty when comparing the results among different devices.

The described calculation of D_{FOV} provides an easy procedure to assess the radiation output of the CBCT device for quality control purposes. It enables comparisons to other devices and the establishment of simple thresholds or suspension levels. Manufacturers of dental CBCT systems are already obliged to report the K_a(FDD) or the D_{FOV} (also called "Dose in the isocentre") in Germany, which allows medical physicists to use this method for acceptance tests and QC. In other countries, the method may be considered among physicists, manufacturers and regulators as a useful dosimetric QC tool.

In conclusion, KAP meters provide a complete assessment of the radiation beam and provide a reliable measure for QC purposes. When these meters cannot be mounted, or whenever they are not available, a simple point measurement of kerma at the flat panel detector (which is always possible in CBCT devices) provides a reliable measurement that can equally well be used for QC purposes.

5.3 | Summary table

TABLE 5.3.1. Summary of the tests of radiation output. One of them may be chosen for the purpose of routine quality control.

Parameter	Frequency			Action level		
	Dental	Interventional radiology	Radiotherapy	Dental	Interventional radiology	Radiotherapy
KAP (Kerma area product)	Annual			KAP larger than 250 mGy cm^2	Not available	Not available
$K_{a,i}$(FDD) (incident air kerma at the detector)				D_{FOV} larger than 50 mGy (following equation 5.1)		

The action level enforced for dental devices in the standard DIN 6868-161[10] for the incident air kerma-metric has been exttended to the other CBCT modalities. The action level for the KAP corresponds to imaging prior to the placement of a maxillary molar implant in a standard adult patient and a field of view of 4 x 4 cm.

Update List

Update January 2018:

- All corrections received from the DIN group regarding the standard 6868-161 and 6868-15 were implemented.
- The title of section "Summary Table" was corrected in chapter 3.
- The table 4.4.1 was updated for consistency with chapter 3.

Update May 2019:

- EURADOS contribution (appendix 7) and corresponding acknowledgment to the EURADOS group.
- Correction of typos
- The definition of uniformity was corrected to comply with DIN.
- Update of references and addition of recent references
- Addition of comments from the praxis regarding the dosimetry chapter.

APPENDIX 1

Outlook Regarding Iterative Reconstruction

APPENDIX 1

Outlook Regarding Iterative Reconstruction

Generally, reconstruction in CBCT systems is based on conventional 3D filtered backprojection (FBP) algorithms (Feldkamp). In conventional CT, all major manufacturers have developed their own iterative reconstruction algorithms, which enable them to acquire patient images at lower doses without losing important diagnostic information for certain indications. Similar iterative reconstruction algorithms have still not been brought into clinical practice with CBCT systems. It can be expected that further optimization of the computational efficiency of iterative reconstruction algorithms in combination with an increasing processing power of reconstruction hardware will result in the clinical implementation of these algorithms in the near future in CBCT. Further improvement in the image quality and even lower dose to the patient might be possible by the use of iterative reconstruction algorithms.

With the possible transition from FBP to iterative reconstruction a paradigm shift in image quality measures will occur, in a similar fashion as in conventional CT. Due to the potential non-linear behaviour of iterative reconstruction, general properties of noise and resolution might not hold anymore. For instance, when compared to FBP, resolution may vary as a function of dose and contrast with iterative reconstruction. With respect to this, for instance new methods for MTF measurement should be applied as the traditional metrics might not apply for iterative reconstruction.

APPENDIX 2

Example of Quality Control Report

APPENDIX 2

Example of Quality Control Report

Monthly CBCT QC report following the EFOMP-ESTRO-IAEA guidelines

User data
Name: *Name of the person performing the tests (or the owner of the CBCT device)*
Facility: *Name and address of the institution*
Telephone number/E-mail: *User contact information*

Device data
Type: *Dental CBCT*
Manufacturer: *Vatech*
Model: *Pax-i3D PHT6500*
S/N: *052-1988*
Effective area of the detector: *71.68 x 11.76 mm*

Phantom data
Manufacturer: *QUART GmbH*
Model: *QUART DVTap*
S/N: *0123*

Analysis software data
Name: *ImageJ & QUART CTtec*
Manufacturer: *NIH & QUART GmbH*
Website: *imagej.nih.gov/ij/ & quart.de*

Scan data
Maximum scan time: *24 s*
kVp/mAs: *89 kV/ 4.9 mA*
Mode: *constancy tests*

Geometric data (see equation 5.1)
Distance from the focal spot to the isocentre Distance from the detector to the focal spot Horizontal diameter of scanned volume: Horizontal diameter of radiation field at the detector

(a): *449 mm*
(b): *642.3 mm*
(c): *80 mm*
(d): *71.68 mm*

Conventional tests

Section	Parameter	Pass/Fail
2	Radiation output: tube potential, leakage, filtration, repeatability, reproducibility	*pass*
2	Beam collimation	*pass*
2	Image display (monitor)	*pass*
2	Artefacts	*pass*
2	Operator protection (report from radiation protection expert is provided)	*pass*

Image quality tests

Section	Parameter	Result	Baseline	Dif. from baseline	Action level	Pass/Fail
3.1	Uniformity (DIN procedure) [-]	*18.7*	*21.9*	-	*<5*	*pass*
3.2	Geometrical evaluation [mm]	*159.1*	*159.4*	*0.3*	*Dif.>0.5*	*pass*
3.3	Voxel density values [HU]	*985*	*991*	*6.0*	*Dif.>240*	*pass*
3.4	Noise[HU]	*38.88*	*37.2*	*-1.68*	*Dif.>20%*	*pass*
3.5	CNR [-]	*16.98*	*18.2*	*1.22*	*Dif>40%*	*pass*
	Acceptance indicator [-]	*627.22*	*671.8*	-	*<100*	*pass*
3.6	Frequency at 10% MTF [lp/mm]	*1.71*	*1.7*	-	*<1*	*pass*
	Frequency at 10% MTFz [lp/mm]	*1.5*	*1.5*	-	*<1*	*pass*

Tests of radiation output

Section	Parameter	M1	M2	M3	Result	Max Dev	Action Level	Pass/Fail
5.3	Air kerma at the detector [mGy]	*8.05*	*8.06*	*8.04*	*8.05*	*0.1%*	*Max Dev > 1%*	*pass*
5.3	Dose to the field of view [mGy]	-	-	-	*11.3*	-	*>50 mGy*	*pass*

Date and signature:

APPENDIX 3

Discussion about Different In-Phantom Dosimetry Indexes

APPENDIX 3

Discussion about Different In-Phantom Dosimetry Indexes

Traditional CTDI metrics

The CTDI is a dose metric originally developed for CT applications. It was introduced in early 1980s by Shope at al.81 as an alternative to multiple scan average dose (MSAD). The CTDI took into account the direct exposure of the primary beam and the scatter radiation contribution from nearby scanned slices. At that time, only axial acquisitions could be performed in CT, with maximum beam collimations of about 1 cm.

The theoretical ideal definition of the CTDI considered an integral sum over infinity:

$$CTDI = \frac{1}{T} \int_{-\infty}^{+\infty} K(z)dz \qquad [A3.1]$$

where T is the nominal x-ray beam collimation in the patient long axis (z-axis) and K(z) the air kerma profile along the z-axis. After the theoretical definitions, two different practical implementations were proposed by FDA and IEC, changing the integral limits from infinity to ± 7 T for FDA and to ± 50 mm for IEC. This last approach became the standard, and the associated index was referred as $CTDI_{100}$:

$$CTDI = \frac{1}{T} \int_{-50mm}^{+50mm} K(z)dz \qquad [A3.2]$$

The $CTDI_{100}$ can be measured free in air or in cylindrical phantoms cast on PMMA (polymethyl methacrylate, density 1.19±0.01 g cm^{-3}), with a pencil ionization chamber, which has a 100 mm length measurement volume (Figure A3.1). Standard CTDI phantoms either represent a “head” (16 cm diameter) or a “body” (32 cm diameter). Thus, measurements with a pencil ionization chamber yield a direct evaluation of the integral in equation A3.2.

The $CTDI_{100}$ is determined by dividing the air kerma reading from the pencil ionization chamber by the nominal x-ray beam collimation.

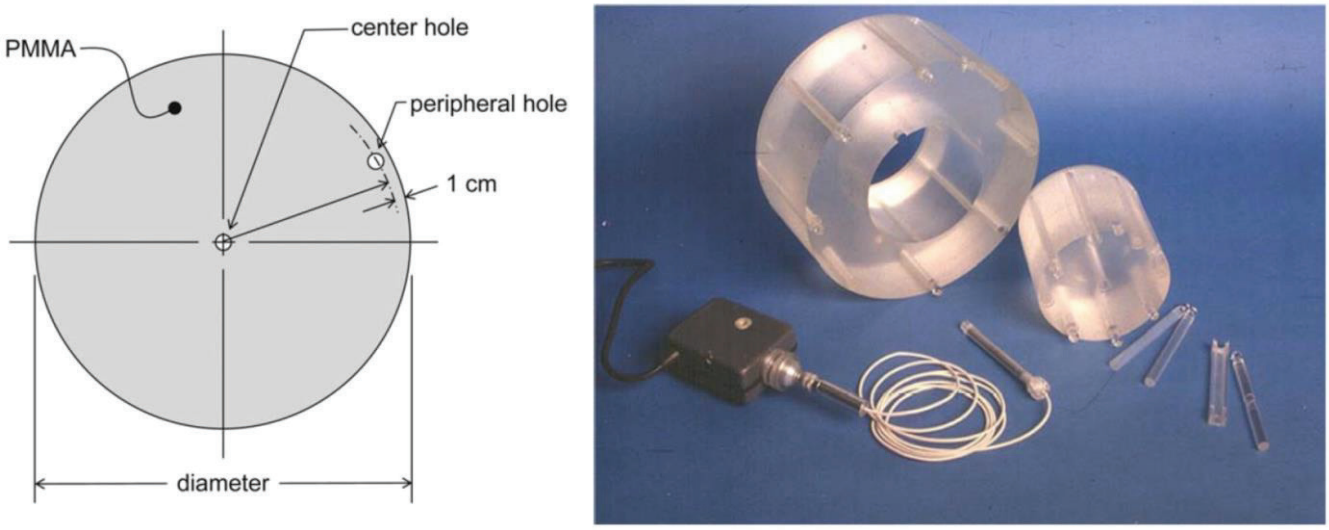

FIGURE A3.1. Left: Schematic image of a CTDI phantom, indicating central and peripheral holes for pencil ionization chamber measurements (Image from reference 61). Right: Pencil ionization chamber and standard CTDI phantoms for head (16 cm diameter) and body (32 cm diameter), respectively (Image from reference 82).

APPENDIX 3 / **Discussion about Different In-Phantom Dosimetry Indexes**

Employing the measurement formalism described, the weighted CTDI ($CTDI_W$), measured in the head or body PMMA phantoms, can be quantified as:

$$CTDI_w = \frac{1}{3} CTDI_{100\,,\,central} + \frac{2}{3} CTDI_{100\,,\,peripheral} \quad [A3.3]$$

where $CTDI_{100,central}$ and $CTDI_{100,peripheral}$ are calculated based on the pencil ionization chamber measurements in the central and peripheral holes applying Eq. A3.2, respectively. Normally for the periphery measurements, four points are considered (north, south, east and west), though other configurations are possible. The $CTDI_W$ metric was defined to represent differences in attenuation for "head" and "body" examinations, as well as for different x-ray beam qualities. The $CTDI_W$ is the most robust and commonly used metric to represent radiation output in CT applications. After the introduction of spiral acquisition, another variation of CTDI was introduced to account for dose dependence on the pitch factor:

$$CTDI_{vol} = \frac{1}{Pitch} CTDI_w \quad [A3.4]$$

It is well known that the information related to dosimetric indexes cannot be translated directly into patient dose quantities, such as organ doses. Considering the $CTDI_W$, the standard body phantom diameter (32 cm of PMMA) is representative of average sized patients but will underestimate the actual absorbed dose for a paediatric patient or overestimate the actual absorbed dose for an obese patient. On the other hand, dosimetric indexes are a useful tool to assess dose reference levels and to compare different protocols and equipment of the same kind. In this sense, while $CTDI_W$ and $CTDI_{vol}$ have served the medical physics community well over the years, technical advances in CT applications have led to increasing difficulties in employing these metrics for patient dose management.

APPENDIX 3 / Discussion about Different In-Phantom Dosimetry Indexes

An important challenge has been the increasing nominal collimations employed in CT applications, which leads to increasing under-representations of patient dose estimates when using the $CTDI_W$ due to systematic underestimation of scatter radiation. The $CTDI_W$ can underestimate the actual dose by 20% for nominal x-ray beam collimations lower than 40 mm, and even more for wider nominal collimations. The use of $CTDI_w$ is also problematic for CT exposures where the patient remains stationary throughout the scan, with single or multiple acquisitions, such as in the case of CT perfusion examinations. In these cases, the sum of scatter and primary radiation resulting from the pencil chamber measurements provide an overestimation of the average dose within the scanned volume and also of the dose to the skin, as shown in figure A3.2 (reference 83).

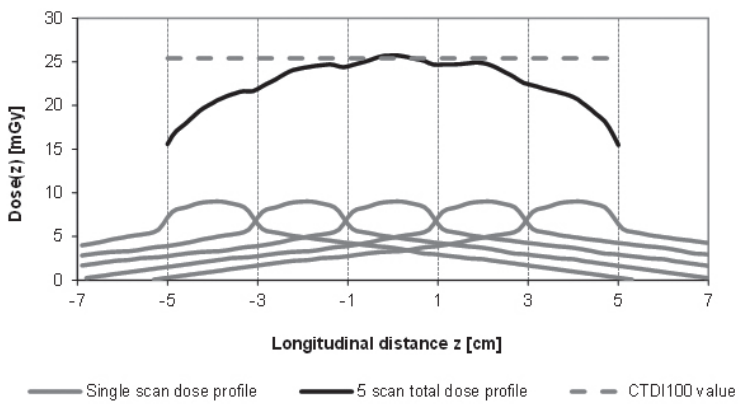

FIGURE A3.2. This plot shows the superposition of 5 single contiguous scan dose profiles measured inside a body phantom with a beam collimation of 2 cm. The black line represents the total dose distribution resulting from the 5 scans and the dotted line represents the $CTDI_{100}$ value, which is close to the total dose in the centre part of the scanned volume. Note that the $CTDI_{100}$ value is in this case about three times the maximum value of the single scan dose profile: when the patient is stationary during the scan, as for example in the case of CT perfusion examinations, the sum of scatter and primary radiation resulting from the pencil chamber measurements provide an overestimation of the average dose within the scanned volume.

APPENDIX 3 / **Discussion about Different In-Phantom Dosimetry Indexes**

For a generic CBCT, we can distinguish two different cases related to the beam collimation along the longitudinal axis. When the collimation is greater than or equal to 100 mm, the $CTDI_{100}$ definition can be adapted by substituting the term "T" in the equation A3.2 with the pencil length of 100 mm. The meaning of this measurement becomes the average dose inside the scanned volume along the central 100 mm, and some[84] call this dosimetric quantity Cone Beam Dose Index (figureA3.3). On the other hand, when the beam collimation is below 100 mm, the original $CTDI_{100}$ definition is applicable, but with an overestimation of average dose inside the scanned volume as previously indicated (see figureA3.2).

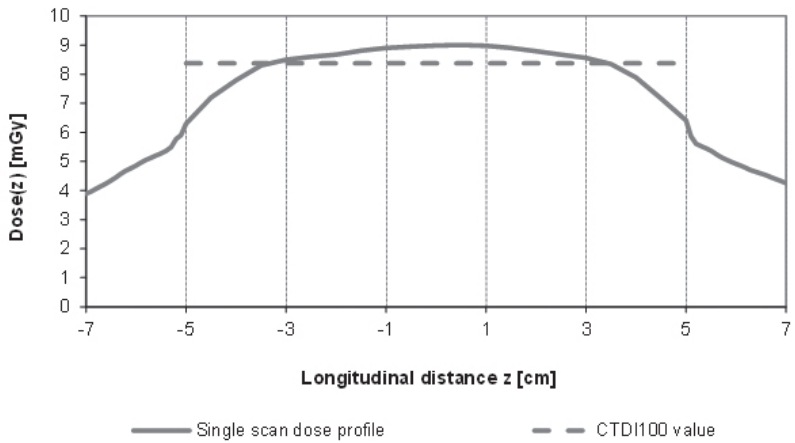

FIGURE A3.3.This plot shows a dose profile of a single scan with a beam collimation of 100 mm. The CTDI (or CBDI) value corresponds to the average dose along the acquired volume, a bit lower than the maximum value of the dose profile.

Another practical issue in applying the CTDI metrics to CBCT is the phantom positioning. While for radiotherapy CBCT and for C-arm CBCT with patient couches it is quite easy to position the phantoms in a similar way of MSCT, for dental CBCT this task is in general complex for different reasons such as:

- the availability of stands to position vertically the phantom;
- the availability of laser lights or other indications to centre the phantom;
- the relative position of FOV and phantom, with the question if it is better to follow a pure geometrical approach (same centre for FOV and phantom) or a more clinical approach (FOV centred peripherally as for an examination of frontal or lateral dental arcade).

IAEA adaptation of CTDI definition for wide beam collimations

In order to account for wide beam collimations, the method proposed by the IAEA considers the evaluation of the CTDI free in air over the entire beam profile, with an integration length of at least NxT + 40 mm, where N is the number of active data channels in a stationary axial scan, and T is the nominal thickness of each data channel[82]. For beam widths greater than 60 mm, the suggested measurement approach is to use of the standard 100 mm CT pencil ionization chamber, and stepping through the beam at regular intervals, usually at a distance equal to the chamber length. For a generic MSCT, in air measurements should be performed for a reference beam collimation with a width lower or equal to 40 mm and for all the other collimations, whereas in phantom dosimetry can be performed measuring the CTDI only for the reference beam collimation. After that, the in phantom $CTDI_{100}$ for a generic collimation NxT can be estimated using the following relationship (Eq. A3.5):

$$CTDI_{100,\,N\times T} = \frac{1}{(N\times T)ref}\left(\int_{-50mm}^{+50mm} D_{ref}(z)dz\right)\times\left(\frac{\mathrm{CTDI}_{free-in-air,N\times T}}{\mathrm{CTDI}_{free-in-air,\,ref}}\right) \qquad [A3.5]$$

APPENDIX 3 / **Discussion about Different In-Phantom Dosimetry Indexes**

This method has been adopted by the IEC and it is reported in the IEC- 60601-2-44 – Ed. 3 Amendment 1 (2010). As a consequence, the future MSCT equipment with wide collimations should use this method for the calculation of the displayed $CTDI_{vol}$ values at the console.

The application of this approach to CBCT raises several issues. First of all, few CBCT equipment allow to define longitudinal beam collimations below 40 mm as a reference. Secondly, even in cases when this collimation would be achievable, this method would be affected by the problem of the inaccurate consideration of scatter contribution, already described in the previous paragraphs for the traditional CTDI definition.

AAPM and ICRU approach for MSCT and CBCT: the cumulative central dose

In 2010, the AAPM task group 111 published a report aimed to give a comprehensive methodology for the evaluation of radiation dose in x-ray computed tomography, including fan beam and cone beam scanning with or without longitudinal translation of the patient table[85]. The described dosimetric approach considers a single point chamber positioned at the centre of a cylindrical head or body phantom. For helical MSCT the measurement procedure is performed by the table translation and accumulation by the point chamber of the scatter and primary beam contributions. The measured quantity is called "cumulative dose" $\mathbf{D_{L(z)}}$. An extensive and well-designed discussion is provided in this report about the relative effects of the scanning and phantom lengths along the longitudinal axis. In particular, the central cumulative dose increases with the scanning length and it approaches an equilibrium value for relative high scanning lengths, of about 45 cm with three stacked CTDI PMMA phantoms. The same quantities and experimental approach is also included in the ICRU 87 report[61], although a different cylindrical phantom is proposed for assessment of dose and image quality. Since the use of a triple phantom can be very hard to manage in routine quality controls, in the ICRU report the proposal is to use single phantoms in the clinical environment and to ask the manufacturer to perform the dose assessment with a triple phantom, together with the calculation of the "approach to equilibrium function", which allow to extrapolate single phantom measurements to triple phantom evaluations.

The situation of the cone-beam scanning without table/phantom translation is also considered in the AAPM TG 111 report. In this case the cumulative dose is a direct punctual measurement of the dose at the centre of the scanned volume and it represents also the maximum value of the dose profile along the longitudinal axis. To apply this method, the same critical aspects of phantom positioning already described for CTDI have to be considered, in particular for dental CBCT. A comparison of single and triple phantom measurements for a radiotherapy CBCT can be found in references 86 and 87.

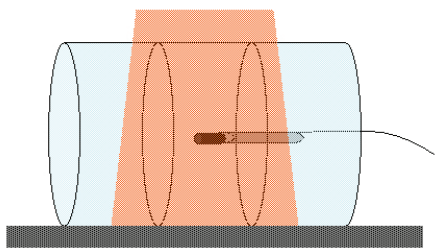

FIGURE A3.4. Setup for the measurement of cumulative central dose in CBCT with a triple CTDI phantom configuration.

IN PHANTOM DOSIMETRIC INDEXES PROPOSED BY THE SEDENTEX-CT PROJECT

For dental CBCT, the SEDENTEXCT project[8] proposed the use of dose indexes obtained from measurements performed with small volume dosemeters positioned in the middle plane of a cylindrical Perspex phantom (recommended diameter of 16 cm).

A first index requires measurements along a diameter of the phantom (Figure A3.5a) and is calculated as the mean of the dosimeter readings. A second index is obtained by measurements at the centre of the phantom and at points around the periphery, as the positions of weighted CTDI. An advantage of Index 1 is the possibility of measurements for on-axis and off-axis exposures, since a simple rotation of the phantom allows having always the isocentre of the FOV on the measuring diameter. On the other hand, index 2 is only suitable for symmetrical dose distributions.

APPENDIX 3 / **Discussion about Different In-Phantom Dosimetry Indexes**

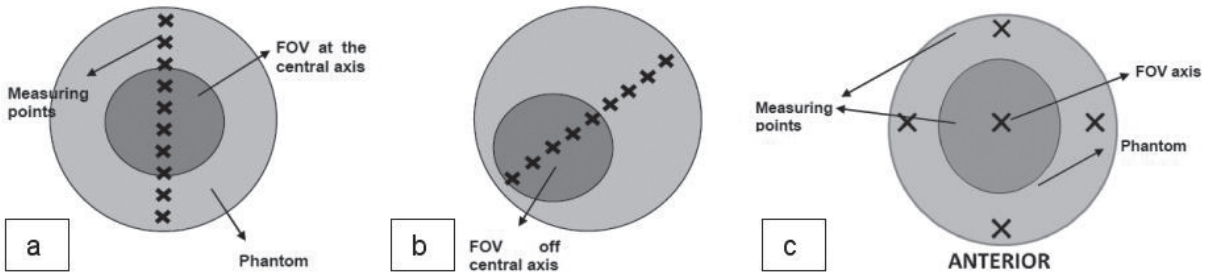

FIGURE A3.5. Sedentex-CT dose indexes: (a) and (b) show two possible configurations of index 1 with dosemeters positioned along the phantom diameter; (c) show the measurement positions for index 2.

These indexes are potential suitable not only for dental CT but also for other CBCT applications. Index 2 is easy to measure with a small volume ionization chamber positioned in a traditional CTDI phantom, and in this sense is similar to the central cumulative dose considered by the AAPM. One of the limitations of index 1 is related to the need of a custom phantom that allows the positioning of the ionization chamber or other dosemeters, such as TLDs along the phantom diameter. Another potential limitation is that it can be a time consuming method. In particular, when using an ionization chamber, about 10 measurements are needed along the diameter of the phantom.

APPENDIX 4

Examples of Free Analysis Software

APPENDIX 4 / **Examples of Free Analysis Software**

A 4.1. | IQWorks

IQWorks is a freely distributed program designed to provide automated image analysis of DICOM images, such as those obtained from CT.

It has a number of built of functions that allow the image quality tests recommended in this report to be carried out including: Region of interest analysis, Distance Measurement, Signal-to-noise ratio, MTF (edge/line analysis and PSF) and Noise Power Spectrum. Another feature of IQWorks is the automatic production of reports detailing the results of the tests.

More details and a download link can be found on the IQWorks website at www.iqworks.org.

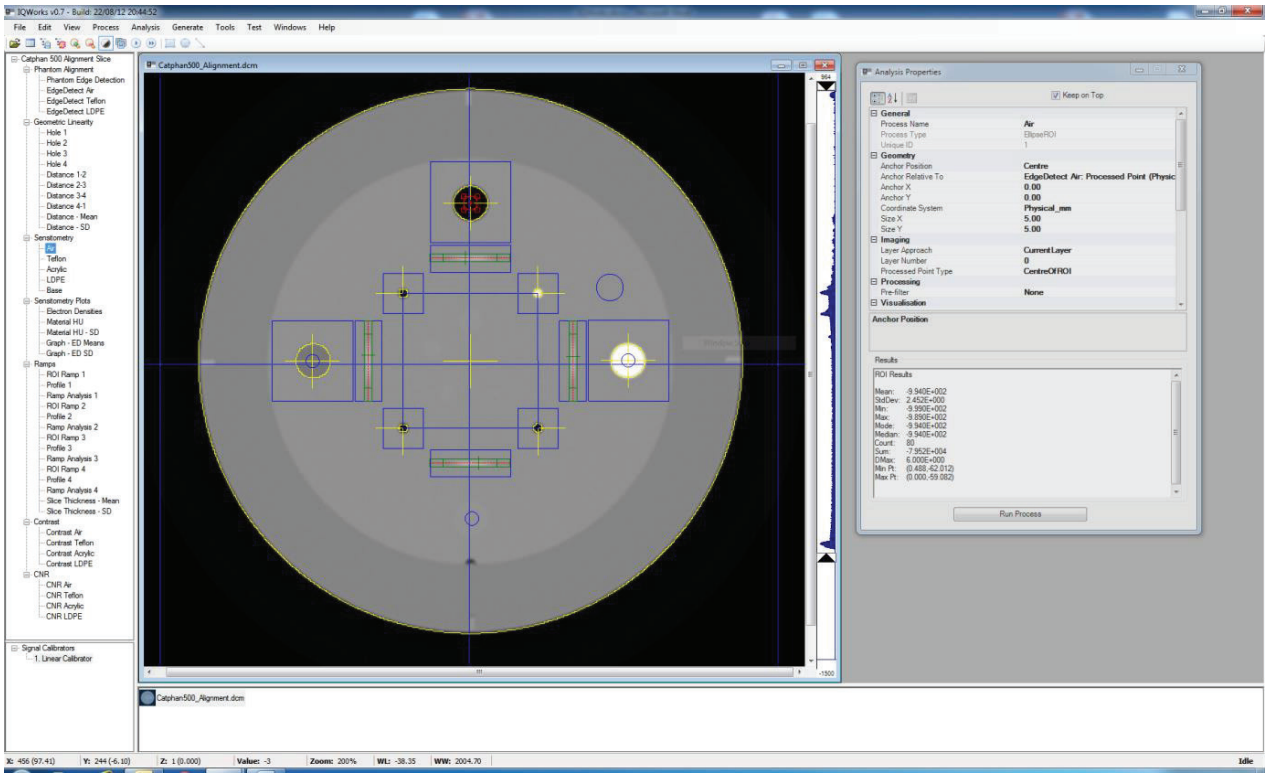

FIGURE A4.1.IQWorks being used to analyse the image of a phantom.

A 4.2. | ImageJ

Examples of ImageJ have been included in the text where appropriate. ImageJ is organized in windows that appear only when you are using their functions. As an example, figure A3.2.1. shows the windows of the main of ImageJ, a window showing a slice of a phantom (with two ROIs in the positions indicated in section 3.5 to measure the CNR), the "window/level" window and the window showing the results from the measurements of these ROIs.

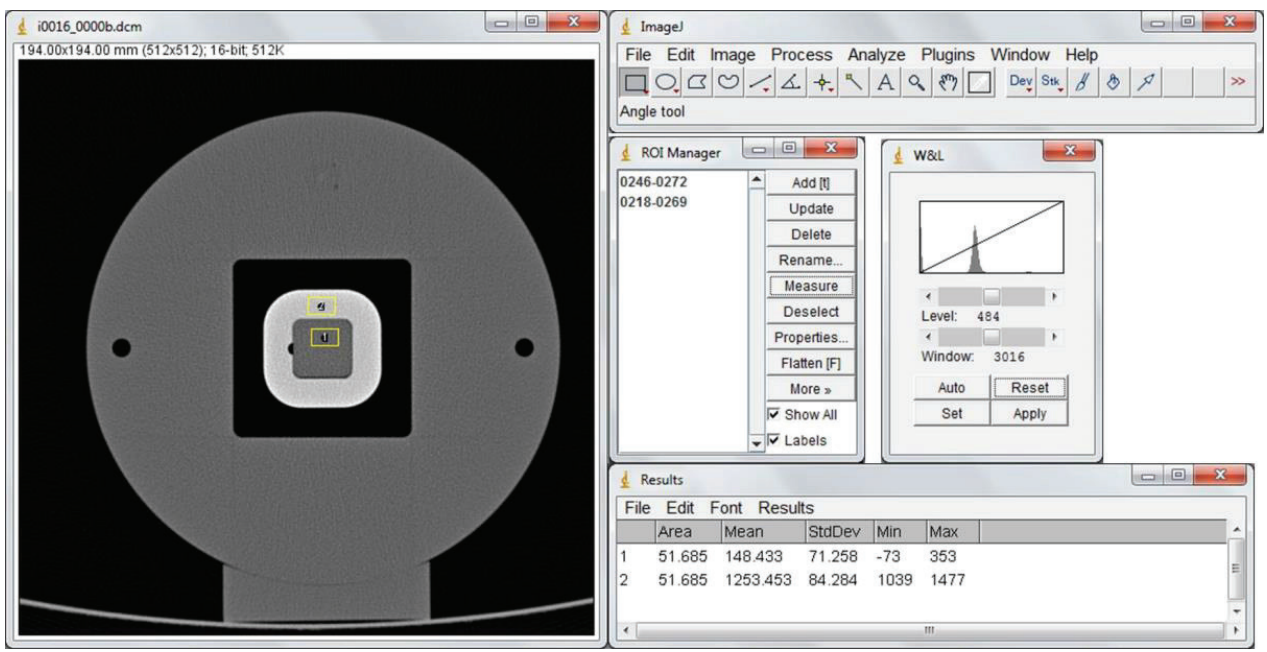

Figure A4.2. ImageJ being used to measure CNR in the slice image of a phantom

APPENDIX 5

Macro for Calculations of Noise Power Spectrum

APPENDIX 5

Macro for Calculations of Noise Power Spectrum

```
////////////////////////////////////////////////////////////////
//NPS_2D
//Computes the average NPS of a stack of 2D images from a uniform phantom
//Julia Garayoa Roca and Pablo Castro Tejero
////////////////////////////////////////////////////////////////

//get stack dimensions
Stack.getDimensions(width, height, channels, slices, frames);
Nim = slices;

//get pixel and image sizes
getPixelSize(unit,w_px,h_px);
H=getHeight();
W=getWidth();

//reset Measurements
run("Set Measurements...","area standard deviation min and max gray value centroid mean");

//set Threshold to locate phantom centre
setThreshold(-2000,-500);
```

```
doWand(H/2,W/2);
run("Measure");
x_c=getResult("X",nResults-1);
y_c=getResult("Y",nResults-1);
resetThreshold;

//create an internal Clipboard for each stack image (ROI 128 px x 128 px).
//subtract ROI mean pixel value
//compute Fourier Transform (FT) and |FT|^2
d = 128; //ROi size in pixel

for(i = 1; i< Nim+1; i++){
setSlice(i);
makeRectangle(x_c/w_px-d/2,y_c/h_px-d/2,d,d);
run("Copy");
run("Internal Clipboard");
run("32-bit");
```

APPENDIX 5 / Macro for Calculations of Noise Power Spectrum

```
//subtract ROI mean pixel value until it reaches a value < 0.0001
vm = 1e6;
     while (abs(vm) > 1e-4){
          selectImage("Clipboard");
          run("Measure");
          vm = getResult("Mean",nResults-1);
          run("Subtract...","value=vm");

    }

     //compute FFT: fft raw
    run("FFT Options...","," raw");
    run("FFT");
    selectImage("Clipboard");
    run("Close");
    selectImage("PS of Clipboard");
    rename(d2s(i,0));
    selectImage(1);
}
```

```
//average the NPS from each image.
run("Images to Stack", "name=NPSs title=[] use");
run("Z Project...", "start=1 stop=96 projection=[Average Intensity]");

//Multiply image by dimensional factors: w_px*h_px/d/d
factor=w_px*h_px/d/d;
run("Multiply...", "value=factor");
```

APPENDIX 6

Other Methods for Low-Contrast Evaluations

APPENDIX 6

Other Methods for Low-Contrast Evaluations

A 6.1. | Subjective methods

Groups of signals of different sizes and intensities are presented to several "observers", who may be medical doctors, physicists, radiographers or trained observers. The observers are asked to identify which of the presented signals are clearly distinguishable. The results from all observers are averaged and a final score is obtained that reflects the low-contrast resolution of the imaging system. These human observer studies are very complex and time consuming, thus they are not practical for quality control.

Apart from that, a great variation appears between the scorings of the same observer in different sessions (intra-observer variation) and between different observers (inter-observer variation). Despite that, subjective methods are indeed better than no quality control at all. Therefore, subjective methods are only acceptable if they are the only alternative that is available.

Example

In the case of one of the traditional phantoms used in CT image quality assessment, (see figure A6.1), the evaluation is strongly biased because the observer knows beforehand the distribution of the objects in the phantom. This can be overcome subtracting samples containing either the signals or background in the phantom images and showing them to the human observers in multiple-alternative forced choice experiments (M-AFC). Thus for each object analysed in the study, a proportion correct (PC) can be obtained for each observer[88]. A certain degree of subjectivity remains though, because different observers (and even the same observer in different moments), may have different opinions about what is "visible".

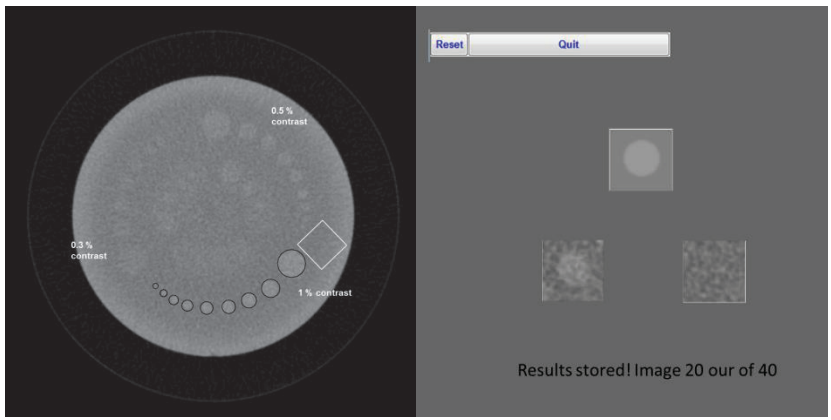

Figure A6.1.Left: A traditional phantom for subjective quality control. Right: Graphical user interface of a program designed to detect the signals of that phantom in an unbiased environment.

A 6.2. | Contrast-detail (using an objective method)

The objective method suggested here is based on Albert Rose's principle, proposed in 1948[89-92] regarding detectability of threshold signals in electronic systems that register photon events, like television cameras. For single photon events, Rose states that a signal which deviates by two standard deviations has a probability of 0.023 of being a noise fluctuation rather than a true, detectable threshold signal. The probability for signals deviating by three standard deviations is 0.0013.

For a two dimensional image of a homogeneous object (flat field image), the standard deviation in Rose's case corresponds to the standard deviation of the mean value for a large number of circular regions of interest (ROIs) of a certain size placed in the central 10% (area) of the slice. Uniformity is a key parameter for which a dental CBCT differs substantially from a medical CT. Due to its acquisition geometry and lack of beam shaping filters, a dental CBCT has, in general, poor uniformity performance.

APPENDIX 6 / **Other Methods for Low-Contrast Evaluations**

The pixel values at the periphery of a homogeneous phantom slice often differ more than 100 pixel units from those at the centre. The corresponding figure for a medical CT is around 3 to 5 pixel units. This is important to consider when evaluating low contrast resolution (the Contrast-Detail Diagram). Because of this lack of uniformity, the ROIs will all need to be placed in a limited area at the centre of the image, in the homogeneous part of the phantom. If not placed so, the mean value of the ROIs will show variation caused by poor uniformity rather than by random variations within a largely homogeneous area. Homogeneity of the phantom is necessary for the validity of Rose's statement[93,94,95]. For this reason, an area covering only the central 10% of the image area should be used for analysis.

The objective method to apply a contrast-detail analysis is reproduced here from Torgersen et *al*[97]. The number of ROIs examined should be around 1000 for a specified ROI size. The ROIs are randomly placed with their centres inside the central 10% area of the slice and are allowed to overlap. The mean pixel value in each ROI is measured and, after completion, the standard deviation of the mean values is calculated. The threshold value for low contrast detectability for an object with a size such as this ROI size is set to three times the standard deviation. This practically eliminates the possibility that a deviating signal is due to random variation. By repeating this procedure with 10 different ROI sizes, where ROI size number n will produce an ROI with a diameter of 2n times 1.5 pixels, a Contrast-Detail diagram can be created. Part of this procedure is illustrated in figure A6.2 below, where ROIs of three different sizes are presented. This objective method for producing a Contrast-Detail diagram has been recommended by the Swedish Radiation Safety Authority for determining the low contrast detectability of conventional medical CT scanners since 1995[96].

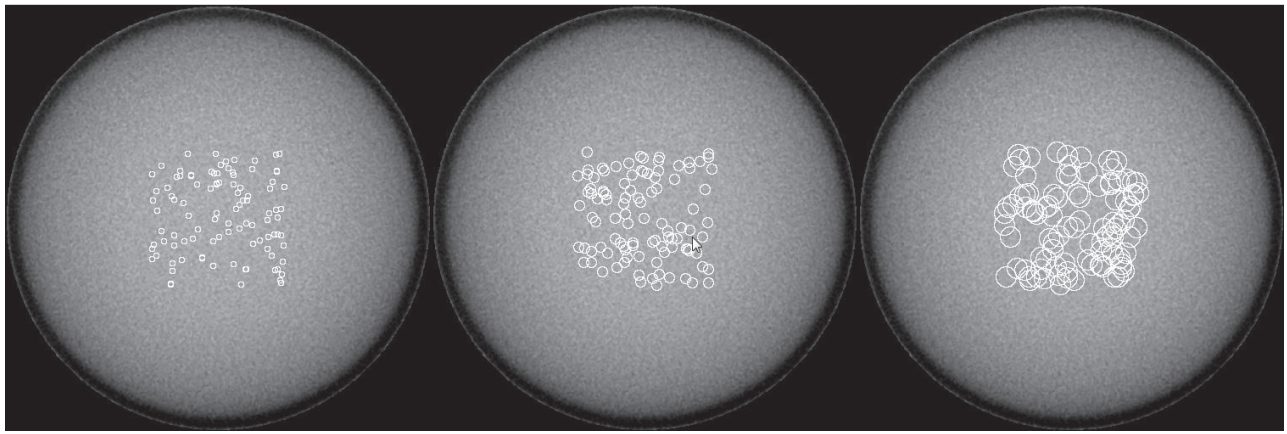

FIGURE A6.2. Placing of ROIs of three different sizes for the determination of the contrast-detail diagram.

The area under the contrast-detail curve can be used as an index to monitor the low contrast properties of the CBCT unit over time. Also, the sum of the mean pixel values for the 10 ROI sizes, which is equal to the signal response from the CBCT unit when exposed at a certain voltage (kV) and charge (mAs), produces a value that reflects the reproducibility and sensitivity of the system.

An example of a contrast-detail diagram for a dental CBCT unit is shown in figure A6.3. The method has been published in the paper by Torgersen et al[97].

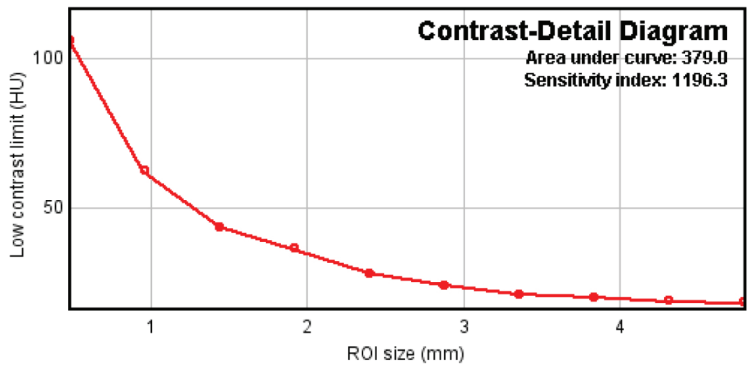

FIGURE A6.3. Contrast-detail diagram for a dental CBCT.

A 6.3. | Model observers

An evolution of subjective methods, which is feasible for digital imaging technologies, is the automatic evaluation of subtle signals by specific software. In general, this method requires the acquisition of many images to obtain a reliable and highly reproducible result. The computer can perform the evaluations very fast, but the acquisition of many images can be a problem in busy facilities and the storage of many tomographic series can be a burden for some PACS. Automatic detection of signals is an active area of research. In particular, the ability of certain software to simulate a human observer is critical, because a computer program can usually detect signals that our brain is not able to process. As opposed to that, sometimes human perception is able to detect signals that are invisible to the computer because they are almost completely hidden within the noisy background; the human brain can distinguish a signal within a pattern only because the person knows it has to be there.

For this reason, models can be useful tools to analyse how different acquisition or reconstruction parameters affect image quality in phantom images, but further research has to be done before using these models for clinical practice applications in CBCT.

Different model observers can be applied in quality control in CT. In particular, the non-prewhitening matched filter with an eye filter (NPWE) and the channelized Hotelling (CHO) model observers have reproduced human trends in low contrast detection tasks scoring CT phantom images acquired at varying dose levels[98,99,100,101]. These models include functions that aim to reproduce the detection process using different strategies. The NPWE model uses an eye filter to include the human contrast sensitivity function and the CHO model emulates the human vision process in the visual cortex as multiple channels, each of them sensitive to a narrow range of spatial frequencies. There are several eye filters and channels available in the literature. The model observer results can be tuned to fit human performance using efficiency parameters or adding internal noise.

The models perform measures in the samples subtracted from the phantom images, after applying different transformations (eye filter or channels), and from the test statistics, calculate a detectability index or d' for each object. The higher d' value implies better detection, as shown in figure A6.4., based on images of a low-contrast phantom and two model observers (NPWE and CHO).

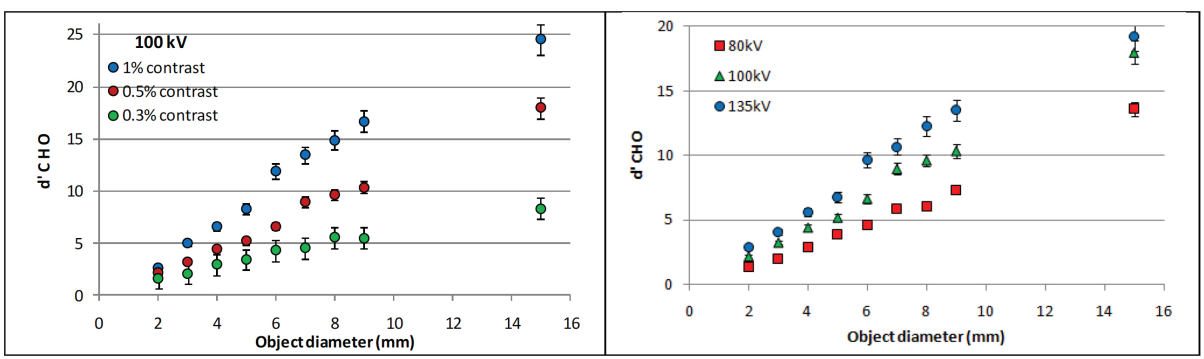

FIGURE A6.4. Examples of detectability evaluations using model observers in a geometrical image quality phantom.

APPENDIX 7

EURADOS-EFOMP Discussion on Patient Dosimetry for CBCT

APPENDIX 7
EURADOS-EFOMP Discussion on Patient Dosimetry for CBCT

Introduction

In recent years there have been several efforts to investigate the most robust dose index metric for CBCT that may be used for quality assurance (QA), as well as for the purpose of estimating patient dose. Although Effective Dose (ED) was by far the dominant dosimetry quantity, a range of other dose metrics was quoted in the published articles. These included Kerma-Area Product (KAP), Dose Length Product (DLP), Dose Height Product (DHP), CTDIw, CTDIvol, $CBDI_{W}$, Central axis dose or "Dose to the field of view" (D_{FOV}), $DPI_{100,c}$ (Dose Product Integral), DI (Dose Index) and incident air kerma. In a recent study a new model of calculation of the incident air kerma at the patient skin is proposed, universally applicable to all MSCT and CBCT equipment [A1].

There is presently no consensus on a standardization of radiation dosimetry for CBCT applications, and the situation with two (or more) QA metrics for radiation dosimetry with CBCT will continue until such consensus is reached. This is also due to the difference in the acquisition technique and the type of exam between the various applications.
In this section, several efforts for estimating patient dose with CBCT applications are summarized for the benefit of the clinical medical physicist responsible for optimization of image quality and radiation dose.

For convenience, the analysis has been made grouping the CBCT applications in three categories:

- Radiotherapy
- Interventional radiology and guided surgery
- Dental and Maxillofacial

For this appendix the references are numbered as A1, A2, A3... etc. The references indicated within the tables are numbered with single figures (1,2,3... etc).

A1 de las Heras Gala H, Schöfer F, Schöfer H, Sánchez Casanueva RM et al. A patient-centric approach to quality control and dosimetry in CT including CBCT. Physica Medica. 2018;47:92-102.

5.4.1 | Radiotherapy applications

CBCT systems were integrated into a radiotherapy treatment room after the publication of Jaffray et. al. [A2;A3] in 1998 and became commercially available in 2005 [A4]. The CBCT system enables a sequence of 2D radiographic projection images to be acquired from a kV source and flat panel detector imaging system as it rotates around the patient either before treatment or during it. The reconstructed CBCT images can be used to correct patient position prior to treatment or as a basis to adapt the treatment plan to the changing anatomy of the patient during the course of their radiotherapy. The introduction of CBCT for Image Guided Radiation Therapy (IGRT) proceeded initially with little regard for the extra radiation dose delivered by the imaging system. The generalized justification for this was that the benefits of IGRT will outweigh the increased risks from the CBCT dose. However, more recently there has been increased concern for the concomitant imaging dose.

Over 120 publications of interest were identified, including 8 review papers. The most relevant results are reported here. They can be grouped in two major categories: studies using physical phantoms combined with different types of dosimeters and studies based on Monte Carlo simulations combined with voxelized phantoms.

The majority of the papers were focused on physical phantom studies. Different types of phantoms have been used: anthropomorphic male/female phantoms, CT and radiotherapy phantoms, different types of custom phantoms. In the same way, several different dosimeters have been adopted (predominantly TLD, followed by MOSFET, ionization chambers, radiochromic films, OSL, diodes, RPL and gel dosimetry) with the purpose of estimating organ dose (including skin dose) as well as point dose.

APPENDIX 7 | EURADOS-EFOMP Discussion on Patient Dosimetry for CBCT

The rest of the papers dealt with Monte Carlo calculations, with or without comparison against experimental results, performed both on adult and paediatric voxel phantoms. There are two main research groups who have developed Monte Carlo (MC) models of CBCT imaging systems. Spezi et al [A5] have developed a model for one commercial CBCT scanner using EGSnrc/BEAMnrc and BEAMPP. Ding et al [A6] have developed their MC model of a different commercial CBCT scanner using the EGSnrc/BEAMnrc code in their early work and more recently with the BEAM/DOSXYZnrc code. Chow [A7] has also modelled one the same commercial system of Spezi using BEAMnrc and a Matlab based implementation of DOSXYZnrc.

An extensive review has been published by Alaei P. and Spezi E. (18). This review summarizes the imaging dose delivered to patients as the result of CBCT imaging performed in radiation therapy using current methods and equipment. It also summarizes methods to calculate imaging dose including the use of Monte Carlo and treatment planning systems. Peripheral dose from CBCT imaging, dose reduction methods, the use of effective dose in describing imaging dose and the measurement of CTDI in CBCT systems are also discussed.

The reviewed publications displayed a wide range of variability for the indication, protocol, system and methodologies used to estimate the doses. $CBDI_w$ (weighted cone-beam dose index) can be adopted as good metrology to compare the different protocols and optimize them.

CBDIw reflects the variation of dose deposition at depth by differentially weighting peripheral (p) and central (c) doses measured in standard CTDI phantoms.

APPENDIX 7 | EURADOS-EFOMP Discussion on Patient Dosimetry for CBCT

Organ doses can be important and should be taken into consideration in order to evaluate the total dose to organs from radiotherapy and associated imaging

The review of existing recommendations and the suggestion of a comprehensive and clinically implementable approach are required. Paediatric patients require more studies with respect to both acquisition protocols and dose optimization. The results have been summarized in table A7.1, which is divided for different body parts (head and neck, chest, abdomen and pelvis, prostate, breast and lung), or purpose (e.g. Spotlight), showing the dose indicator used in the paper, the used methodology and the related reference identification.

Treatment	Dose indicator	Range	Methodology	Ref.
Head and neck	Effective Dose	0.03 ÷ 0.06 mSv	MC simulations (GATE), ICRP voxel phantoms linac CBCT	*1*
		8.54 mSv	MC simulations MCNPX Computational phantom	*2*
		2.8 ÷ 10 mSv	TLD + Phantom	*3,4*
		0.11 ÷ 0.76 mSv/100 mAs	MC simulations (DOSXYZnrc)	*21*
	Organ Doses	0.82 ÷ 1.01 mGy	TLD + anthropomorphic phantom Organs entirely within the irradiation field linac CBCT	*5*
		4.09 ÷ 8.28 cGy	Standard mode, Cardiac torso phantom, Geant4 Application for Tomographic Emission (GATE)	*6*

Table A7.1. Summary of the range of doses, represented as (minimum dose ÷ maximum dose or value ± uncertainty) for different body parts, dose indicators and methodologies retrieved from the reviewed papers for radiotherapy applications.

APPENDIX 7 | EURADOS-EFOMP Discussion on Patient Dosimetry for CBCT

Treatment	Dose indicator	Range	Methodology	Ref.
Head and neck	Organ Doses	1.61 ÷ 1.89 cGy	Low dose mode, Cardiac torso phantom, Geant4 Application for Tomographic Emission (GATE)	*6*
		0.03 ÷ 4.91 cGy	Radiochromic films, Anthropomorphic phantom	*7*
		5 ÷ 23 cGy	Vanderbilt-Monte-Carlo-Beam-Calibration algorithm, Pediatric (29 m)	*8*
		3.2 ÷ 3.5 mGy	Optically stimulated luminescence dosimeters (OSLD), linac CBCT	*9*
		0.27 ÷ 5.78 mGy/100 mAs	MC simulations (DOSXYZnrc)	*21*
		6.38 ÷ 8.30 mGy	Monte Carlo (MCNP6 and GATE)	*22*
	Phantom dose	0.09 ÷ 0.11 cGy	Head phantoms, Farmer cylindrical chamber	*10*
	$CBDI_W$	5.17 mGy (Varian) 0.98 mGy (Elekta)	Pencil chamber CTDI phantom	*11*
	D_{FOV}	4.2 ÷ 8.8 mGy	Solid-state probe	*19*
	KAP	1.5 ÷ 2.7 Gy cm^2	KAP meter	
	Incident air kerma	1.5 ÷ 3.2 mGy (pending further validation)	PAKT method Solid-state probe	
Chest	Effective Dose	1.38 ÷ 3.19 mSv	MC simulations (GATE) ICRP voxel phantoms, linac CBCT	*1*
		24 mSv	TLD + Phantom	*4*
		1.04 ÷ 5.60 mSv/100 mAs	MC simulations (DOSXYZnrc)	*21*
	Organ Doses	7.9 ÷ 22.3 mGy	TLD + anthropomorphic phantom, Organs entirely within the irradiation field, linac CBCT	*5*
		1.33 ÷ 1.85 cGy/scan	MC simulations, Computational phantoms, linac CBCT	*12*
		0. 70 ÷ 3.15 cGy	Radiochromic films, Anthropomorphic phantom	*7*
		0.61 ÷ 17.28 mGy/100 mAs	MC simulations (DOSXYZnrc)	*21*
		15.17 ÷ 16.88 mGy	Monte Carlo (MCNP6 and GATE)	*22*

APPENDIX 7 | EURADOS-EFOMP Discussion on Patient Dosimetry for CBCT

Treatment	Dose indicator	Range	Methodology	Ref.
Chest	Phantom dose	2.19 ÷ 2.51 cGy	Body phantoms Farmer cylindrical chamber	*10*
	$CBDI_W$	6.14 mGy (Varian) 16.62 mGy (Elekta)	Pencil chamber CTDI phantom	*11*
	D_{FOV}	8.8 ± 0.5 mGy	Solid-state probe	*19*
	KAP	4.5 ± 0.3 Gy cm^2	KAP meter	
	Incident air kerma	3.9 ± 0.3 mGy (pending further validation)	PAKT method Solid-state probe	
Abdomen and Pelvis	Effective Dose	1.11 ÷ 2.80 mSv	MC simulations (GATE) ICRP voxel phantoms linac CBCT	*1*
		14.3 mSv	TLD + Phantom	*3*
		2.73 ÷ 13.99 mSv/100 mAs	MC simulations (DOSXYZnrc)	*21*
	Organ Doses	13.5 ÷ 22.3 mGy	TLD + Rando Alderson phantom Organs entirely within the irradiation field linac CBCT	*5*
		4.30 ÷ 7.48 cGy	Standard mode Cardiac torso phantom Geant4 Application for Tomographic Emission (GATE)	*6*
		0.79 ÷ 1.85 cGy	Low dose mode Cardiac torso phantom Geant4 Application for Tomographic Emission (GATE)	*6*

APPENDIX 7 | EURADOS-EFOMP Discussion on Patient Dosimetry for CBCT

Treatment	Dose indicator	Range	Methodology	Ref.
Abdomen and Pelvis	Organ Doses	0.50 ÷ 6.50 cGy	Radiochromic films Anthropomorphic phantom	*7*
		3 ÷ 17 cGy	Vanderbilt-Monte-Carlo-Beam-Calibration algorithm Pediatric (29 m)	*8*
		2.22 ÷ 47.94 mGy/100 mAs	MC simulations (DOSXYZnrc)	*21*
		24.15 ÷ 53.70 mGy	Monte Carlo (MCNP6 and (GATE)	*22*
	Absorbed Dose	0.0 ÷ 7.2 cGy	5y Anthropomorphic phantom MOSFET	*13*
	$CBDI_w$	21.57 mGy (Varian) 24.13 mGy (Elekta)	Pencil chamber CTDI phantom	*11*
	D_{FOV}	35 ± 2 mGy	Solid-state probe	*19*
	KAP	18 ± 2 Gy cm^2	KAP meter	
	Incident air kerma	15.5 ± 1.0 mGy (pending further validation)	PAKT method Solid-state probe	
Prostate	Effective Dose	6.25 mSv	MC simulations MCNPX, Computational Phantom	*2*
	Organ Doses	2.5 ÷ 3. 1 cGy	Anthropomorphic phantoms TLDs	*14*
		29.1 ÷ 30.2 mGy Other organs: 0.1 ÷ 37.8 mGy	Rando phantom with TLD and PCXMC estimations	*20*
	Phantom dose	2.94 ÷ 3.51 cGy	Body phantoms Farmer cylindrical chamber	*10*
	$CBDI_w$	17.2 mGy (Varian)	Pencil chamber CTDI phantom	*15*

APPENDIX 7 | EURADOS-EFOMP Discussion on Patient Dosimetry for CBCT

Treatment	Dose indicator	Range	Methodology	Ref.
Breast	Effective Dose	2.01 mSv left breast setup 2.45 mSv right breast setup	Female anthropomorphic phantom and TLD	*16*
		15.3 mSv	Phantom TLD	*3*
	Organ Doses	3.9 ÷ 6.4 mGy	Female anthropomorphic phantom and TLD	*16*
Lung	Organ dose	10 ÷ 50 mGy	Anthropomorphic phantoms TLD	*17*
Spotlight	D_{FOV}	44 ± 3 mGy	Solid-state probe	*19*
	KAP	13.8 ± 0.9 Gy cm2	KAP meter	
	Incident air kerma	16.3 ± 0.9 mGy (pending further validation)	PAKT method Solid-state probe	

References of the radiotherapy part

A2 Jaffray D A, Drake D G, Pan C and Wong J W 1996 Cone beam CT using a clinical fluoroscopic portal imager EPI 96, 4th Int. Workshop on Electronic Portal Imaging (10-12 June 1996, Amsterdam)

A3 Jaffray DA, Drake DG, Moreau M, Martinez AA, Wong JW. A radiographic and tomographic imaging system integrated into a medical linear accelerator for localization of bone and soft-tissue targets. 1999 International Journal of Radiation Oncology Biology Physics. 45: 773-789.

A4 Sykes JR, Lindsay R, Iball G and Thwaites DI. Dosimetry of CBCT: methods, doses and clinical consequences, Journal of Physics: Conference Series 444 (2013) 012017.

APPENDIX 7 | EURADOS-EFOMP Discussion on Patient Dosimetry for CBCT

A5 Spezi E, Downes P, Radu E, Jarvis R. Monte Carlo simulation of an x-ray volume imaging cone beam CT unit. Med Phys. 2009 Jan;36(1):127-36.

A6 Ding GX, Duggan DM, Coffey CW. Accurate patient dosimetry of kilovoltage cone-beam CT in radiation therapy. Med Phys. 2008;35(3):1135–44.

A7 Chow JC. Cone-beam CT dosimetry for the positional variation in isocenter: a Monte Carlo study. Med Phys. 2009 Aug;36(8):3512-20.

1 Marchant TE, Joshi KD. Comprehensive Monte Carlo study of patient doses from cone-beam CT imaging in radiotherapy. J Radiol. Prot. 2017;37(1):13–30.

2 Gu J, Bednarz B, Xu XG, Jiang SB. Assessment of patient organ doses and effective doses using the VIP-Man adult male phantom for selected cone-beam CT imaging procedures during image guided radiation therapy. Radiat Prot Dosimetry. 2008;131(4):431–43.

3 Sawyer LJ, Whittle SA, Matthews ES, Starritt HC, Jupp TP. Estimation of organ and effective doses resulting from cone beam CT imaging for radiotherapy treatment planning. Br J Radiol. 2009;82(979):577–84.

4 Kan MW, Leung LH, Wong W, Lam N. Radiation dose from cone beam computed tomography for image-guided radiationtherapy. Int J Radiat Oncol Biol Phys. 2008;70(1):272–79.

APPENDIX 7 | EURADOS-EFOMP Discussion on Patient Dosimetry for CBCT

5 Osvaldo Rampado, Francesca Romana Giglioli, Veronica Rossetti, Christian Fiandra, Riccardo Ragona, and Roberto Ropolo, Evaluation of various approaches for assessing dose indicators and patient organ doses resulting from radiotherapy cone-beam CT, Medical Physics, 3, 2515 (2016); doi: 10.1118/1.4947129

6 Kihong Son, Seungryong Cho, Jin Sung Kim, Youngyih Han, Sang Gyu Ju, Doo Ho Choi, Evaluation of radiation dose to organs during kilovoltage cone-beam computed tomography using Monte Carlo simulation, Journal of applied Clinical Medical physics Vol 15, 2, 2014

7 Ahmad Nobah, Saad Aldelaijan, Slobodan Devic, 3 Nada Tomic, Jan Seuntjens, Mohammad Al-Shabanah, Belal Moftah, Radiochromic flm based dosimetry of image-guidance procedures on different radiotherapy modalities, Journal of applied Clinical Medical physics Vol 15, 6, 2014

8 Ding GX, Coffey CW. Radiation dose from kilovoltage cone beam computed tomography in an image-guided radiotherapy procedure. Int J Radiat Oncol Biol Phys. 2009;73(2):610–17.

9 Smith L, Mamoon H, Morales J et al. Radiation dose measurements of on-board imager X-ray unit using optically-stimulated luminescence dosimeters
Australasian Physical & Engineering science in Medicine 2015;38(4):665–669.

10 Daniel Scandurra, and Catherine E. Lawford, A dosimetry technique for measuring kilovoltage cone-beam CT dose on a linear accelerator using radiotherapy equipment, Journal of applied Clinicl Medical Physics Vol 15, 4, 2014

APPENDIX 7 | EURADOS-EFOMP Discussion on Patient Dosimetry for CBCT

11 Hyer DE, Hintenlang DE Estimation of organ doses from kilovoltage cone-beam CT imaging used during radiotherapy patient position verification. Med Phys. 2010 Sep;37(9):4620-6.

12 Zhang Y, Wu H, Chen Z, Knisely JPS, Nath R, Feng Z, Bao S, Deng J. Concomitant Imaging Dose and Cancer Risk in Image Guided Thoracic Radiation Therapy
Int J Radiat Oncol Biol Phys. 2015;93(3):523–531.

13 Kim S, Yoshizumi TT, Frush DP, Toncheva G, Yin FF. Radiation dose from cone beam CT in a pediatric phantom: risk estimation of cancer incidence., AJR Am J Roentgenol. 2010 Jan;194(1):186-90. CHILDREN PAPER

14 Jeng S-C, Tsai C-L, Chan W-T, Tung C-J, Wu J-K, Cheng JC-H. Mathematical estimation and in vivo dose measurement for cone-beam computed tomography on prostate cancer patients. Radiother Oncol. 2009;92(1):57–61.

15 Walter C, Boda-Heggemann J, Wertz H, et al. Phantom and in-vivo measurements of dose exposure by imageguided radiotherapy (IGRT): MV portal images vs. kV portal images vs. cone-beam CT. Radiother Oncol. 2007;85(3):418–23.

16 Alexandra Quinn, Lois Holloway, PJ Jarrad Begg, Vinod Nelson, and Peter Metcalfe, FinstP, Kilovoltage cone-beam CT imaging dose during breast radiotherapy: A dose comparison between a left and right breast setup, Med Dosim. 2014 Summer;39(2):190-3.

APPENDIX 7 | EURADOS-EFOMP Discussion on Patient Dosimetry for CBCT

17 Steiner E, Stock M, Kostresevic B, Ableitinger A, Jelen U, Prokesch H, Santiago A, Trnková P, Wolf A, Wittig A, Lomax A, Jäkel O, Baroni G, Georg D., Imaging dose assessment for IGRT in particle beam therapy., Radiother Oncol. 2013 Dec;109(3):409-13.

18 Alaei P, Spezi E. Imaging dose from cone beam computed tomography in radiation therapy Phys Med. 2015; 31(7):647-658.

19 de las Heras Gala H, Schöfer F, Schöfer H, Sánchez Casanueva RM et al. A patient-centric approach to quality control and dosimetry in CT including CBCT. Physica Medica. 2018;47:92-102.

20 Wood TJ, Moore CS, Saunderson JR, Beavis AW. Validation of a technique for estimating organ doses for kilovoltage cone-beam CT of the prostate using the PCXMC 2.0 patient dose calculator. J. Radiol. Prot. 2015;35:153–163.

21 Abuhaimed A and Martin CJ. Evaluation of coefficients to derive organ and effective doses from cone-beam CT (CBCT) scans: a Monte Carlo study. J. Radiol. Prot. 2018;38:189–206.

22 Ardenfors O, Henry T, Gudowska I, Poludniowski G and Dasu A. Organ doses from a proton gantry-mounted cone-beam computed tomography system characterized with MCNP6 and GATE. Physica Medica. 2018;53:56-61.

5.4.2 | Interventional applications

C-arm cone-beam CT (often called Flat detector CT or FD-DT) provides high- and low-contrast soft tissue ("CT-like") images in multiple viewing planes. Because of this enhanced 3D imaging capability, C-arm cone-beam CT offers more subtle vascular and soft tissue information and constitutes a substantial improvement over conventional single-planar digital subtraction angiography (DSA) and fluoroscopy. Although C-arm cone-beam CT has been in development for the past two decades, it has only been applied in the interventional radiology clinic in recent years. Potential vascular applications of C-arm cone-beam CT include its use for pre-procedure anatomic diagnosis and treatment planning, intra-procedure device or implant positioning assessment, and post-procedure assessment of procedure endpoints.

C-arm cone-beam CT image-guided tumour therapy is one of the fastest growing applications in radiology; it applies to all body regions and includes tumour embolization and radiofrequency ablation. Vascular interventions for treatment of aneurysms and arteriovenous malformations, stent imaging and angioplasties are also growing in importance. Angiographic C-arm cone-beam CT is particularly helpful during neuro-interventional procedures, i.e. intracranial stenting for cerebrovascular stenosis, stent- assisted coil-embolization of wide-necked cerebral aneurysms and embolization of arteriovenous malformations of the brain. Additionally, by providing morphologic images of the brain within the angio suite C-arm, cone-beam CT is able to work up periprocedural haemorrhage in the rare cases of intraprocedural aneurysm or AVM rupture and may thus significantly improve immediate complication management without the need to transfer the patient to the CT suite. Spinal interventions such as kyphoplasty or vertebroplasty also benefit from Flat Detector CT.

Intra-operative imaging has also shown an impressive upward trend over the past few years. It is focused on orthopaedic and trauma surgery, such as joint replacements and spine surgery. Similar to the situation in the interventional suite, it allows immediate and conclusive control of the surgical intervention, as for example the correct placement of screws without impairment of joint function.

APPENDIX 7 | EURADOS-EFOMP Discussion on Patient Dosimetry for CBCT

A literature review focusing on C-arm cone-beam CT imaging was undertaken. Over 60 relevant papers were identified. The papers dealing with dosimetry for procedures performed with C-arms have been divided in the following sub-categories:

- Neuro-interventions
- Vascular Procedures
- Non-Vascular procedures
- Surgery

All dose evaluations have been performed either in phantoms (e.g. adult Alderson Rando) using TLDs and Mosfets and estimating organ doses and effective dose and on procedures performed on real patients, simulating the irradiation with the PCXMC software (Stuk, Helsinki, FI*) based on the ICRP 103 [A8] weight coefficients and the KAP provided by the equipment (derived from the RDSR for irradiation event or an average) as original value.

The results of the reviewed paper for this appendix have been summarized in table A7.2, which is divided into different procedures (neuro, vascular, non-vascular and surgery), showing the dose indicator used in the paper, the used methodology and the related reference identification.

* See website: http://www.stuk.fi/palvelut/pcxmc-a-monte-carlo-program-for-calculating-patient-doses-in-medical-x-ray-examinations

APPENDIX 7 | EURADOS-EFOMP Discussion on Patient Dosimetry for CBCT

Table A7.2. Summary of the range of doses, represented as (minimum dose ÷ maximum dose) or (average ± st. dev) for different procedures (neuro, vascular, non-vascular and surgery) dose indicators and methodologies retrieved from the reviewed papers for interventional applications.

Procedure	Dose indicator	Range	Methodology	Ref.
Neuro	CTDI	9 mGy (high contrast) 75 mGy (soft tissue)	105 Clinical patients (217 scans) 172 high contrast 45 soft tissue	1
	Effective Dose	0.30 ± 0.08 mSv	48 patients Monte Carlo (PCXMC, STUK, FI) TLDs using a human-shaped phantom.	2
		Soft tissue: 0.4 mSv (low dose) 1.87 mSv (high dose) High Contrast: 0.16 mSv (low dose) 0.24 mSv (high dose)	Organ dose (mosfet + anthropomorphic adult male phantom) Monte Carlo (PCXMC, STUK, FI)	3
		0.83 ÷ 1.6 mSv	99 clinical procedures + anthropomorphic adult male phantom	4
		0.47 ÷ 1.2 mSv	anthropomorphic phantom small sized silicon-photodiode	5

Neuro	Effective Dose	0.38 ÷ 0.87 mSv	Anthropomorphic adult male phantom MOSFET	6
		0.3 ± 0.08 mSv	Anthropomorphic phantom TLD, CTDI Phantom Pencil Chamber	7, 13
		4.4 ÷ 5.4 mSv	Anthropomorphic adult phantom TLD High and low dose protocols	10
	KAP	9.41 ± 2.50 Gy·cm^2	48 patients KAP meter	2
		11.75 ÷ 23.5 Gy·cm^2	99 clinical procedures + Anthropomorphic adult male phantom	4
		5.99 ÷ 9.61 Gy·cm^2	Anthropomorphic adult male phantom MOSFET	6
		9.4 ± 2 Gy·cm^2	Anthropomorphic phantom TLD	7
		9 ÷ 43 Gy·cm^2	KAP meter	31
	Organ Dose	Brain dose: 16 ÷ 32 mGy	99 clinical procedures + anthropomorphic adult male phantom	4
		Brain dose: 14 ÷ 37 mGy	Anthropomorphic phantom Small sized silicon-photodiode	5
		Brain dose: 5 ÷ 6 mGy	Anthropomorphic adult male phantom MOSFET	6
		Brain dose: 6 mGy	Anthropomorphic phantom TLD	7

APPENDIX 7 | EURADOS-EFOMP Discussion on Patient Dosimetry for CBCT

Neuro	D_{FOV}	21 ÷ 88 mGy	Solid-state probe	31
	Incident air kerma	7.6 ÷ 32.2 mGy (pending further validation)	PAKT method Solid-state probe	
Vascular	Effective Dose	4 ÷ 5 mSv	Abdominal protocol Anthropomorphic phantom Small sized silicon-photodiode	5
		1.1 ÷ 7.4 mSv	40 patients – Abdominal Aneurysm Monte Carlo (PCXMC, STUK, FI)	8
		15 ÷ 37 mSv	Anthropomorphic adult phantom TLD High and low dose abdomen protocols	10
		11.5±2.3 mSv (male) 11.3±3.0 mSv (female)	125 patients – liver embolization Anthropomorphic adult phantom TLD	11
		1.9 mSv (small ph.) 2.2 mSv (medium ph.) 2.1 mSv (large ph.)	Anthropomorphic phantom (3 sizes) TLD + Monte Carlo	12
		6.01 ÷ 7.32 mSv (chest) 7.04÷ 7.48mSv (abdomen)	Anthropomorphic phantom TLD	7
	KAP	3.7 ÷ 25.6 Gy·cm^2	40 patients – Abdominal Aneurysm Monte Carlo (PCXMC, STUK, FI)	8
		21.58 ÷ 42.62 Gy·cm^2	126 patients – TACE	9
		61.0 ± 6.6 Gy·cm2 (male) 52.2 ± 8.3 Gy·cm2 (female)	125 patients – liver embolization	11

APPENDIX 7 | EURADOS-EFOMP Discussion on Patient Dosimetry for CBCT

Vascular	Entrance Surface Dose	81.36 ÷ 157.83 mGy	126 patients – TACE	9
	Organ dose	0.3 ÷ 13. 3 mGy	Anthropomorphic phantom (3 sizes) TLD + Monte Carlo	12
Non vascular	Effective Dose	0.98 ÷ 1.15 mSv	Anthropomorphic phantom (3 sizes) TLD Endobronchial procedure	15
		7.6 mSv (upper thorax) 12.3 mSv (lower thorax) 16.1 mSv (upper abdomen) 13.4 mSv (lower abdomen)	MonteCarlo calculations	16
		5.4 ÷ 8.39 mSv (Spine) 17.10 ÷ 36.59 mSv (Biliar)	Anthropomorphic adult male phantom MOSFET	6
	Organ Doses	0.32 ÷ 0.48 mSv (Lungs)	Anthropomorphic phantom (3 sizes) TLD Endobronchial procedure	15
	KAP	16.5 ÷ 126.5 Gy·cm^2	Renal biopsy – 41 procedures KAP meter	17
		8.39 ÷ 36.59 Gy·cm^2 (spine) 4.63 ÷ 24.31 Gy·cm^2 (biliar)	Anthropomorphic adult male phantom MOSFET	6

APPENDIX 7 | EURADOS-EFOMP Discussion on Patient Dosimetry for CBCT

Non vascular	$CTDI_w$ – like	1.2 ÷ 12.50 mGy Lumbar spine 3.70 ÷ 11.5 mGy Thoracic spine	CTDI Phantom Pencil Chamber	13
		1.8 mGy (thoracic bone) 3.2 mGy (lumbar bone) 4.3 mGy (thoracic soft tissue) 10.6 mGy (lumb. soft tissue)	CTDI Phantom 0.6 cc Farmer chamber	14
Surgery	Effective Dose	0.5 ÷ 5.9 mSv (1y) 0.5 ÷ 6.3 mSv (5y) 0.4 ÷ 8.3 mSv (12y)	Spine surgery(O-arm) Pediatrics PCXMC Standard and low dose protocols	19
		0.02 ÷ 0.8 mSv	Head and neck surgery PMMA cylindrical head phantoms 0.6 cc Farmer chamber	20
		0.35 ÷ 17.1 mSv	Urology Anthropomorphic phantom TLD	21
		7 ÷ 9 mSv	Pediatric Spine surgery DLP and conversion factors	23, 24,25

Surgery	Effective Dose	0.2 ÷ 1.1 mSv (Thoracic) 0.1 ÷ 8.6 mSv (Lumbar) 0.3 ÷ 20 mSv (Whole)	Spine surgery (O-arm) Adolescent PCXMC	26
		3.24 ± 0.04 mSv (small) 6.48 ± 0.08 mSv (medium) 9.72 ± 0.12 mSv (large)	Spine surgery (O-arm) TLD	27
		0.064 mSv (Low Dose) 0.15 mSv (High Quality)	Extremities surgery Dedicated cone-beam CT system 15 cm PMMA phantom 0.6 cc farmer chamber	28
		0.06 mSv	Extremities surgery PMMA Phantom TLD	30
	$CTDI_w$	1.2 ÷ 16.6 mGy (1y) 1.5 ÷ 14.4 mGy(5y) 1.6 ÷ 14.5 mGy (12y)	Spine surgery (O-arm) Pediatrics PMMA cylindrical phantoms (1y, 5y, 12y) Pencil chamber Standard and low dose protocols	19
		0.025 ÷ 0.11 mGy/mAs	Head and neck surgery PMMA cylindrical head phantoms 0.6 cc Farmer chamber	20
		1.7 ÷ 2.2 mGy	Extremities CTDI provided by the unit	29
	DLP	446.62 Gy·cm	Orthopedy (O-arm) 23 patients	22
	Organ dose	0.01 ÷ 33.6 mGy (Thoracic) 0.03 ÷ 7.9 mGy (Lumbar)	Spine surgery (O-arm) Adolescent PCXMC	26

APPENDIX 7 | EURADOS-EFOMP Discussion on Patient Dosimetry for CBCT

References of the interventional part

A8 The 2007 Recommendations of the International Commission on Radiological Protection; ICRP 103

1 Y. Kyriakou et al Neuroradiologic Applications with Routine C-arm Flat Panel Detector CT: Evaluation of Patient Dose Measurements, AJNR 29 Nov-Dec 2008
2 Mei Bai, Xianghua Liu, Bin Liu Effective patient dose during neuroradiological C-arm CT procedures, Diagn Interv Radiol 2013; 19:29–32
3 Wang C et al; Evaluation of patient effective dose of neurovascular imaging protocols for C-arm cone-beam CT; AJR Am J Roentgenol. 2014 May;202(5):1072-7. doi: 10.2214/AJR.13.11001
4 Sanchez RM et al; Brain radiation doses to patients in an interventional neuroradiology laboratory; AJNR Am J Neuroradiol. 2014 Jul;35(7):1276-80
5 Koyama S, Aoyama T, Oda N, et al.Radiation dose evaluation in tomosynthesis and C-arm cone-beam CT examination with an an-thropomorphic phantom.Med Phys2010;37:4298–306
6 Kim S, Sopko D, Toncheva G, et al.Radiation dose from 3D rotational X-ray imaging: organ and effective dose with conversion factors.Radiat Prot Dosimetry 2012;150:50–54
7 Bai M, Liu X, Liu B..Effective patient dose during neuroradiological C-arm CT procedures. Diagn Interv Radiol2013;19:29–32
8 Anna M. Sailer et al; Radiation Exposure of Abdominal Cone Beam Computed Tomography; Cardiovasc Intervent Radiol (2015) 38:112–120
9 Paul et al; Radiation dose and image quality of X-ray volume imaging systems: cone-beam computed tomography, digital subtraction angiography and digital fluoroscopy; Eur Radiol (2013) 23:1582–1593
10 Y. M. Kwok et al; Effective dose estimates for cone beam computed tomography in interventional radiology; Eur Radiol (2013) 23:3197–3204
11 Tyan YS et al; The effective dose assessment of C-arm CT in hepatic arterial embolisation therapy; Br J Radiol. 2013 Apr;86(1024):20120551

12 Suzuki S et al; Evaluation of effective dose during abdominal three-dimensional imaging for three flat-panel-detector angiography systems; Cardiovasc Intervent Radiol. 2011 Apr;34(2):376-82
13 Mei Bai et al; The comparison of radiation dose between C-arm flat-detector CT (DynaCT) and multi-slice CT (MSCT): A phantom study; European Journal of Radiology 81 (2012) 3577– 3580
14 Schafer S, Nithiananthan S, Mirota DJ, et al. Mobile C-arm cone-beam CT for guidance of spine surgery: image quality, radiation dose, and inte-gration with interventional guidance. Med Phys2011; 38:4563– 4574
15 Wolfgang Hohenforst-Schmidt et al; Radiation Exposure of Patients by Cone Beam CT during Endobronchial Navigation - A Phantom Study; Journal of Cancer 2014; 5(3): 192-202
16 Braak SJ et al; Effective dose during needle interventions: cone-beam CT guidance compared with conventional CT guidance; J Vasc Interv Radiol. 2011 Apr;22(4):455-61. doi: 10.1016/j.jvir.2011.02.011
17 Braak SJ et al; 3D cone-beam CT guidance, a novel technique in renal biopsy--results in 41 patients with suspected renal masses; Eur Radiol. 2012 Nov;22(11):2547-52
18 Schulz B et al; Radiation exposure to operating staff during rotational flat-panel angiography and C-arm cone beam computed tomography (CT) applications; Eur J Radiol. 2012 Dec;81(12):4138-42
19 Asger Greval Petersen et al; Dose optimisation for intraoperative cone-beam flat-detector CT in paediatric spinal surgery; Pediatr Radiol (2012) 42:965–973
20 Daly MJ et al; ntraoperative cone-beam CT for guidance of head and neck surgery: Assessment of dose and image quality using a C-arm prototype; Med Phys. 2006 Oct;33(10):3767-80
21 Schegerer AA et al; Dose and image quality of cone-beam computed tomography as compared with conventional multislice computed tomography in abdominal imaging; Invest Radiol. 2014 Oct;49(10):675-84
22 Cheng EY et al; Radiation dosimetry of intraoperative cone-beam compared with conventional CT for radiofrequency ablation of osteoid osteoma; J Bone Joint Surg Am. 2014 May 7;96(9):735-42 doi: 10.2106/JBJS.M.00874
23 O'Donnell C et al; Comparative radiation exposure using standard fluoroscopy versus cone-beam computed tomography for posterior instrumented fusion in adolescent idiopathic scoliosis; Spine (Phila Pa 1976). 2014 Jun 15;39(14)

APPENDIX 7 | EURADOS-EFOMP Discussion on Patient Dosimetry for CBCT

24 Petersen AG , Eiskjær S , Kaspersen J . Dose optimisation for intra-operative cone-beam fl at-detector CT in paediatric spinal surgery . Pediatr Radiol2012 ; 42 : 965 – 73 .

25 Van de Kelft E , Costa E , Van Der Planken D , et al. A prospective multicenter registry on the accuracy of pedicle screw placement in the thoracic, lumbar, and sacral levels with the use of the O-arm imaging system and StealthStation Navigation . Spine2012 ; 37 : 1580 – 7 .

26 Abul-Kasim K et al; Optimization of radiation exposure and image quality of the cone-beam O-arm intraoperative imaging system in spinal surgery; J Spinal Disord Tech. 2012 Feb;25(1):52-8.

27 Lange J et al; Estimating the effective radiation dose imparted to patients by intraoperative cone-beam computed tomography in thoracolumbar spinal surgery; Spine (Phila Pa 1976). 2013 Mar 1;38(5):E306-12.

28 Zbijewski W et al; A dedicated cone-beam CT system for musculoskeletal extremities imaging: design, optimization, and initial performance characterization; Med Phys. 2011 Aug;38(8):4700-13.

29 Ramdhian-Wihlm R et al; Cone-beam computed tomography arthrography: an innovative modality for the evaluation of wrist ligament and cartilage injuries; Skeletal Radiol. 2012 Aug;41(8):963-9

30 Faccioli N et al; Finger fractures imaging: accuracy of cone-beam computed tomography and multislice computed tomography; Skeletal Radiol. 2010 Nov;39(11):1087-95.

31 de las Heras Gala H, Schöfer F, Schöfer H, Sánchez Casanueva RM et al. A patient-centric approach to quality control and dosimetry in CT including CBCT. Physica Medica. 2018;47:92-102.

5.4.3 | Dental Cone Beam CT (CBCT)

Intraoral, panoramic and cephalometric radiographs are the basic imaging techniques in dentomaxillofacial radiology (DMFR), allowing two-dimensional (2D) imaging of oral hard tissue. 2D radiographic images have been used in dentistry for decades. However, the maxillofacial region includes fairly complex 3D anatomy where traditional dental modalities may fail to provide optimal visualisation of adjacent overlaying structures, which might overlap in any single projection. Technological advances have led to the introduction of new cone beam CT (CBCT) in dentomaxillofacial radiology (DMFR). Dental CBCT technology first emerged in 1995. Dental CBCT utilises a cone- or pyramid-shaped X-ray beam covering the intended maxillofacial field-of-view (FOV). Most of the modern CBCT scanners use flat panel detectors (FPD).

A literature review focusing on dosimetry in dental CBCT imaging was undertaken. A total of 85 relevant papers were identified, including some relevant paper reviews.

Experimental studies used phantoms of various types in conjunction with TLDs, small volume chambers, radiochromic film, MOSFET or OSL detectors. Adult phantoms were predominantly used, although a very small number of studies used child/paediatric phantoms. There is no commercially available adolescent phantom on the market at present. While organ doses and/or effective doses were detailed for numerous phantom studies, only one patient study was identified in the literature. Monte Carlo approaches were also adopted to estimate Effective Dose.

APPENDIX 7 | EURADOS-EFOMP Discussion on Patient Dosimetry for CBCT

Default exposure protocols were routinely applied, although some authors digressed from these programs and adjusted the exposure parameters. The various permutations resulted in multiple protocols being available to users, with one author citing 72 protocols available on one system [9]. Adult protocols were primarily selected but a small number of papers covered adolescent and/or paediatric/child imaging protocols. In general, when clinical protocols were citied, there was a lack of detail given, with respect to the important exposure parameters affecting patient dose as X-ray tube voltage, tube current, angle of rotation and Field of View (FOV). In particular, classification to small, medium and large FOV was used in numerous studies, but there is a large discrepancy among them in terms of classification criteria.

A large range in Effective Dose measurements was noted, with one author quoting a 20-fold difference between CBCT devices [1]. It was also noted reviewing the publications, an existing significant variation in conversion factors to estimate of Effective Dose be calculated from Entrance Surface Dose, DHP or KAP. Limited information was available in relation to the establishment of Diagnostic Reference Levels (DRLs). Finland has established DRLs for a number of adult examinations [28] while the UK has published an “achievable dose”, quoted as a KAP of 250 mGy·cm2 for the upper 1st molar implant for an adult patient [2].

Additional low-dose and high image quality definition protocols, available on some systems have contributed to the wide dose range currently being achieved. A 15-fold difference in dose was observed for the same FOV between low dose and high-resolution protocols [3].

A significant variation in conversion factors to allow an estimate of Effective Dose be calculated from Entrance Surface Dose, DHP or KAP was also noted in the publications. One author recorded a 7.5-fold range of Effective Dose/KAP values for varying adult exposures between various systems and a 3.8-fold range for large to small FOVs using a single CBCT system [3].

APPENDIX 7 | EURADOS-EFOMP Discussion on Patient Dosimetry for CBCT

Some relevant results are summarized in table A7.3. Following the guidelines of the European Commission on cone beam CT for dental and maxillofacial Radiology [4], studies were divided into “dentoalveolar” (small) and “craniofacial” (large FOV). A medium FOV category was added for studies of temporomandibular joint (medium FOV). The height of the dentoalveolar FOVs is smaller than 5cm, the medium FOV is between 5 and 10 cm, allowing imaging of the lower and upper jaws. For the craniofacial FOVs, the height is greater than 10cm allowing maxillofacial imaging. Additionally, paediatric studies have been added when available.

An extensive review has been published by Kiljunen T et al. [5]. This review summarizes the characteristics of commercial dental CBCT systems, including the dose delivered (in terms of KAP or CTDI).

Overall, the literature on dosimetry in dental CBCT imaging is difficult to interpret at times and also challenging to compare. This is due to variations in phantom design and composition, test methodologies and dose metrics used. The limited technical information provided by some authors also contributed to the difficulties in comparing data. The variability in protocol parameters and in particular, the difference in FOV definitions also influenced the scale of the disparity in dosimetry measurements.

It is clear from the literature that specific protocols are required to be developed that will address an imaging goal. It is also evident that the most appropriate dose metric for dental CBCT imaging has yet to be agreed upon. However, the International Electro technical Commission stated that Dental extra-oral "Equipment shall be provided with an indication of the dose area product (DAP)” [A9] and also the RP 172 [A10] stated that manufacturers of dental CBCT equipment should provide a read-out of Kerma-Area Product (KAP) after each exposure. So KAP is already a common quantity displayed by the most of present dental equipment and it is expected to have this indication provided by all the new equipment.

Doses often vary in very wide ranges. Very low values of few μGy are usually associated to organ exposed only to scatter radiation (such as lens or thyroid) and relative high values of thousands of μGy are associated to organ entirely included in the primary beam, such as oral mucosa or salivary glands.

APPENDIX 7 | EURADOS-EFOMP Discussion on Patient Dosimetry for CBCT

Table A7.3. Summary of the range of doses, represented as (minimum dose ÷ maximum dose) or (value ± uncertainty) for different field of view sizes (dentoalveolar, temporo-mandibular joint, craniofacial and paediatric) dose indicators and methodologies retrieved from the reviewed papers for dental applications.

Field of view	Dose indicator	Range	Methodology	Ref.
Dentoalveolar	Effective Dose	9.7 ÷ 197 µSv	Review	6
		10 ÷ 21 µSv	Rando head Radiochromic films	7
		81.46 ± 0.13 µSv	KAP meter Coefficients (E/KAP)	8
		37 ÷ 107 µSv	Anthropomorphic head OSL	9
		32 ÷ 60 µSv	Anthropomorphic head TLD	10
		20.2 ÷ 30.24 µSv	Anthropomorphic phantom TLD	11
		19 ÷ 44 µSv	Anthropomorphic head TLD	1
		27 ÷ 101 µSv	Anthropomorphic head TLD	12
		32.8 ÷ 114.8 µSv	Anthropomorphic head TLD	13
		9.3-51.2 µSv	Anthropomorphic head TLD	14
	Organ Dose	1 ÷ 1890 µGy	Anthropomorphic head Radiochromic films	7

APPENDIX 7 | EURADOS-EFOMP Discussion on Patient Dosimetry for CBCT

Dentoalveolar	Organ Dose	25.2 ÷ 3395 µGy	Anthropomorphic phantom Radiochromic films	11
		14 ÷ 2011 µGy	Anthropomorphic head TLD	12
	KAP	101.1 ÷ 457.9 mGy·cm^2	KAP meter	15
		637.4 ± 0.97 mGy·cm^2	KAP meter	6
		429 ÷ 644 mGy·cm^2	Head phantom TLD KAP meter	16
		850 ± 57 mGy·cm^2	KAP meter	29
	D1, D2	0.468 ÷ 1.891 mGy 0.673 ÷ 2.837 mGy	Technical Phantom Ionisation chamber	15
	D_{FOV}	23.1 ± 1.4 mGy	Solid-state probe	29
	Incident air kerma	2.85 ± 0.17 mGy (pending further validation)	PAKT method Solid-state probe	
Temporo-mandibular joint	Effective Dose	3.9 ÷ 6.74 µSv	Review	6
		56 ÷ 129 µSv	Anthropomorphic head Radiochromic films	7
		154.5 ÷ 273.7 µSv	KAP meter Coefficients (E/KAP)	8
		36 ÷ 100 µSv	Anthropomorphic head OSL	9

APPENDIX 7 | EURADOS-EFOMP Discussion on Patient Dosimetry for CBCT

Temporo-mandibular joint	Effective Dose	83.09 ÷ 332.4 μSv	Anthropomorphic head TLD	17
		58 ÷ 113 μSv	Anthropomorphic head TLD	10
		39.92 ÷ 43.27 μSv	Anthropomorphic phantom TLD	11
		92 μSv	Anthropomorphic head TLD	18
		18 ÷ 28 μSv	Computational phantoms MC code	19
		28 ÷ 265 μSv	Anthropomorphic head TLD	1
		62 ÷ 211 μSv	Anthropomorphic head TLD	12
		61.6 ÷ 183.7 μSv	Anthropomorphic head TLD	13
		17.6-52.0 μSv	Anthropomorphic head TLD	14
	Organ Dose	20 ÷ 5700 μGy	Anthropomorphic head Radiochromic films	7
		18 ÷ 10747 μGy	Anthropomorphic head TLD	17
		53.6 ÷ 10328.4 μGy	Anthropomorphic phantom Radiochromic films	11

	Organ Dose	15 ÷ 2195 µGy	Anthropomorphic head TLD	18
		26 ÷ 4203 µGy	Anthropomorphic head TLD	12
	KAP	1085 ÷ 2140 mGy·cm^2	KAP meter	8
		126.7 ÷ 1476.9 mGy·cm^2	Blue-tinted film OSL	20
		956 ÷ 1910 mGy·cm^2	Anthropomorphic head TLD KAP meter	16
		117 ÷ 214 mGy·cm^2	KAP meter	19
	Absorbed Dose	1.10 ÷ 1.43 mGy	PMMA Ion chamber	21
Craniofacial	Effective Dose	8.8 ÷ 1073 µSv	Review	6
		153.9 ÷ 428.3 µSv	KAP meter Coefficients (E/KAP)	8
		48 ÷ 102 µSv	Anthropomorphic head OSL	9
		98.7 µSv	Anthropomorphic head TLD	22
		63 µSv	Anthropomorphic head TLD	23
		77 µSv	Anthropomorphic head TLD	10

APPENDIX 7 | EURADOS-EFOMP Discussion on Patient Dosimetry for CBCT

Craniofacial	Effective Dose	60 ÷ 932 μSv (left parotid gland) 148 ÷ 932 μSv (submandibular gland)	Anthropomorphic head OSL	24
		16 ÷ 66 μSv	Computational phantoms MC code	19
		68 ÷ 368 μSv	Anthropomorphic head TLD	1
		169 ÷ 303 μSv	Anthropomorphic head TLD	12
		107 ÷ 117 μSv	Anthropomorphic head Radiochromic film, TLD	25
		44.5 ÷ 169.7 μSv	Anthropomorphic head TLD	13
		43.1 ÷ 111.5 μSv	Anthropomorphic head TLD	14
	Organ Dose	14.1 ÷ 3368.2 μGy	Anthropomorphic head TLD	22
		2.6 ÷ 1066.3 μGy	Anthropomorphic head TLD	23
		72 ÷ 6861 μGy	Anthropomorphic head TLD	12
		56 ÷ 2705 μGy	Anthropomorphic head Radiochromic, TLD	25

Craniofacial	Organ Dose	117 ÷ 935 μGy (skin at thyroid) 36.7 ± 21.0 mGy (skin at female breast) 12.1 ± 7.6 mGy (skin at back) 0.8 ± 1.0 mGy (skin at gonads)	Anthropomorphic body solid-state chamber	28
	KAP	1081 ÷ 3349 mGy·cm^2	KAP meter	8
		3023 mGy·cm^2	KAP meter	11
		2485 ÷ 4499 mGy·cm^2	Anthropomorphic head phantom TLD KAP meter	16
		98 ÷ 556 mGy·cm^2	KAP meter	19
	Absorbed Dose	1.33 ÷ 1.58 mGy	PMMA Ion chamber	21
Paediatric	Effective Dose	11 ÷ 1160 μSv	Review	27
		50.77 ± 0.18 μSv (small FOV) 141.9 ÷ 171.0 μSv (medium FOV) 133.4 ÷ 255.9 μSv (large FOV)	KAP meter Coefficients (E/KAP)	8

APPENDIX 7 | EURADOS-EFOMP Discussion on Patient Dosimetry for CBCT

	KAP	237 ÷ 282 µSv (10 y small FOV) 214 µSv (10 y medium FOV) 28 µSv adolescent (10 y large FOV) 188 ÷ 216 µSv (adolescent small FOV) 70 µSv (adolescent medium FOV) 32 µSv (adolescent large FOV)	Anthropomorphic phantom TLD	26
		395.8 ± 1.4 mGy·cm^2 (small FOV) 996.7 ÷ 1337 mGy·cm^2 (medium FOV) 1006 ÷ 2001 mGy·cm^2 (large FOV)	KAP meter	8
	Absorbed Dose	1.83 ÷ 2.00 mGy (child medium FOV) 2.00 ÷ 2.20 mGy (child large FOV) 1.53 ÷ 1.70 mGy (adolescent medium FOV) 1.69 ÷ 1.99 mGy (adolescent large FOV)	PMMA Ion chamber	21

APPENDIX 7 | EURADOS-EFOMP Discussion on Patient Dosimetry for CBCT

References of the dental part

A9 International Electrotechnical Commission 60601-2-63:2012; Medical electrical equipment - Part 2-63: Particular requirements for the basic safety and essential performance of dental extra-oral X-ray equipment

A10 European Commission RP 172: Cone beam CT for dental and maxillofacial radiology (Evidence-based guidelines); 2012

1. Pauwels R, Beinsberger J, Collaert B, Theodorakou C, et al. Effective dose range for dental cone beam computed tomography scanners. Eur J Radiol. 2012; 81: 267–271.
2. HPA. Health Protection Agency Recommendations for the design of X-ray facilities and quality assurance of dental Cone Beam CT (Computed tomography) systems. HPA-RPD-065. Chilton, UK; Health Protection Agency; 2010.
3. Ludlow JB, Timothy R, Walker C, Hunter R, Benavides E, et al. Effective dose of dental CBCT—a meta analysis of published data and additional data for nine CBCT units. Dentomaxillofac Radiol. 2015; 44: 20140197.
4. European Commission. Radiation Protection No. 172. Cone beam CT for dental and maxillofacial Radiology (evidence based guidelines). 2012.
5. Kiljunen T, Kaasalainen T, Suomalainen A, Kortesniemi M. Dental cone beam CT: A review. Physica Medica. 2015; 31: 844–860.
6. Al-Okshi A, Lindh C, Sale H, Guinnarisson M, et al. Effective dose of cone beam CT (CBCT) of the facial skeleton: a systematic review. Br J Radiol. 2015; 88 (1045): 20140658.
7. Al-Okshi A, Nilsson M, Petersson Q, Wiese M, et al. Using Gaf Chromic film to estimate the effective dose from dental cone beam CT and panoramic radiography Dentomaxillofac Radiol. 2013; 42: 20120343.
8. Shin HS, Nam KC, Park H, Choi HU, Kim HY et al. Effective doses from panoramic radiography and CBCT (cone beam CT) using dose area product (DAP) in dentistry. Dentomaxillofac Radiol. 2014; 43: 20130439.
9. Chambers D, Bohay R, Kaci L, Barnett R, Battista J. The effective dose of different scanning protocols using the Sirona GALILEOS® comfort CBCT scanner. Dentomaxillofac Radiol. 2015; 44, 20140287.

APPENDIX 7 | EURADOS-EFOMP Discussion on Patient Dosimetry for CBCT

10. Davies J, Johnson B, Drage N. Effective doses from cone beam CT investigation of the jaws. Dentomaxillofac Radiol. 2012; 41: 30–36.
11. Hirsch E, Wolf U, Heinicke F, Silva MA. Dosimetry of the cone beam computed tomography Veraviewepocs 3D compared with the 3D Accuitomo in different fields of view. Dentomaxillofac Radiol. 2008; 37(5): 268–273.
12. Pauwels R, Zhang G, Theodorakou C, Walker A, et al. Effective radiation dose and eye lens dose in dental cone beam CT: effect of field of view and angle of rotation. Br J Radiol. 2014; 87(1042): 20130654.
13. Schilling R, Geibel MA. Assessment of the effective doses from two dental cone beam CT devices. Dentomaxillofac Radiol. 2013; 42: 20120273.
14. Soares MR, Batista WO, de Lara Antonio P, Caldas LVE, et al. Study of Effective Dose of Various Protocols in Equipment Cone Beam CT. Ap Rad Iso. 2015; doi. 10.1016/j.apradiso.2015.01.012.
15. Araki K, Patil S, Endo A, Okano T. Dose indices in dental cone beam CT and correlation with dose–area product. Dentomaxillofac Radiol. 2013; 42: 20120362.
16. Kim DS, Rashsuren O, Kim EK. Conversion coefficients for the estimation of effective dose in cone-beam CT. Imaging Sci Dent. 2014; 44: 21-29
17. Dae-Kyo Jeong et al. Comparison of effective dose for imaging of mandible between multi-detector CT and cone-beam CT. Imaging Science in Dentistry. 2012; 42 : 65-70.
18. Kadesjo N, Benchimol D, Falahat B, Näsström, et al. Evaluation of the effective dose of cone beam CT and multislice CT for temporomandibular joint examinations at optimized exposure levels. Dentomaxillofac Radiol. 2015; 44: 20150041.
19. Morant JJ, Salavado M, Hernandez-Giron I, Casanovas R, et al. Dosimetry of a cone beam CT device for oral and maxillofacial radiology using Monte Carlo techniques and ICRP adult reference computational phantoms. Dentomaxillofac Radiol. 2013; 42: 92555893.
20. Endo A, Katoh T, Vasudeva SB, Kobayashi I et al. A preliminary study to determine the diagnostic reference level using dose–area product for limited-area cone beam CT. Dentomaxillofac Radiol. 2013; 42: 20120097.

21. Choi E, Ford NL. Measuring absorbed dose for i-CAT CBCT examinations in child, adolescent and adult phantoms. Dentomaxillofac Radiol. 2015; 44(6): 20150018.
22. Chinem LA, de Souza Vileella B, de Pinho Mauricio CL, Canevaro LV, et al. Digital orthodontic radiographic set versus cone-beam computed tomography: an evaluation of the effective dose. Dental Press J Orthod. 2016; 21(4): 66-72.
23. De Cock J, Zanca F, Canning J. A comparative study for image quality and radiation dose of a cone beam computed tomography scanner and a multislice computed tomography scanner for paranasal sinus imaging. Eur Radiol. 2015; 25: 1891–1900.
24. Jadu F, Yaffe MJ, Lam EW. A comparative study of the effective radiation doses from cone beam computed tomography and plain radiography for sialography. Dentomaxillofac Radiol. 2010; 39: 257–263.
25. Rampado O, Bianchi SD, Cornetto AP, Rossetti V, et al. Radiochromic films for dental CT dosimetry: A feasibility study. Physica Medica. 2014; 30(1): 18-24.
26. Theodorakou C, Walker A, Horner K, Pauwels R, et al, The SEDENTEXCT Project Consortium. Estimation of paediatric organ and effective doses from dental cone beam CT using anthropomorphic phantoms. The British Journal of Radiology 2012; 85: 153–160.
27 Reference levels for patient radiation exposure in cone-beam computed tomography examinations of adults' head region, STUK, 12/3020/2016, 7 November 2016.
28. Schulze RKW, Sazgar M, Karle H, de las Heras Gala H. Influence of a Commercial Lead Apron on Patient Skin Dose Delivered During Oral and Maxillofacial Examinations under Cone Beam Computed Tomography (CBCT). Health Physics 2017 113(2): 129–134.
29. de las Heras Gala H, Schöfer F, Schöfer H, Sánchez Casanueva RM et al. A patient-centric approach to quality control and dosimetry in CT including CBCT. Physica Medica. 2018;47:92-102.

References

References

[1] Official Journal of the European Union. COUNCIL DIRECTIVE 2013/59/EURATOM of 5 December 2013, laying down basic safety standards for protection against the dangers arising from exposure to ionising radiation, and repealing Directives 89/618/Euratom, 90/641/Euratom, 96/29/Euratom, 97/43/Euratom and 2003/122/Euratom. Definition 71 (chapter 2, article 4).

[2] Dance DR, Christofides S, Maidment ADA, McLean ID, Ng KH, editors. Diagnostic radiology physics: A handbook for teachers and students. Vienna: International Atomic Energy Agency (IAEA); 2014.

[3] European Commission. Radiation Protection No 162: Criteria for acceptability of medical radiological equipment used in diagnostic radiology, nuclear medicine and radiotherapy. Luxembourg: Office for Official Publications of the European Communities; 2012.

[4] European society of radiology.EuroSafe: Imaging together – for patient safety. [Online] Available: http://www.eurosafeimaging.org/.

[5] The alliance for radiation safety in pediatric imaging. Image Gently. [Online] Available: http://www.imagegently.org/

[6] Image Wisely: Radiation safety in adult medical imaging. [Online] Available: http://www.imagewisely.org/

[7] Korreman S, Rasch C, McNair H, Verellen D, Oelfke U, Maingon P, Mijnheer B, Khoo V. The European Society of Therapeutic

[8] European Commission.Radiation Protection No 172: Cone beam CT for dental and maxillofacial radiology. Evidence based guidelines. Luxembourg: Office for Official Publications of the European Communities; 2012.

[9] Health Protection Agency. HPA-CRCE-010 :Guidance on the safe use of dental cone beam CT equipment. Chilton, UK: Health Protection Agency ; 2010.

[10] Deutsches Institut für Normung. DIN 6868-161: Image quality assurance in X-ray departments - Part 161: RöV acceptance testing of dental radiographic equipment for digital cone beam computed tomography. English translation of DIN 6868-161:2013-01. Berlin: Deutsches Institut für Normung; 2016. Original and English translation available at https://www.beuth.de/en/standard/din-6868-161/164214522.

[11] Leary D, Robar JL. CBCT with specification of imaging dose and CNR by anatomical volume of interest. Med Phys 2014;41(1):011909.

[12] Droege RT, Morin RL. A practical method to measure the MTF of CT scanners. Med Phys 1982;9(5):758-60.

References

[13] Lin PJP, Beck TJ, Borras C, Cohen G, Jucius RA, Kriz RJ, et al. AAPM task group report No 39: Specification and acceptance testing of computed tomography scanners. New York: American Association of Physicists in Medicine; 1993.

[14] Chiarot CB, Siewerdsen JH, Haycocks T , Moseley DJ, Jaffray DA. An innovative phantom for quantitative and qualitative investigation of advanced x-ray imaging technologies. Phys Med Biol 2005;50(21):N287-97.

[15] Popescu LM, Myers KJ. CT image assessment by low contrast signal detectability evaluation with unknown signal location. Med Phys 2013;40:111908.

[16] Steiding C, Kolditz D, Kalender WA. A quality assurance framework for the fully automated and objective evaluation of image quality in cone-beam computed tomography. Med Phys 2014;41:031901.

[17] Chen R, Geschwind JF, Wang Z, Tacher V, Lin M. Quantitative assessment of lipiodol deposition after chemoembolization: Comparison between cone-beam computed tomography and multidetector computed tomography. J VascIntervRadiol 2013;24(12):1837-44.

[18] Esmaeili F, Johari M, Haddadi P. Beam hardening artifacts by dental implants: Comparison of cone-beam and 64-slice computed tomography scanners. Dent Res J (Isfahan) 2013;10(3):376-81.

[19] Brisco J, Fuller K, Lee N, Andrew D. Cone beam computed tomography for imaging orbital trauma-image quality and radiation dose compared with conventional multislice computed tomography. Br J Oral MaxillofacSurg 2013;52(1):76-80.

[20] Thongvigitmanee SS,Pongnapang N, Aootaphao S, Yampri P, Srivongsa T, Sirisalee, P, et al, Radiation dose and accuracy analysis of newly developed cone-beam CT for dental and maxillofacial imaging. Proc IEEE Eng Med BiolSoc 2013;2356-9.

[21] Kyriakou Y, Kolditz D, Langner O, Krause J, Kalender W. Digital volume tomography (DVT) and multislice spiral CT (MSCT): an objective examination of dose and image quality. RoFoFortschrRontg 2011;183(2):144-53 [in German].

[22] Rehani MM, Gupta R, Bartling S, Sharp GC, Pauwels R, Berris T, et al. ICRP publication 129: Radiological protection in cone beam computed tomography (CBCT). Ann. ICRP 2015;44(1):7-127.

[23] Deutsches Institut für Normung.DIN 6868-15:Image quality assurance in X-ray departments - Part 15: RöV constancy testing of X-ray installations for dental radiographic equipment for digital cone-beam computed tomography. Berlin: Deutsches Institut für Normung; 2015 [in German].

[24] Société Française de Physique Médicale (SFPM). Radiothérapie Guidée par l'Image - Contrôle de qualité des équipements à rayons X. Delpon G (coordinator). RAPPORT SFPM N° 29 [in French]; 2014. Download here: http://www.sfpm.fr/download/fichiers/docs_sfpm/sfpm_2014-29_cq_igrt.pdf

References

[25] Bissonnette JP, Balter PA, Dong L, Langen KM, Lovelock DM, Miften M, et al. Quality assurance for image-guided radiation therapy utilizing CT-based technologies: A report of the AAPM TG-179. Med Phys 2012;39(4):1946-63.

[26] "Dental cone beam computed tomography: safe usage - Publications - GOV.UK." [Online]. Available: https://www.gov.uk/government/publications/dental-cone-beam-computed-tomography-safe-usage. [Accessed: 15-Apr-2016].

[27] "Radiation: protection and safety guidance for dental cone beam CT equipment - Publications - GOV.UK." [Online]. Available: https://www.gov.uk/government/publications/radiation-protection-and-safety-guidance-for-dental-cone-beam-ct-equipment. [Accessed: 15-Apr-2016].

[28] International Electrotechnical Commission. IEC 60601-2-63:2012. Medical electrical equipment - Part 2-63: Particular requirements for the basic safety and essential performance of dental extra-oral X-ray equipment. September 2012.

[29] "Dental practitioners: safe use of x-ray equipment - Publications - GOV.UK." [Online]. Available: https://www.gov.uk/government/publications/dental-practitioners-safe-use-of-x-ray-equipment. [Accessed: 15-Apr-2016].

[30] "Test Protocol for Dental Cone-beam Computed Tomography x-ray Apparatus 2016." Environment Protection Authority of South Australia, 2016.

[31] "Test Protocol for Medical, Veterinary and Chiropractic x-ray Apparatus Used for Plain Radiography 2016." Environment Protection Authority of South Australia, 2016.

[32] Popova Y, Hersemeule G, Klausz R,Souchay H. Description and benefits of dynamic collimation in digital breast tomosynthesis. Radiat Prot Dosimetry 2015 Jul;165(1-4):321-4.

[33] EFOMP. Quality controls in digital mammograph – Protocol of the EFOMP mammo working group. Gennaro G (group leader). 2015. Download here: http://www.efomp.org/index.php/scientific-guidance-and-protocols/351-mammo-protocol

[34] Hsieh J. Computed Tomography Principles, Design, Artifacts, and Recent Advances, 2nd Edition. SPIE, Bellingham, Washington, USA and John Wiley & Sons, Inc, Hoboken, New Jersey, USA;. 2009.

[35] "GAEC circular for radiological laboratory testing protocols (in application of § 1.1.4.7.1 of the Radiation Protection Regulations)." Greek Atomic Energy Commission, 2006.

[36] International Electrotechnical Commission. IEC Report No 61223-3-5: Evaluation and routine testing in medical imaging departments – Part 3-5: Acceptance tests – Imaging performance of computed tomography X-ray equipment. Geneva: International Electrotechnical Commission; 2004.

References

[37] Feldkamp LA, Davis LC, and Kress JW. Practical cone-beam algorithm. J. Opt. Soc. Am. A 1984;1:612-619.

[38] Klein EE, Hanley J, Bayouth J, Yin FF, Simon W, Dresser S, et al. Task Group 142 report: Quality assurance of medical accelerators. Med Phys. 2009;36(9):4197-212.

[39] Bissonnette JP, Moseley DJ, Jaffray DA. A quality assurance program for image quality of cone beam CT guidance in radiation therapy. Med Phys 2008;35(5)1807-15.

[40] Rasband WS. ImageJ. Bethesda, MD, USA: National Institutes of Health; 1997-2015. [Online] Available: http://imagej.nih.gov/ij/

[41] Lutz W, Winston KR, Maleki N. A system for stereotactic radiosurgery with a linear accelerator.Int J RadiatOncolBiol Phys 1988;14(2):373-81.

[42] Sharpe MB, Moseley DJ, Purdie TG, Islam M, Siewerdsen JH, Jaffray DA. The stability of mechanical calibration for a kV cone beam computed tomography system integrated with linear accelerator. Med Phys 2006;33(1):136-44.

[43] Yin FF, Wong J, Balter JM, Benedict S, Craig J, Dong L, et al. The role of in-room kV X-Ray imaging for patient setup and target localization: A report of AAPM task group 104. College Park, MD, USA: American Association of Physicists in Medicine; 2009.

[44] Cho Y, Moseley DJ, Siewerdsen JH, Jaffray DA. Accurate technique for complete geometric calibration of cone-beam computed tomography systems. Med Phys 2005;32(4):968-83.

[45] Bissonnette JP. Quality assurance of image-guidance technologies.SeminRadiatOncol 2007;17(4):278-86.

[46] Sumida I, Yamaguchi H, Kizaki H, Yamada Y, Koizumi M, Yoshioka Y, et al. Evaluation of imaging performance of megavoltage cone-beam CT over an extended period. J Radiat Res 2014;55(1):191-9.

[47] Sykes JR, Lindsay R, Dean CJ, Brettle DS, Magee DR, Thwaites DI.Measurement of cone beam CT coincidence with megavoltage isocenter and image sharpness using the QUASAR™ Penta-Guide phantom. Phys Med Biol 2008;53(19):5275-93.

[48] Benedict SH, Yenice KM, Followill D, Galvin JM, Hinson W, Kavanagh B, et al. Stereotactic body radiation therapy: The report of AAPM Task Group 101. Med Phys 2010;37(8):4078-101.

[49] Fotina I. et al: Feasibility of CBCT-based dose calculation: Comparative analysis of HU adjustment techniques. Radiother Oncol 2012;104(2): 249-256.

[50] Schulze R, Heil U, Groß D, Bruellmann DD, Dranischnikow E, Schwanecke U, et al. Artefacts in CBCT: a review. Dentomaxillofac Rad 2011;40:265-73.

References

[51] http://www.impactscan.org/

[52] Abramoff MD, Magelhaes PJ, Ram SJ. Image processing with ImageJ.BiophotonicsInt 2004;11:36–42.

[53] Carl P. Radial Profile Extended plugin for ImageJ.Bethesda, MD, USA: National Institutes of Health; 2006-2014. [Online] Available: http://rsb.info.nih.gov/ij/plugins/radial-profile-ext.html

[54] Linnenbrügger N. FFTJ and DeconvolutionJ plugin for ImageJ. Bethesda, MD, USA: National Institutes of Health; 2001-2002. [Online] Available: http://rsb.info.nih.gov/ij/plugins/fftj.html

[55] Schmid B. ImageJ 3D Viewer plugin.Bethesda, MD, USA: National Institutes of Health; 2007-2009. [Online] Available:http://imagej.nih.gov/ij/plugins/3d-viewer/

[56] Thilander-Klang A, Ledenius K, Hansson J, Sund P, Båth M. Evaluation of subjective assessment of the low-contrast visibility in constancy control of computed tomography. RadiatProtDosim 2010;139(1-3):449-54.

[57] Steiding C, Kolditz D, Kalender WA. A quality assurance framework for the fully automated and objective evaluation of image quality in cone-beam computed tomography. Med Phys 2014;41:031901.

[58] Siewerdsen JH, Jaffray DA. Cone-beam computed tomography with a flat-panel imager: Magnitude and effects of x-ray scatter. Med Phys 2001;28(2):220-31.

[59] Ozaki Y, Watanabe H, Nomura Y, Honda E, Sumi Y, Kurabayashi T. Location dependency of the spatial resolution of cone beam computed tomography for dental use. Oral Surg Oral Med O 2013;116(5):651-5.

[60] Dougherty G. Effect of sub-pixel misregistration on the determination of the point spread function of a CT imaging system. Med Eng Phys 2000;22(7):503–7.

[61] International Commission on Radiation Units & Measurements. ICRU report 87: Radiation dosimetry and image quality assessment in computed tomography. Stockholm: International Commission on Radiation Units & Measurements; 2012.

[62] Kwan AL, Boone JM, Yang K, Huang SY. Evaluation of the spatial resolution characteristics of a cone-beam breast CT scanner. Med Phys 2007;34:275-81.

[63] Boone JM. Determination of the presampled MTF in computed tomography. Med Phys 2001;28:356–60.

[64] Institute of Physics and Engineering in Medicine. IPEM report 91: Recommended standards for the routine performance testing of diagnostic X-Ray systems. York, UK: Institute of Physics and Engineering in Medicine; 2005.

References

[65] Wallace MJ, Kuo MD, Glaiberman C, Binkert CA, Orth RC, Soulez G. Three-dimensional C-arm cone-beam CT: applications in the interventional suite. J VascIntervRadiol.2009;20(7):S523-37.

[66] Fahrig R, Dixon R, Payne T, Morin RL, Ganguly A, Strobel N. Dose and image quality for a cone-beam C-arm CT system. Med Phys 2006;33(12):4541-50.

[67] Schafer S, Nithiananthan S, Mirota DJ, Uneri A, Stayman JW, Zbijewski W, Schmidgunst C, Kleinszig G, Khanna AJ, Siewerdsena JH.Mobile C-arm cone-beam CT for guidance of spine surgery: image quality, radiation dose, and integration with interventional guidance.Med Phys. 2011 Aug;38(8):4563-74.

[68] Toporek G, Wallach D, Weber S, Bale R, Widmann G. Cone-beam computed tomography-guided stereotactic liver punctures: a phantom study. Cardiovasc Inter Rad 2013;36(6):1629-37.

[69] Kenngott HG, Wagner M, Gondan M, Nickel F, Nolden M, Fetzer A, et al. Real-time image guidance in laparoscopic liver surgery: first clinical experience with a guidance system based on intraoperative CT imaging. SurgEndosc 2014;28(3):933-40.

[70] Daly MJ, Siewerdsen JH, Cho YB, Jaffray DA, Irish JC. Geometric calibration of a mobile C-arm for intraoperative cone-beam CT. Med Phys 2008;35(5):2124-36.

[71] Chan MF, Yang J, Song Y, Burman C, Chan P, Li S. Evaluation of imaging performance of major image guidance systems. Biomed Imaging Interv J. 2011;7(2):e11.

[72] European Commission. EUR 16262 EN: European guidelines on quality criteria for computed tomography. Luxembourg: Office for Official Publications of the European Communities; 1999. [Online] Available: http://www.drs.dk/guidelines/ct/quality/.

[73] Stock M, Pasler M, Birkfellner W, Homolka P, Poetter R, Georg D. Image quality and stability of image-guided radiotherapy (IGRT) devices: A comparative study. RadiothOncol 2009;93(1):1-7.

[74] Dixon RL, Anderson JA, Bakalyar DM, Boedeker K, Boone JM, Cody DD, et al. Comprehensive methodology for the evaluation of radiation dose in X-ray computer tomography: A new measurement paradigm based on a unified theory for axial, helical, fan-beam, and cone-beam scanning with or without longitudinal translation of the patient table. Report of AAPM Task Group 111: The future of CT dosimetry. College Park, MD, USA: American Association of Physicists in Medicine; 2010.

[75] International Atomic Energy Agency. Dosimetry in Diagnostic Radiology: An International Code of Practice. Technical Reports Series 457. Vienna: International Atomic Energy Agency (IAEA); 2007.

References

[76] International Atomic Energy Agency. Implementation of the International Code of Practice on Dosimetry in Diagnostic Radiology (TRS 457): Review of Test Results. IAEA Human Health Reports 4. Vienna: International Atomic Energy Agency (IAEA); 2011.

[77] Andersson J, Pavlicek W. Patient organ dose with computed tomography - a review of present methodology and DICOM information: executive summary of the joint report of AAPM task group 246 and EFOMP. 2016 In: ECR 2016 Book of Abstracts, 2016, Vol. 7, no 1, B0303

[78] Larsson JP1, Persliden J, Sandborg M, Carlsson GA. Transmission ionization chambers for measurements of air collision kerma integrated over beam area. Factors limiting the accuracy of calibration. Phys Med Biol. 1996;41(11):2381-98.

[79] Servomaa A and Tapiovaara M. Organ Dose Calculation in Medical X Ray Examinations by the Program PCXMC. RadiatProtDosimetry 1998;80(1-3):213-19.

[80] ICRU, 2005. Patient dosimetry for X rays used in medical imaging. ICRU Report 74. J. ICRU 5, 1–113.

[81] T. B. Shope, R. M. Gagne, and G. C. Johnson, "Method for describing the doses delivered by transmission x-ray computed tomography," Med. Phys. 8, 488–495 (1981).

[82] IAEA Human Health Reports No. 5 Subject Classification: 0103-Medical physics "Status of Computed Tomography Dosimetry for Wide Cone Beam Scanners" STI/PUB/1528 (ISBN:978-92-0-120610-7).

[83] McCollough CH, Leng S, Yu L, Cody DD, Boone JM, McNitt-Gray MF CT dose index and patient dose: they are not the same thing. Radiology. 2011 May;259(2):311-6.

[84] A. Amer, T. Marchant, J. Sykes, J. Czajka, and C. Moore, "Imaging doses from the Elekta Synergy x-ray cone beam CT system," Br. J. Radiol. 80, 476–482 (2007).

[85] American Association of Medical Physics, "Report of AAPM Task Group 111: the future of CT dosimetry," AAPM, CollegePark (2010).

[86] Hu N1, McLean D. Measurement of radiotherapy CBCT dose in a phantom using different methods. Australas Phys Eng Sci Med. 2014 Dec;37(4):779-89. doi: 10.1007/s13246-014-0301-x. Epub 2014 Sep 23.

[87] Rampado O, Giglioli FR, Rossetti V, Fiandra C, Ragona R, Ropolo R.Evaluation of various approaches for assessing dose indicators and patient organ doses resulting from radiotherapy cone-beam CT.Med Phys. 2016 May;43(5):2515.

[88] Hernández-Girón I, Calzado A, Geleijns J, Joemai RMS, Veldkamp WJH. Comparison between human and model observer performance in low-contrast detection tasks in CT images: application to images reconstructed with filtered back projection and iterative algorithms. Br J Radiol 2014; 87(1039):20140014.

References

[89] Rose A. Television pickup tubes and the problem of vision. In: Marton L, editor. Advances in Electronics. New York: Academic Press 1948;1:131-66.

[90] Rose A. Quantum effects in human vision. In: Lawrence JH, Tobias CA, editors. Advances in Biological and Medical Physics. New York: Academic Press 1957;5:211-42.

[91] Rose A. Vision: Human and Electronic. New York: Plenum Press; 1974.

[92] Burgess AE. The Rose model, revisited. J Opt Soc Am A 1999;16(3):633-46.

[93] Baek J, Pelc NJ. Local and global 3D noise power spectrum in cone-beam CT system with FDK reconstruction. Med Phys 2011,38:2122-31.

[94] Oliveira ML, Tosoni GM, Lindsey DH, Mendoza K, Tetradis S, Mallya SM. Influence of anatomical location on CT numbers in cone beam computed tomography. Oral Surg Oral Med O 2013;115(4):558-64.

[95] Mah P, Reeves TE, McDavid WD. Deriving Hounsfield units using grey levels in cone beam computed tomography. Dentomaxillofac Rad 2010;39(6):323-35.

[96] Swedish Radiation Safety Authority. SSMFS 2008:42: Strålsäkerhetsmyndighetens allmänna råd om prestandaspecifikationer vid upphandling av utrustning för röntgendiagnostik (Recommendations on Performance Specifications for Equipment used in Diagnostic Radiology). Stockholm: Swedish Radiation Safety Authority; 2009 [in Swedish].

[97] Torgersen GR, Hol C, Møystad A, Hellén-Halme K, Nilsson M. A phantom for simplified image quality control of dental cone beam computed tomography units. Oral Surg Oral Med O 2014;118(5):603-11.

[98] Hernández-Girón I, Geleijns J, Calzado A, Veldkamp WJH. Automated assessment of low contrast sensitivity for CT systems using a model observer. Med Phys 2011;38:S25–35.

[99] Hernández-Girón I, Calzado A, Geleijns J, Joemai RMS, Veldkamp WJH. Low contrast detectability performance of model observers based on CT phantom images: kVp influence. Phys Med 2015;31(7):798–807. doi: 10.1016/j.ejmp.2015.04.012.

[100] Yu L, Leng S, Chen L, Kofler JM, Carter RE, McCollough CH. Prediction of human observer performance in a 2-alternative forced choice low-contrast detection 650 task using channelized Hotelling observer: impact of radiation dose and reconstruction algorithms. Med Phys 2013;40:041908.

[101] Leng S, Yu L, Zhang Y, Carter RE, Toledano AY, McCollough CH. Correlation between model observer and human observer performance in CT imaging when lesion location is uncertain. Med Phys 2013;40:081908.

References

[102] Pauwels R, Beinsberger J, Collaert B, Theodorakou C, Rogers J, Walker A, Cockmartin L, Bosmans H, Jacobs R, Bogaerts R, Horner K. Effective dose range for dental cone beam computed tomography scanners. Eur J Radiol. 2012 Feb;81(2):267-71.

[103] Araki K, Patil S, Endo A, Okano T. Dose indices in dental cone beam CT and correlation with dose–area product. Dento-maxillofac Rad2013;42:20120362.

[104] de Oliveira MVL, Santos AC, Paulo G, Campos PSF, Santos J. Application of a newly developed software program for image quality assessment in cone-beam computed tomography. Imaging Sci Dent (2017), 47(2):75-86.

Quality control in cone-beam computed tomography (CBCT)

EFOMP-ESTRO-IAEA protocol